THE FLORIDA STATE UNIVERSITY

COLLEGE OF ARTS AND SCIENCES

THE EFFECT OF THE BENTHIC BOUNDARY LAYER ON THE PHYSICS OF INTENSE MESOSCALE EDDIES

by

GERMANA PEGGION

A Dissertation submitted to the
Geophysical Fluid Dynamics Program
in partial fulfillment of the
requirements for the degree of
Doctor of Philosophy

Approved:

James J. O'Brien
Professor Co-Directing Dissertation

George L. Weatherly
Professor Co-Directing Dissertation

Doron N.F.

R. Krishnamurti

Christopher Tam

April, 1985

THE EFFECT OF THE BENTHIC BOUNDARY LAYER ON THE PHYSICS OF INTENSE MESOSCALE EDDIES

(Publication No.)

Germana Peggion, Ph.D.
The Florida State University, 1984

Professor Co-Directing Dissertation: James O'Brien, Ph.D.
Professor Co-Directing Dissertation: Georges Weatherly, Ph.D.

The Benthic Boundary Layer is a region close the ocean bottom with features distinct from the oceanic interior. Near the bottom the ocean is turbulent and the resultant mixing leads to a neutrally stratified bottom layer. Turbulent closure models have been applied to investigate how the structure of the Benthic Boundary Layer is affected by the flow and the stratification above the layer.

The object of the present research is to analyze how the benthic region affects the dynamics of the forcing flow. More specifically, a numerical model based on the level 2 1/2 closure scheme of Mellor and Yamada is developed to examine the decay of deep mesoscale eddy-like flows.

It is found that the decay of the flow occurs through conversion of kinetic to potential energy and through dissipation by bottom friction. The relative importance of both processes is expressed by the Rossby number $\varepsilon=U/fR$ and by the stratification parameter $s=N^2H^2/f^2R^2$ (where H is the total depth of the eddy, R the radius, U the velocity scale, N the Brunt-Vaiasala frequency, and f

the Coriolis parameter). A larger Rossby number and stratification parameter lead to a larger conversion of kinetic to potential energy, but a smaller mechanical dissipation of the same energy.

Examination of the structure of the Benthic Boundary Layer indicates that a clear distinction should be made between the mixed layer, or the region neutrally stratified, and the Bottom Boundary Layer, or the region where most of the turbulent activity occurs. It is found that the structure of the Bottom Boundary Layer depends also on the magnitude of the flow above the benthic region, but the mixed layer depends also on the sign of the mesoscale activity. Under a cyclonic flow, the mixed layer is defined by vertical advection and it is usually much thicker than the Bottom Boundary Layer. The mixed layer of an anticyclonic flow is the result of both vertical advection and near bottom turbulence, and the ambiguity between the mixed layer and Bottom Boundary Layer is notably reduced.

ACKNOWLEDGEMENT

This research was supported by the Office of Naval Research under grants to Dr. James O'Brien and Dr. Georges Weatherly. Partial support was offered by Dr. Richard Pfeffer with funds of the Geophysical Fluid Dynamics Institute.

My gratitude is equally divided among Drs. James O'Brien and Georges Weatherly for serving as my major professors. It is with the deepest respect and affection that I thank Dr. James O'Brien for the countless opportunities which he has given me during my graduate career. His continuous guidance and support will never be forgotten. I thank Dr. Georges Weatherly for his interest and the motivation he supplied throughout the course of this work. This dissertation would not have become a reality without his ideas, comments and enthusiasm. I am also grateful for the time taken by Drs. R. Krishnamurti, D. Nof, and C. Tam while serving on my doctoral committee.

I also wish to mention all my colleagues and friends who have shared the ups and downs of these past years. Sincere appreciation is extended to Mrs. Ruth Pryor, Jim Merritt, and David Legler for their constant assistance. Thanks goes to Helen McKelder for her endless patience during the typing of the manuscript.

Grazie

TABLE OF CONTENTS

PAGE

PAGE

LIST OF TABLES

LIST OF FIGURES

PAGE

1. INTRODUCTION.

Measurements of temperature and salinity made close to the bottom of the ocean showed a well-mixed bottom layer a few tens of meters thick bounded by a sharp interface above which there is a nearly-uniformly stratified region. The characteristic well-mixed region of this Benthic Boundary Layer generally does not form a pool or have a distinctive water mass; thus the layer is formed by mixing of the stratified deep ocean (Armi and D'Asaro, 1980; Armi and Millard, 1976; Bowden, 1978; Weatherly and Niiler, 1974). The spatial variability of the bottom region sometimes exhibits evidence of a differential horizontal advection suggestive of forcing due to mesoscale activity. Armi and D'Asaro (1980) reported explicit variations in the horizontal structure of the layer with length scales up to 20 km. Energetic fluctuations within the mixed bottom layer respond mainly to near-inertial and tidal frequencies. Near the bottom there is less near-inertial energy than in the upper levels, but more energy in the high frequency band. These high frequency velocities, which are modulated by tidal currents and by the variations of the flow above the layer, have been considered as measures of the boundary layer turbulent activity (D'Asaro, 1982). Thus a clear distinction should be made between the mixed layer, or the region neutrally stratified, and the Bottom Boundary Layer (BBL)

or the region where most of turbulent activity occurs.

The dynamic role of the BBL was first investigated in relation with coastal and fluvial regions. Its role in sediment transport processes is determinant (Nowell, 1983). Typically in such regions, the near-bottom velocities are not negligible compared to the near-surface flows, and the BBL has been considered as the dominant mechanism by which the input of energy by winds and tides is dissipated (Csanady, 1978).

On the other hand, very little is known about the role of the BBL on the dynamics of the ocean circulation, and the few observations available are often controversial. Weatherly (1972) indicated that bottom friction under the Florida Current is not important, but the same author (1984) estimated that bottom friction in the North Atlantic Ocean may effectively dissipate the energy input by the wind at the surface.

According to Worthington (1976) and the observations of Richardson et al. (1981), and Schmitz (1977), the general circulation of the deep North Atlantic Ocean is composed of a well-defined southward flow along the American continental slope and a northward flow further to the east enclosed in an anticyclonic subtropical gyre. The northward and eastward flow of the gyre is adjacent to the Gulf Stream axis, and it is a fundamental question whether or not the Gulf Stream extends to and interacts with the ocean bottom circulation. Recent studies (Kelley et al., 1982;

Richardson, 1983; Weatherly and Kelley, 1984) supported the hypothesis that the Gulf Stream system influences the entire water column and excursion of the surface Gulf Stream affects near-bottom currents.

Following the hypothesis that the Gulf Stream may extend to the bottom, Clarke (1976) suggested that warm core eddies in the Slope Water region may extend to the bottom as well. The assumption was supported by McCartney et al. (1978). The authors reported that the structure of cold core rings appears to extend all the way to the bottom. The vertical profile of velocity showed a cyclonic flow in the upper levels and a level of no motion near 2000 m of depth with a weak anticyclonic circulation beneath. Kelley (1984) indicated that energetic fluctuations with time scale of 30-90 days in the records of near-bottom deep ocean current meters in the lower Scotian Rise are the results of the barotropic components of Gulf Stream meanders and warm-core rings. Holland (1978) developed a quasi-geostrophic two layer model and postulated that the deep flow might be due to barotropic and baroclinic instabilities generated by the motion in the upper strata of the ocean. Numerical simulations of the model indicated that a mean flow is induced in the lower layer in the same direction as the current in the upper layer. Schmitz and Holland (1982) made a detailed comparison of deep ocean observation in the Gulf Stream region with the results of Holland's model and indicated that although the model is a crude formulation of the North

Atlantic circulation, it provides a convincing explanation of the deep high energetic circulation.

Despite the fact that all those studies have suggested that bottom friction forces may be an efficient dissipative mechanism in the spin-down and decay of rings, up to now this physical process has been neglected. In general, the decay of mesoscale eddies has been attributed to dissipation of kinetic energy either through internal viscous effects or through dispersive spreading of Rossby waves at their own characteristic wave speed. Flierl (1977) examined the decay of isolated linear vortices in absence of frictional forces and showed that they dissipated rapidly under the dispersive effect of a beta-plane. Mied and Lindemann (1979), McWilliams and Flierl (1979) showed that nonlinearity stabilizes the eddies against beta-dispersion and allows the vortices to propagate westwards as a stable entity for longer periods of time. The decay of a ring under the influences of momentum and bouyancy diffusion has been considered by Molinari (1970) and Flierl (personal communication), but both authors neglected bottom friction. Thus in these studies the primary mechanism for the decay is the absorption of the ring in the surrounding waters.

The aim of the present study is to investigate how bottom friction may contribute to the decay of an isolated vortex extending to the bottom of the ocean. Highlights of the sections in which the work is divided are as follows:

In Section Two we present the model formulation which consists

of two distinct parts: one for the flow far from the bottom, and one for the Benthic Boundary Layer together with appropriate matching conditions. In deriving the governing equations for the interior, we develop the model on an f-plane and we assume that the flow is incompressible and hydrostatic. In modelling the turbulent BBL equations, we adopt a modified Mellow and Yamada level 2 1/2 closure scheme (1982).

Section Three is the explanation of the numerical model. Computational efficiency requires consideration of a two-dimensional formulation of the model. This is achieved by assuming that the motion is uniform in one of the horizontal coordinates and parametrizing a mesoscale eddy as an infinite slab. Perhaps, the best justification for such a model is its wide range of applications.

Section Four includes an application of the model for analyzing the structure of the Benthic Boundary Layer forced by a steady flow. Under the assumption that the motion is horizontally homogeneous, we verify the validity of the model by comparing results obtained for neutrally and stably stratified flows with the correspondent values derived by other turbulence models. When the Benthic Boundary Layer is forced by mesoscale activity with a steady barotropic component, the numerical experiments emphasize the different roles that the mixed layer and BBL play in the dynamics of the system.

The decay of an homogeneous and linear vortex is presented in Section Five. An analytical formulation of the problem is presented

and compared with the results of the numerical experiments. Since the analytical model has been conceived as an independent entity, we apologize for the unavoidable repetitions and the different symbols in this section.

Section Six combines the results of Sections Four and Five, and considers the spin-down of a stably stratified and nonlinear flow. Under the hypothesis that the eddy is stationary, the effects of stratification and advection on its decay are analyzed. When the eddy is assumed to be nonstationary, the study investigates how its spin-down is affected by a uniform and steady westward translation

Finally, Section Seven summarizes and discusses this research.

2. MODEL FORMULATION.

We consider a deep eddy-like flow extending from the bottom of the ocean to the thermocline. The eddy has radius R and total depth H. The bottom of the ocean is taken to be flat. The problem is formulated on an f-plane with a Cartesian coordinate system (x,y,z) chosen such that in the northern hemisphere the x-coordinate increases eastwards, the y-coordinate northwards, and the vertical coordinate, z, is zero at the bottom and increases upwards.

We assume that the flow is homogeneous in the north-south direction. The ocean is hydrostatic and incompressible and the density is a linear function of temperature alone (Fofonoff, 1962).

Since close to the bottom the horizontal frictional force due to turbulent mixing of momentum becomes dominant, the most convenient approach to the problem is through boundary layer theory. Thus it is appropriate to present the model equations for the interior and the BBL separately.

2.1. The model equations for the interior flow

The equations governing the motion are those of momentum, mass and heat conservations, viz:

$$u_t + uu_x + wu_z - fv = - g\eta_x - \frac{1}{\rho_o} p_x + (A_x u_x)_x + \nu u_{zz} \tag{2.1.1a}$$

$$v_t + uv_x + wv_z + fu = (A_{xy} v_x)_x + \nu v_{zz} \tag{2.1.1b}$$

$$0 = - p_z - g\rho \tag{2.1.1c}$$

$$u_x + w_z = 0 \tag{2.1.1d}$$

$$T_t + uT_x + wT_z = (A'_x T_x)_x + kT_{zz} \tag{2.1.1e}$$

$$\rho = \rho_o(1 - \alpha(T - T_o)) \tag{2.1.1f}$$

The subscripts (x,z,t) denote partial differentiation; the variables (u,v,w) are the components of the eastward, poleward, and vertical velocities respectively. The variable η (henceforth indicated as the displacement of the thermocline) is the barotropic forcing; ρ and T are the deviations of density and temperature from density and temperature associated with a state of rest expressed by the constants of reference ρ_o and T_o. The variable p is the hydrostatic pressure associated with the density distribution ρ; A_x and A'_x and A_{xy} are the eddy coefficients of horizontal viscosity and conductivity respectively; ν and k are the eddy coefficients of vertical viscosity and conductivity respectively; α is the coefficient of thermal expansion; g is the gravitational acceleration, and f the Coriolis parameter.

The matching conditions between the interior and the BBL solutions provide the dissipative mechanism that governs the spin-down process of the flow.

Equations (2.1.1) must be satisfied in the region $h \leq z \leq H$, $-x_o \leq x \leq x_o (x_o > R)$. At the top of the BBL the boundary conditions are specified by matching the BBL and the interior solutions; at the free surface the heat flow is assigned and the velocities u, and v kept equal to their relative barotropic components. Outside the region of interest, the ocean is in a state of rest. The specific conditions are:

$$(u,v,w) = (\bar{u},\bar{v},\bar{w}) \qquad \text{at } z = h \tag{2.1.2}$$

$$T = \bar{T}$$

where bar indicates the BBL solutions.

$$(u,v) = (U_g,V_g) \qquad \text{at } z = H \tag{2.1.3}$$

$$T_z = \Theta_z$$

$$(u,v) = (0,0) \qquad \text{at } |x| = x_o \tag{2.1.4}$$

$$T = T_B(z)$$

where $T_B(z)$ is the temperature distribution of the ocean at rest.

2.2. The model equations for the Bottom Boundary Layer

Using the same notations introduced in Section 2.1 the BBL equations are written as follows:

$$\bar{u}_t + \overline{uu}_x + \overline{wu}_z - f\bar{v} = -g\eta_x - \frac{1}{\rho_o}\bar{p}_x + (A_x\bar{u}_x)_x - (\overline{w'u'})_z \tag{2.2.1a}$$

$$\text{(2.2.1b)} \qquad \bar{v}_t + \overline{uv}_x + \overline{wv}_z + fu = (A_{xy}\bar{v}_x)_x - (\overline{w'v'})_z$$

$$\text{(2.2.1c)} \qquad 0 = -\bar{p}_z - g\bar{\rho}$$

$$\text{(2.2.1d)} \qquad \bar{u}_x + \bar{w}_z = 0$$

$$\text{(2.2.1e)} \qquad \bar{T}_t + \overline{uT}_x + \overline{wT}_z = (A'_x\bar{T}_x)_x - (\overline{w'\theta'})_z$$

In the equations, the terms $-\overline{u'_j u'_i}$, and $-\overline{u'_j \theta'}$ (we will use the usual tensor notation when it does not create ambiguities) represent Reynolds average turbulent fluxes. The equations (2.2.1) must be satisfied in the region $0 \leq z \leq h$, $-x_o \leq x \leq x_o$. At the top of the layer and at the lateral boundaries, the boundary conditions are specified as in (2.1.2) and (2.1.4), respectively. At the rigid surface, the boundary conditions are specified by prescribing the no-slip boundary condition and no flux of heat, viz.:

$$\text{(2.2.2)} \qquad (\bar{u},\bar{v},\bar{w}) = (0,0,0) \quad \text{at } z = 0$$

$$\bar{T}_z = 0$$

Since we have assumed that turbulence is mainly confined to the BBL region, we must require that the Reynolds stresses vanish at $z = h$. Unfortunately, it is not possible to have a priori knowledge of the BBL thickness. Therefore, for numerical purposes, it is convenient to remove the upper boundary at a depth, d, derived from observations and measurements, chosen such that: $h \leq d \leq H$ and assume:

$$(2.2.3) \qquad -\overline{u_j'u_i'} = \overline{u_j'\theta'} = 0 \qquad \text{at } z = d$$

The remaining problem is to specify the Reynolds stresses, $-\overline{u_j'u_i'}$, and, $-\overline{u_j'\theta'}$, so that the equations (2.2.1) are a closed set of equations.

2.3 The closure scheme

A rigorous theory for analyzing the structure of turbulent flows is not available, and most of the difficulties lie in the definition of the turbulent fluxes. For many applications it is sufficient to assume:

$$(2.3.1.) \qquad -\overline{u_j'u_i'} = K \frac{\partial u_i}{\partial x_j}$$

with the eddy coefficient K kept constant and defined from observations and measurments. Unfortunately, this assumption is not advisable for our study. Parameterizing turbulence with constant eddy coefficients cannot represent turbulent processes that are of scale smaller than the grid system of the numerical model. Therefore, the use of constant eddy viscosity implies a grid so fine that is not suitable for numerical computations (Sommeria,1976).

Deardoff (1973) suggested the use of the entire second-order momentum equations for modelling the Reynolds stresses. In order to resolve the higher order stresses that appear in the equation, the method implies the addition of at least ten time-dependent equations, and the scheme is not efficient.

The most common closure schemes resolve the Reynolds stresses by postulating empirical definitions for the higher order stresses. These models are generally derived by one of two different approaches, depending on the nature of the problem. Thus if the purpose of the analysis is to study the response of the boundary layer to the variations of the forcing flow or its spectral distribution, it is necessary to consider closure schemes where the Reynolds stresses are defined from individual transport equations. On the other hand, if the analysis is focused on the effects of the boundary layer on the circulation above that layer, it is sufficient to develop closure schemes that parameterize the effects of turbulence via eddy coefficients and calculate only the mean value of the quantities.

For the latter approach, Mellor and Yamada (1974) obtained an expression for the turbulent fluxes. They are related to the shear of the mean flow via eddy coefficients proportional to the square root of the local value of the turbulent kinetic energy $q^2 = \frac{1}{2}\ \overline{u_j' u_i'}$, and a mixing length scale ℓ dependent upon the distance from the wall

through a proportional coefficient which takes into account the stratification of the fluid, i.e.:

$$(2.3.2a) \qquad (-\overline{w'u'}, -\overline{w'v'}) = S_M \ell q (u_z, v_z)$$

$$(2.3.2b) \qquad -\overline{w'\theta'} = S_T \ell q T_z$$

Thus the problem is closed when one specifies:

i) an equation for the turbulent kinetic energy, q^2

ii) an equation for the mixing length scale, ℓ

iii) the functions S_M and S_T

2.3.1 The turbulent kinetic energy equation

The equation for the turbulent kinetic energy of the flow may be derived by formulating the dynamics equations for the velocity fluctuations and forming the time-averaged equations for the stress components (Monin and Yaglom, 1971). This yields an equation which contains correlation terms that must still be parameterized. The nature of the assumptions made in order to close the q^2-equation leads to different turbulence models. We adopt the turbulent kinetic energy equation according to the level 2 1/2 closure scheme of Mellor and Yamada (1982). The equation is written as follows:

$$(2.3.3) \qquad 1/2(q_t^2 + uq_x^2 + wq_z^2) = P_d + P_s + P_b - \varepsilon$$

where the term P_d represents vertical diffusion of the turbulent kinetic energy. In analogy with the definitions (2.3.2), it is defined as:

$$P_d = (1/2)(S_Q \ell q (q^2)_z)_z \tag{2.3.4a}$$

The function S_Q is usually kept constant.

The term P_s is the production of turbulent kinetic energy by the mean flow, i.e.:

$$P_s = - (\overline{w'u'}\, u_z + \overline{w'v'}\, v_z) \tag{2.3.4b}$$

The term P_b is the gravitational potential energy of the turbulent flow, i.e.:

$$P_b = g\alpha\, \overline{w'\theta'} \tag{2.3.4c}$$

The term $-\varepsilon$ represents dissipation of the turbulent kinetic energy by internal friction. Under the Kolmogorov hypothesis it is dimensionally correct to define:

$$- \varepsilon = q^3/c\ell \tag{2.3.4d}$$

where the constant c must be defined empirically.

2.3.2 The turbulent length scale

There are many ways to define the turbulent length scale. It may be specified empirically from the gross features of the flow

geometry, or it may be predicted from a semi-empirical dynamical differential equation. Using the latter approach, Rotta (1951) derived an equation for the quantity $q^2-\ell$. However, in order to specify the terms in the equation, it is necessary to introduce more parameters than in the case of the Reynolds stresses equations, where many of the terms are determined precisely without recourse to further parameterization. Therefore, the $q^2-\ell$ equation is less convincing than some other model equations and more likely to be substituted by other ℓ-closure schemes.

Vager and Nadezhina (1975) used a differential equation for ℓ obtained by manipulation from the original $q^2-\ell$ equation. The expression is still dependent on many constants that must somehow be determined. The Laykhtman-Zilitinkevich relation, which is basically a further simplification of the ℓ-equation, is widely used in the Soviet literature.

It appears fairly clear that the turbulent length scale cannot exceed some some fraction of the total spread of the turbulent region (represented by the variable, ℓ_o), and that somewhere in the neighborhood of the wall, it should be proportional to the distance from the wall. Therefore there are two fundamental conditions for the quantity ℓ:

$$\ell \sim z \quad \text{as } z \to 0$$

$$\ell \sim \ell_o \text{ as } z \to \infty.$$

From those simple constraints, Mellor and Yamada (1974) used an algebraic expression for ℓ:

$$(2.3.5) \qquad \ell = \frac{\kappa z}{(\kappa z/\ell_o + \ell)}$$

where κ is the Karman constant.

The maximum scale ℓ_o is defined as follows:

$$(2.3.6) \qquad \ell_o = \gamma \int_o^\infty zqdz / \int_o^\infty qdz$$

where γ is an empirical constant.

In this study, the variable ℓ is determined from (2.3.5) and (2.3.6) rather than from the $q^2\ell$ equation which is an intrinsic component of the level 2 1/2 closure scheme.

2.3.3. The functions S_M and S_T.

From the Mellor and Yamada (1982) level 2 closure scheme, it is possible to derive algebraic expressions for the functions S_M and S_T as functions of either flux Richardson number:

$$(2.3.7) \qquad R_f = P_b/P_s$$

or gradient Richardson number:

$$(2.3.8) \qquad R_i = \frac{g\alpha T_z}{(u_z)^2 + (v_z)^2}$$

The level 2 closure scheme differs from the 2 1/2 level as the eddy kinetic energy equation does not contain a time derivative and

the diffusion terms. It is our belief that the model will not be particularly susceptible to variations of the functions S_M and S_T and, following Yamada (1983), we take:

$$(2.3.9a)\quad S_M = \begin{cases} 1.96\,\dfrac{(0.1912 - R_f)(0.2341 - R_f)}{(1 - R_f)\,(0.2231 - R_f)} & R_f < 0.16 \\ 0.085 & R_f > 0.16 \end{cases}$$

$$(2.3.9b)\quad S_T = \begin{cases} S_M\,\dfrac{(0.2231 - Rf)}{(0.2341 - R_f)}1.318 & R_f < 0.16 \\ 0.095 & R_f \geq 0.16 \end{cases}$$

Therefore our closure scheme is intermediate to the Mellor and Yamada levels 2 and 2 1/2 and we propose calling it a level 2.3.

3. THE NUMERICAL MODEL.

Turbulent closure schemes have been intensively applied to study the atmospheric planetary boundary layer, and many numerical models are available for that purpose (Brown, 1970; Mason and Sykes, 1980; Sommeria, 1976; Yamada, 1979, 1982, and 1983). However, there exists a need at present to develop numerical models for the Benthic Boundary Layer to understand the dynamic role which that region has on the oceanic circulation.

Weatherly and Martin (1978) developed a one-dimensional model derived from the level 2 closure scheme of Mellor and Yamada (1974); Richardson (1982a, 1982b, and 1984) presented one-dimensional and two-dimensional models applied to a multi-layered ocean, where the Reynolds stresses are defined from individual transport equations. The aim of all those studies is to investigate how the flow and the stratification above the BBL affects the structure and the thickness of the benthic region. However, to my knowledge, no attempts have been made to analyze how the Benthic Boundary Layer affects the structure of the forcing flow.

The numerical model described in this section is specifically designed to examine the decay of a deep eddy-like flow subjected to bottom friction forces.

3.1 The numerical model equations

Define (u_o, v_o) to be the velocity components representing the migration of the eddy in the ocean; in order to reduce the number of the mesh points and increase the efficiency of the scheme, the model equations are rewritten in a coordinate system $(\tilde{x},\tilde{y},\tilde{z})$ moving with the eddy. This is achieved by applying the transformation:

$$x = \tilde{x} + u_o t$$

(3.1.1) $$y = \tilde{y} + v_o t$$

$$z = \tilde{z}$$

If u_o and v_o are assumed to be constant, in the new coordinate system the model equations are as follows:

(3.1.2a) $$u_t + uu_x + wu_z - f(v + v_o) = - g\eta_x - \frac{1}{\rho_o} p_x + (A_x u_x)_x + (K_M u_z)_z$$

(3.1.2b) $$v_t + uv_x + wv_z + f(u + u_o) = (A_{xy} v_x)_x + (K_M v_z)_z$$

(3.1.2c) $$0 = - p_z - g\rho$$

(3.1.2d) $$u_x + w_z = 0$$

(3.1.2e) $$T_t + uT_x + wT_z = (A_x' T_x)_x + (K_T T_z)_z$$

(3.1.2f) $$1/2(q_t^2 + uq_x^2 + wq_z^2) = 1/2(K_Q(q^2)_z)_z + K_M(u_z^2 + v_z^2) + K_T(- g\alpha T_z) - q^3/c\ell$$

(3.1.2g) $K_M = \nu + S_M \ell q$; $K_T = k + S_T \ell q$; $K_Q = S_Q \ell q$

where tilde has been dropped.

The set of equations (3.1.2) is resolved in the region $0 \leq z \leq h$; $-x_o \leq x \leq x_o$, with the boundary conditions:

(3.1.3) $(u,v,w) = (-u_o, -v_o, 0)$ at $z = 0$
$T_z = q_z = 0$

(3.1.4) $(u,v) = (U_g, V_g)$ at $z = H$
$T_z = 0$

(3.1.5) $q = 0$ at $z = d$

(3.1.6) $(u,v) = (-u_o, -v_o)$
$T = T_B(z)$ at $|x| = x_o$
$q = 0$

The value of the depth d and of the other constants used in the numerical simulations are given in Table 3.1.

Let h be the thickness of the BBL, integration over depth of the continuity equation (2.1.1d) leads to:

(3.1.7a) $$\int_h^H u_x dz = \frac{d\eta}{dt} + w_e$$

(3.1.7b) $$w_e = \frac{dh}{dt} + w(x,h(x))$$

Equations (3.1.7) imply that the spin-down process acts primarily on the depth averaged components of the motion. Thus it is convenient to rewrite the functions u,v, and T as:

$$u = u' + U_g$$

$$v = v' + V_g \qquad (3.1.8)$$

$$T = T' + T_g$$

where $(\ )_g$ represents the barotropic component of the motion associated with thermocline displacement.

With the decomposition (3.1.8) it is possible to introduce two different time scales intrinsic to the physical nature of the problem: the larger time scale (hereafter, expressed by the variable, τ) that controls the decay of the flow, and the smaller time scale (hereafter, expressed by the variable, t) that controls the deviations of the fields from their barotropic components (which can be regarded as constant with respect to this time scale). (See Section 5.1.1 for a complete dimensional analysis of the equations 2.1.1). If we assume that advection, diffusion, and thermal wind effect respond to the smaller time scale, we derive the following equations for the barotropic motion:

$$U_{g_\tau} - fV_g = - g\eta_x \qquad (3.1.9a)$$

$$V_{g_\tau} + fU_g = 0 \qquad (3.1.9b)$$

(3.1.9c) $$T_{g\tau} = 0$$

(3.1.9d) $$U_{gx} + \frac{1}{H-h} w_e = 0$$

Equation (3.1.9d) has been written under the rigid lid approximation. The term $w_e/(H-h)$ of (3.1.9d) is defined from average value over the period $\Delta\tau$. Furthermore, in resolving equations (3.1.9) it is necessary also to define the thickness of the BBL. In general, the thickness of the BBL is defined as the height at which the flow is parallel to the forcing flow but slightly greater in magnitude, or as the height at which the turbulent kinetic energy is reduced by a factor of 99% with respect to its value at the surface. Since the model includes advective terms and the thermal wind effect which affects the vertical profile of the velocity distribution, we prefer to relate the BBL thickness to the turbulent kinetic energy.

No special treatment is required in the integration of the equations (3.1.9). Therefore we focus our attention on the resolution of the system (3.1.2).

3.2. The grid system.

The equations (3.2.1) are solved using a grid of spatially staggered variables, chosen so that application of the boundary conditions is made easier. Since the vertical structure of the turbulent eddies is

small near the bottom and increases upwards, a vertical grid equally spaced in a log-plus-linear vertical coordinate is often used. This varies approximately logarithmically at the bottom and linearly at the higher levels; i.e.

$$Z = c_1 z + c_2 \ln(z/z_o)$$

where Z is the transformed coordinate, z_o the roughness parameter, c_1 and c_2 constants (Yamada,1978). Because our study is not particularly focused in the lower levels of the BBL, but in the region of transition between the boundary layer and the interior flow, we prefer to introduce a variable vertical grid, where the distance between two levels is function of height.

3.3. The treatment of the equations.

The numerical scheme chosen in the treatment of the equations (3.1.2) is based on the centered difference method. Since the system uses a variable vertical resolution, the value of any given function ϕ at any mesh point between two consecutive ϕ-levels (not necessarly the middle point) is computed by linear interpolation.

All the terms are leapfrogged in time except for horizontal and vertical diffusion and for the term, $-\varepsilon$, of equation (2.3.4d), that are treated using the Dufort-Frankel, The Crank-Nicholson, and a semi-implicit scheme, respectively. This scheme is affected only by the CFL stability condition applied to the advective terms:

$$(3.3.1) \qquad \frac{W\Delta t}{(\Delta z)_{min}} << 1$$

where W is the scale of the vertical velocity and $(\Delta z)_{min}$ the smallest distance between two consecutive levels.

With the Crank-Nicholson scheme, the equations containing vertical diffusion are reduced to a system of linear algebraic equations for the variables at time step (n+1) and horizontal location j, where all the variables at the time steps n and (n-1) are known. Because of its tridiagonal nature, matrix solutions can be efficiently obtained by a special form of the Gaussian Elimination Method (Carnaham et al., 1969).

Unfortunately, the Crank-Nicholson scheme requires that the vertical eddy coefficients be computed at time step (n+1). This constraint complicates the solution of the q^2-equation. A reasonable approximation is to compute the eddy coefficient K_Q of (3.1.2f) at time step n. However, once q is known at time step (n+1), the eddy coefficients K_M and K_T can be defined at the new time step, and the Crank-Nicholson scheme is applied naturally in the resolution of the momentum and heat conservation equations.

Following Yamada (1978), the horizontal eddy coefficients are defined as follows:

$$(3.3.2) \qquad A_x = A_x' = A_{xy} = 2a(\Delta x)^2|u_x| + \nu$$

where a is a constant of proportionality.

The numerical procedure described above is computationally very efficient; the time step is suitable for long term simulations and computer storage is limited. We retain the variables for two consecutive time steps except for the eddy coefficients K_M and K_T, which must be saved for three time steps. Furthermore, no artificial conditions are required during the numerical experiments except in the definition of q when the q^2-equation presents negative values of the turbulent kinetic energy. In this case, dissipation exceeds production of the same energy, and the variable q is set equal to zero.

Unfortunately, if numerical computations are performed for an extended period of time (greater than 8-9 months), it is necessary to correct the scheme to prevent nonlinear instability. It is well known that the use of the leapfrog scheme in the treatment of the advective terms induces a distortion in the values of speed and group velocities. The computational error affects the short waves: the smallest waves resolved by the scheme (wave-length $2\Delta x$) have zero computational speed velocity and their energy is propagated in the opposite direction to the correct group velocity (Grotjahn and O'Brien, 1976). In order to control computational inaccuracy, numerical schemes are usually developed that include such additional frictional terms such as harmonic or biharmonic terms (Richards, 1984) or smoothing procedures (Yamada, 1978). However, the

corrections might alter the physics of the problem, reducing the contribution of advection in favor of a merely dissipative regime.

In our case, we must modify the numerical scheme to prevent the consequences of the nonlinear instability essentially at the center of the eddy where the short waves induce a horizontal convergence or divergence of energy contrary to the physics of the problem. Thus in order to improve the accuracy of the leapfrog scheme, horizontal advective terms and the continuity equation are resolved by a centered fourth-order space differencing (Grotjahn and O'Brien, 1976) and the horizontal eddy viscosity coefficients are specified as follows:

$$A_x = A_x' = \nu_H + 10a(\Delta x)^2|u_x|$$
$$A_{xy} = 10A_x \qquad (3.3.3)$$

where ν_H is a computational horizontal eddy viscosity coefficient.

Although the choice of the horizontal eddy coefficients has been suggested merely by computational arguments, equations (3.3.3) may be partially justified as follows. According to Ragallo and Monin (1984), for three-dimensional numerical models, the horizontal eddy coefficients may be computed from:

$$A_x = A_x' = 2a\Delta x\Delta y(u_x^2 + v_y^2)^{1/2}$$
$$A_{xy} = 2a\Delta x\Delta y(u_x^2 + v_y^2)^{1/2} \qquad (3.3.4)$$

Furthermore, a two-dimensional formulation of the model equations (3.1.2) implicitly contains the assumptions:

$$\begin{aligned} & L_x \ll L_y \\ & U \ll V \end{aligned} \tag{3.3.5}$$

where L_x and L_y are the dimensional length scales of x- and y-directions, respectively, and U and V the dimensional scales of the x- and y-components of the geostrophic motion respectively. Thus with the constraints (3.3.5), equation (3.3.4) can be reduced to (3.3.3).

3.4 The treatment of the boundary conditions

At the lower boundary it is assumed that the velocity varies logarithmically with height above the bottom :

$$|\underline{u}(z)| = \frac{1}{\kappa} u_* \, \ell n(z/z_o) \tag{3.4.1}$$

where u_* is the friction velocity and κ is the Karman's constant (Bowden, 1978). Measurements made close to the oceanic floor indicate that the relation is certainly applicable in the region just above the surface (Wimbush and Munk, 1971; Kundu, 1976; Weatherly, 1977). Thus our model considers the lower boundary not at the effective rigid wall but at a height z_1 where the logarithmic profile is still valid. Therefore, in order to apply the new boundary condition we must specify the friction velocity u_* and the direction of the flow at the level z_1.

Consistent with the level 2 1/2 closure scheme and observations, the friction velocity is computed from the turbulent eddy kinetic energy at the lowest grid point:

$$u* = q/(B)^{1/3} \tag{3.4.2}$$

where B is constant.

The direction of the flow at the lowest grid points is specified equal to the direction of the flow at the second level, henceforth represented by the angle α. The assumption is justified by observations and experiments that indicate that the Ekman veering is about constant in the lowest levels of the BBL (Kundu, 1976).

A new problem now arises because of the chosen coordinate system. We assume that the logarithmic layer is moving with the eddy as unity and the boundary conditions (3.1.3) are changed into:

$$u = -u_o + \frac{1}{\kappa} u* \cos(\alpha) \ell n(z_1/z_o)$$

$$v = -v_o + \frac{1}{\kappa} u* \sin(\alpha) \ell n(z_1/z_o) \qquad \text{at } z = z_1 \tag{3.4.3}$$

$$T_z = q_z = 0$$

At the lateral boundaries the ocean is assumed to be at rest. However, the eddy induces a recirculation in its closest neighborhood which must supply (absorb) the mass of water pumped in (out) the BBL. Thus in order to preserve the number of mesh points without closing

the recirculation inside the domain, the boundary conditions (3.1.6) are modified by requiring that both the u-velocity and the temperature distribution be horizontally uniform.

3.5 The initial conditions

In the following discussion, let the superscript o indicate the initial values of the relative variables, assigned for two consecutive time steps. The thickness h^o of the BBL is taken to be:

$$h^o = 0.4\, u_*^o/f \tag{3.5.1}$$

where the friction velocity u_*^o is computed as:

$$u_*^o = 0.03((U_g^o + u_o)^2 + (V_g^o + v_o)^2)^{1/2} \tag{3.5.2}$$

(Weatherly and Martin, 1978).

Above the BBL the functions u^o, v^o, and T^o are specified and q^o is kept equal to zero. At the lowest grid points the initial value q^o is computed from (3.4.2) and the velocity components from (3.4.3), specifying a ten degree Ekman veering. After the functions u, v, and q are defined at the lowest levels, they are matched with their relative values above the BBL by linear interpolation.

The initial temperature profile considers a bottom layer neutrally stratified, assuming a complete mixing of the temperature distribution. Although the initial mixed layer and BBL are identical, it is advisable to underestimate their thickness so as not to

alter the final temperature profile. If the initial mixed layer is too thick, no physical process can reestablish stratification inside it.

The vertical eddy coefficients are computed from the initial distribution of the turbulent kinetic energy, with the functions S_M and S_T given for neutrally stratified flows.

The scheme results not particularly sensitive to the adjustment process from the previous initial conditions. In general, the steady state configuration is reached after about three or four days, the period necessary to mix the upper strata of the BBL.

3.6 The choice of the time steps

Numerical tests indicate that if a coarse near-bottom vertical resolution is used, the logarithmic layer does not instantaneously respond to the variations of the flow at the upper points. Thus to preserve the computational efficiency of the scheme, it is necessary to apply equations (3.4.3) with the variable q of (3.4.2) and values of the angle α averaged values over a period ΔT_f.

Therefore the numerical procedure illustrated in the previous sections depends upon which of the following parameters is chosen:

- Δt the time step used for the resolution of the equations (3.1.2).
- $\Delta \tau$ the time step used for the correction of the barotropic flow.

- ΔT_f the average period used for the adjustment of the velocity field at the lower grid points.
- Δs the shift between the time steps $\Delta\tau$ and ΔT_f.

It appears natural to consider the time steps $\Delta\tau$, ΔT_f, and Δs multiples of Δt and to choose $\Delta\tau$ as a multiple of ΔT_f to avoid the shift Δs being a function of time.

First, let us consider the parameter ΔT_f. Since turbulent flows respond to inertial oscillations (D'Asaro, 1980), the natural choice is ΔT_f = 12 hours.

With respect to the parameter $\Delta\tau$, we must choose a time step short enough to avoid the flow reaching a steady state at each correction (we do not want to start repeatedly from initial conditions), but long enough to allow the BBL to adjust itself to the new state. Numerical simulations indicate that the evolution of the flow above the BBL is not sensitive to the choice of $\Delta\tau$; however, for large time steps a noise of frequency $1/(2\Delta\tau)$ can appear in the BBL thickness configuration. The phenomenon, known as $2\Delta x$-instability (Lilly, 1965; Phillips, 1959), is a consequence of the fact that the BBL time variations are modulated on two different time scales: the inertial period associated with the BBL time scale and the much larger time scale that controls the variations of the forcing flow. Thus if $\Delta\tau$ is too large, the scheme cannot adequately resolve the inertial oscillations that are incorrectly interpreted as frequencies

of order $1/(2\Delta\tau)$. To filter the high frequency noise as much as possible , numerical experiments suggest a period $\Delta\tau$ = 48 hours.

In order to define the parameters Δs, we have essentially considered the cases Δs = 0 and Δs = 6 hours. Numerical tests indicate that inside the BBL, for any given interval $\Delta\tau$, the flow might present different instantaneous configurations, but averaged values over the period ΔT_f and the evolution of the flow above the layer do not present substantial differences. Thus we conclude that the scheme is not affected by the shift Δs.

Table 3.1: Values of constants used in the numerical experiments.

Symbol	Value	Remark
α	$2\times10^{-4}(C^{o})^{-1}$	Thermal expansion coefficient.
ν	$1cm^4s^{-1}$	Vertical viscosity coefficient.
ν_H	$10^5cm^2s^{-1}$	Computational eddy coefficient.
k	$0.1cm^2s^{-1}$	Vertical conductivity coefficient.
T_o	$2\ C^{o}$	Reference temperature.
ρ_o	$1\ gmcm^{-3}$	Reference density.
f	$10^{-4}s^{-1}$	Coriolis paramater.
g	$981cm^2s^{-1}$	Gravitational acceleration.
R	10^7cm	Radius of the eddy.
x_o	1.75×10^7cm	Domain extent.
H	4×10^5cm	Total depth of the eddy.
d	1.3×10^4cm	Level of maximum possible penetration for turbulence.
Δx	1.25×10^6cm	Horizontal grid size.
$(\Delta z)_m$	100cm	Minimum vertical grid size.
$(\Delta z)_M$	2×10^4cm	Maximum vertical grid size.
Δt	1hour	Time step.
$\Delta\tau$	48 hours	Time step for the barotropic components.
ΔT_f	12 hours	See Section 3.4.
Δs	0	See Section 3.4.

z_1	25cm	See Section 3.4.
S_Q	0.2	See equation (2.3.6a)
c	15.	See equation (2.3.6d)
γ	0.20	See equation (2.3.8)
a	0.01	See equation (3.3.2).
B	16.6	See equation (3.4.2).
κ	0.4	Karman's constant.

4. PRELIMINARY ANALYSIS OF THE MODEL: STRUCTURE AND DYNAMICS OF THE BENTHIC BOUNDARY LAYER.

The aims of this section are to study the structure of the Benthic Boundary Layer forced by a mesoscale activity and to investigate how the Benthic Boundary Layer might affect the dynamics of the forcing flow. For the present, we assume that dissipation by bottom friction does not affect the barotropic component of the motion, so that the the thermocline displacement is kept constant with time.

As we have already discussed, the numerical model described in the previous sections has been developed with particular attention to its applicability to long term simulations. Storage and computer time are reduced by the use of an unequally spaced vertical resolution and of the logarithmic law at the lowest levels. Although for an accurate analysis of the Benthic Boundary Layer structure the model should be applied with very fine mesh point, we prefer to present results obtained with a coarse grid (the minimum vertical increment is 1m), and discuss how computational efficiency affects the accuracy of the solutions.

4.1. Horizontally homogeneous flow.

Although the present case is irrelevant in the dynamics of mesoscale motions, it makes it possible to analyze the structure of

the Benthic Boundary Layer as a function of various velocities and to test the accuracy of the scheme by comparing the numerical results with predictions derived by previous works on turbulence.

Working on the hypothesis of horizontally homogeneous flows, most of the studies have related turbulent quantities such as the BBL thickness, friction velocity, and Ekman veering to the forcing flow. It can be showed that the friction velocity and the Ekman veering satisfy the relations:

$$(4.1.1.) \qquad u* = \sqrt{C_D}\,(U_g^2 + V_g^2)^{1/2}$$

$$(4.1.2.) \qquad \sin\alpha = b_D \sqrt{C_D}$$

where $u*$ is the friction velocity, U_g and V_g are the velocity components of the forcing flow, α is the magnitude of the Ekman veering at the surface, C_D the drag coefficient, and b_D a constant of proportionality (Csanady, 1967; Blackadar and Tennekes, 1968; Monin and Yoglom, 1971; Tennekes and Lumley, 1972). It is usually considered that the drag coefficient is a monotonic decreasing function of the surface Rossby number $Ro = |\underline{U}_g|/fz_o$, such that for a representative oceanic range $10^6 < R_o < 10^7$, $0.03 < \sqrt{C_D} < 0.04$ (Deardoff, 1970; Weatherly, 1972). Yamada (1975) suggested a value $b_D = 7.55$ for flows with small velocities and weak stratification, such as those considered in our experiments.

More intriguing is the definition of the BBL thickeness. Several authors have defined the BBL thickness as the height, h_E, at which the flow is parallel to the forcing flow but slightly greater in magnitude (Wimbush & Munk,1970; Kundu,1976; Caldwell,1976). The same and other authors predicted the thickness of the BBL as the height $h*$ such as:

(4.1.3) $$h* = .4\ u*/f$$

(Weatherly, 1972; Richards, 1984). A physically more realistic definition is to consider the height, h_q, at which the BBL-generated turbulence goes to zero (Weatherly & Martin,1978). Finally, Richards (1982a) has related the BBL thickness to the temperature profile and defined the BBL thickness as the height, h_T, at which the temperature gradient is maximum. This definition is the least convincing because it identifies the BBL with the mixed layer. As we will discuss later, this relation creates some ambiguities and imprecisions.

In the following sections, we present the values of turbulent quantities for neutrally and stably stratified flows. All the numerical simulations have been made for forcing flow within the range of the deep ocean values. However, values have been restricted to those greater than $0.03ms^{-1}$ because the coarse grid does not allow a correct application of the logarithmic law for smaller velocities.

4.1.1. Neutrally stratified flow.

The results of the case are depicted in Fig. 4.1., 4.2, and 4.3. The values of the friction velocity were determined by considering the values of the turbulent kinetic energy at the lowest levels as in equation (3.4.2) or by evaluating the bottom stresses, i.e.:

$$\rho u_*^2 = ((\tau^x)^2 + (\tau^y)^2)^{1/2} \tag{4.1.4a}$$

where

$$\tau^x = f\int_{z_o}^{H} (v-V_g)dz$$

$$\tau^y = -f\int_{z_o}^{H} (u-U_g)dz \tag{4.1.4b}$$

Obviously, the magnitude of the drag coefficient computed from equation (4.1.4a) is in a better agreement with observations and predictions, but in neither case are the drag coefficient or the Ekman veering a decreasing function of the forcing flow. However, the range of velocities used in our experiments is too narrow for presenting marked evidence of monotony.

The ambiguity in defining the depth of the BBL is clearly illustrated by the numerical simulations. The defintion (4.1.2) leads to the thinner BBL, but the function, h_*, is definitely correlated with the variable h_E. The best fit between h_* and h_E is obtained for $h_* \simeq 0.65u_*/f$. On the other hand, relating the BBL thickness to

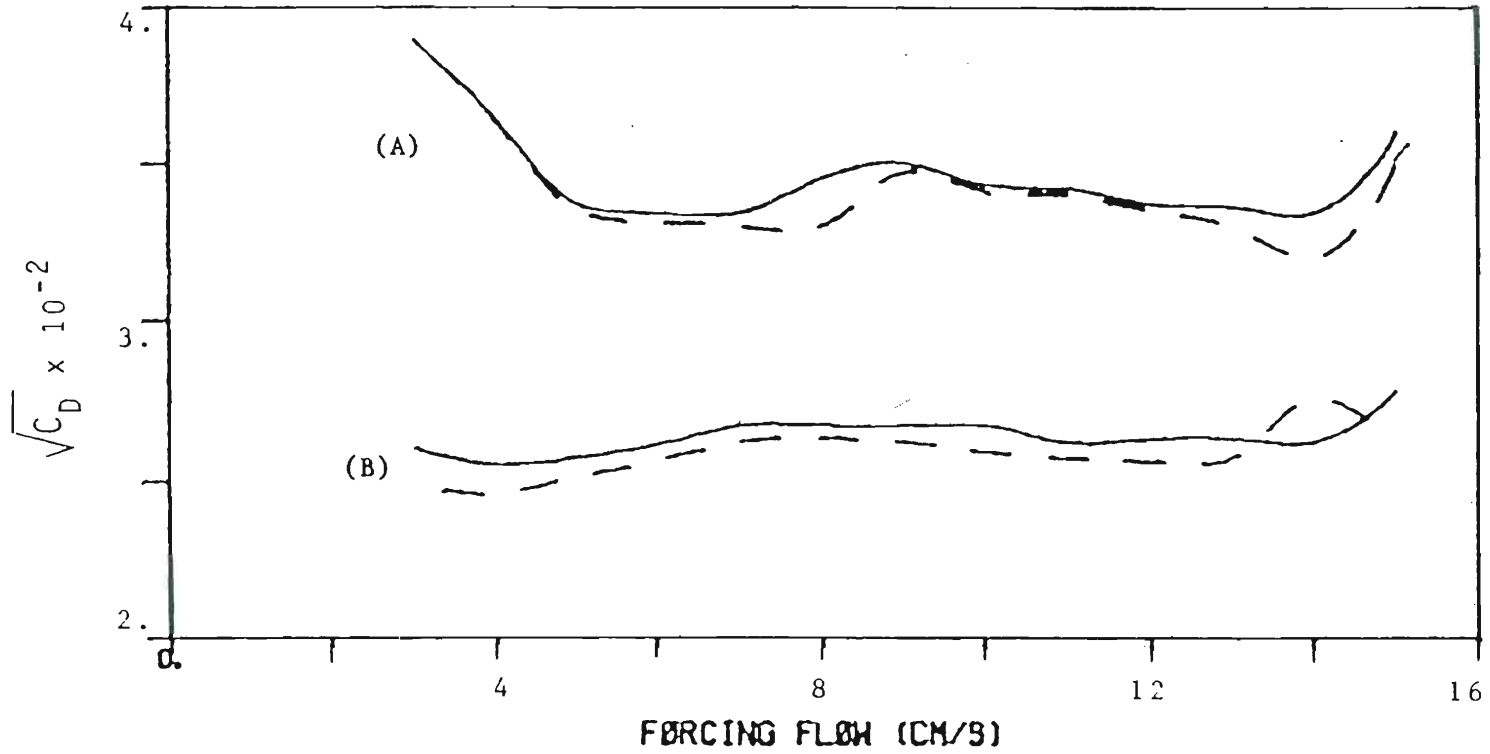

Figure 4.1. The square root of the drag coefficient as function of the forcing flow computed for neutrally stratified flows (dashed lines) and stably stratified flows (solid lines). A calculates tge friction velocity from equation (4.1.1); B calculates the friction velocity from the turbulent kinetic energy at the lowest grid points.

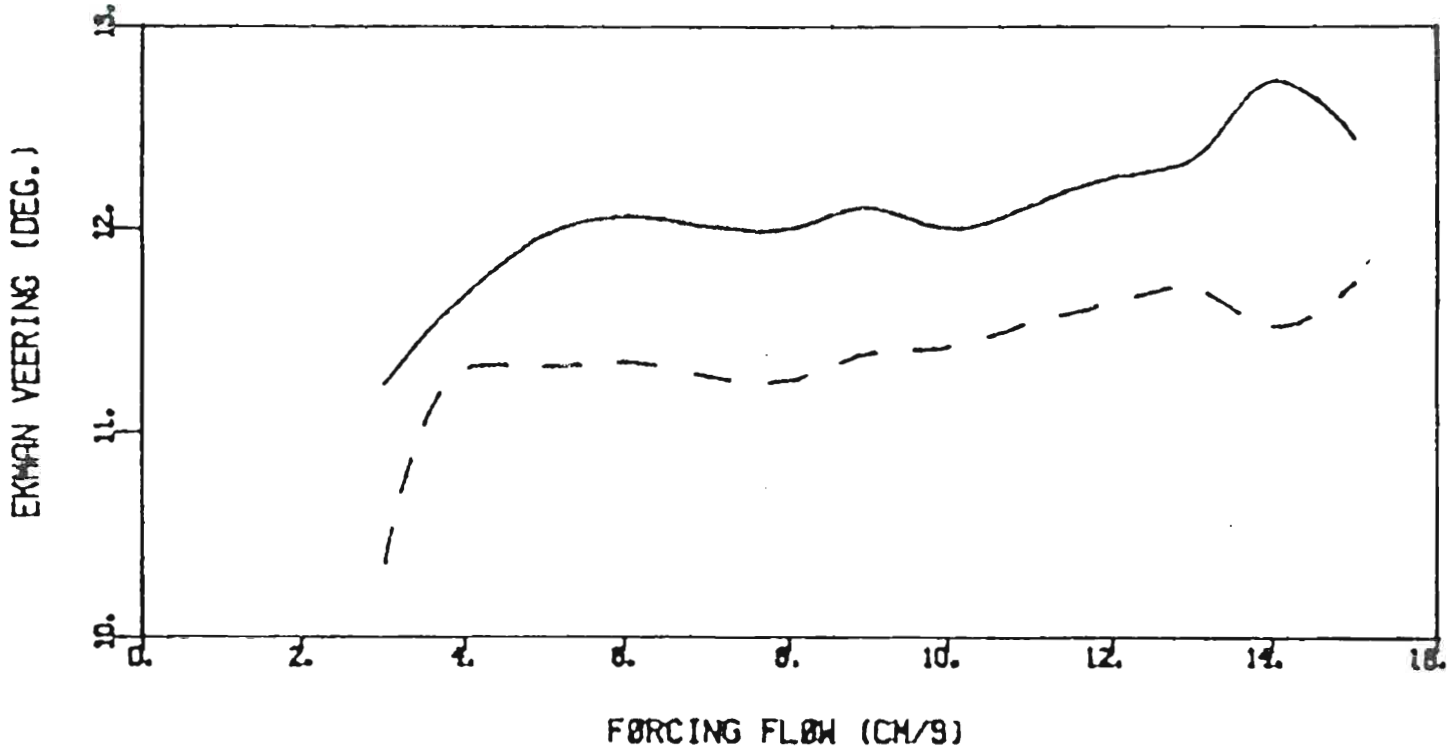

Figure 4.2. The Ekman veering computed as a function of the forcing flow. Neutrally stratified flows (dashed line); stably stratified flows (solid line).

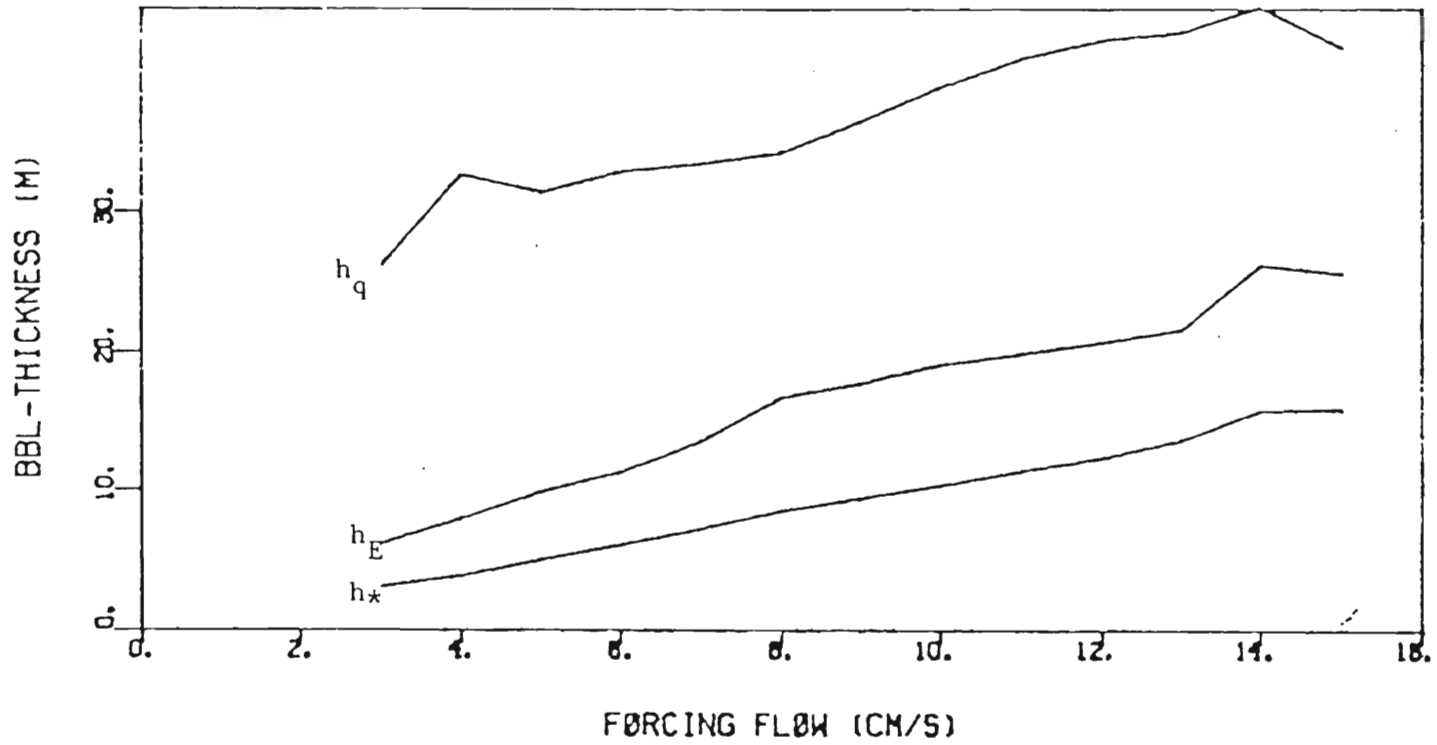

Figure 4.3. The BBL thickness as a function of the neutrally stratified forcing flows.

the turbulent kinetic energy gives the largest value: turbulence not inhibited by the buoyancy forces propagates upwards where the last residuals of the Ekman spiral can be still found.

4.1.2. Stably stratified flow.

All the results presented in the following section consider a Brunt-Vaiasala frequency $N=7.6\times10^{-4}s^{-1}$.

Both Ekman veering and drag coefficient have the same distortion found for neutrally stratified flow (Fig. 4.1, and 4.2), but the ambiguity between the functions $h*$, h_E, and h_q is highly reduced (Fig. 4.4). However, the numerical simulations confirm that the mixed layer and the BBL cannot be identified with one another. The mixed layer is much thicker than BBL and is a measure of the level at which the Ekman spiral vanishes. In the upper strata of the mixed layer the work done against the buoyancy forces balances the input of turbulent kinetic energy by the shear of the mean flow, and no turbulent activity can be maintained at those heights.

For the completeness of our analysis, the vertical profiles of the mean flow, temperature distribution, turbulent kinetic energy, and momentum vertical eddy viscosity coefficient are depicted in Fig. 4.5. Since those quantities exhibit similar patterns for neutrally stratified flows (except for the level of zero turbulence), we do not present the relative profiles.

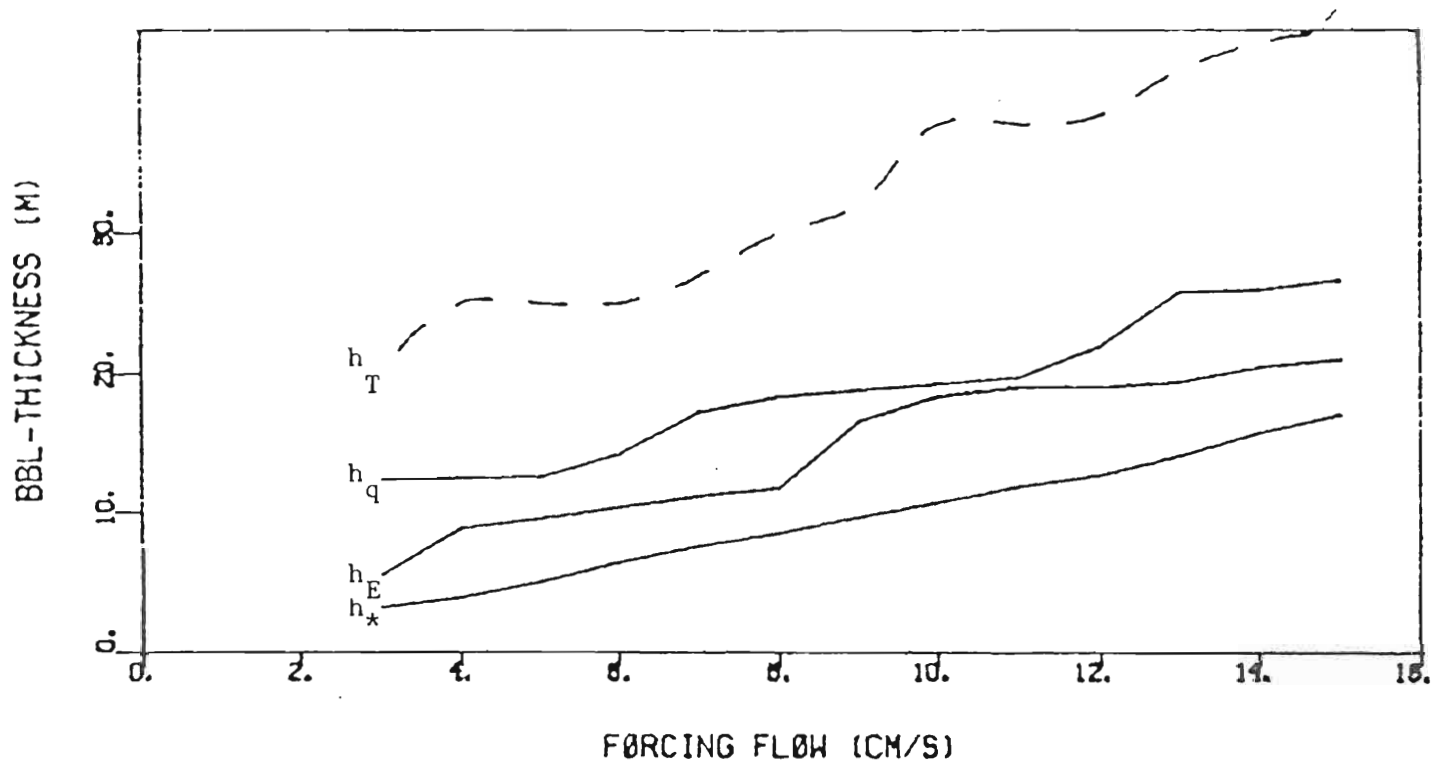

Figure 4.4. The BBL thickness as a function of stably stratified forcing flows.

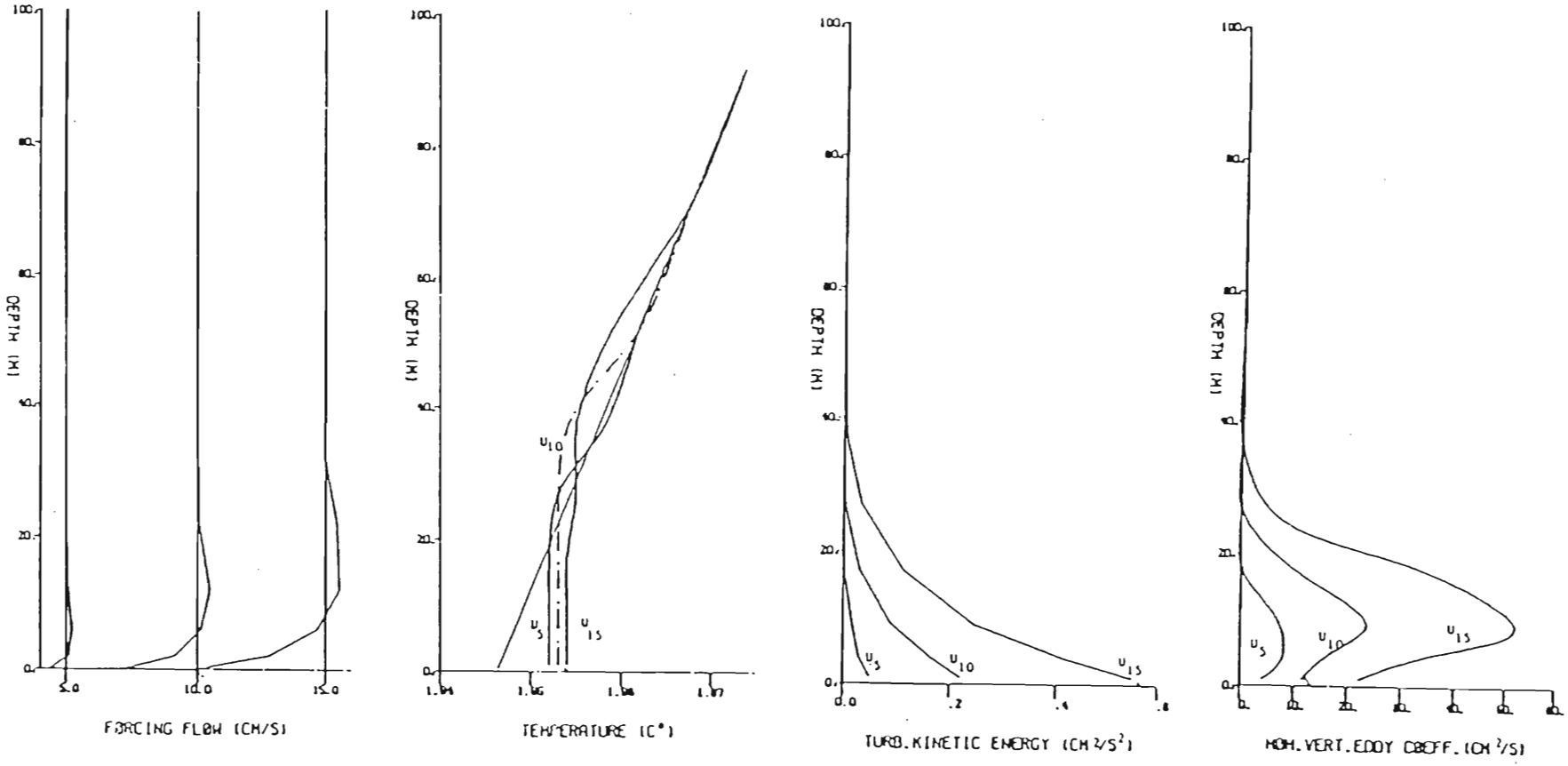

Figure 4.5. Profiles of velocity (a), temperature (b), turbulent kinetic energy (c),and momentum vertical eddy coefficient (d) computed for stably stratified flow of speed 0.05, 0.1, and 0.15ms^{-1}, respectively. The abscissa represents the height above the bottom. It is expressed in m.

4.1.3. Discussion.

We now briefly compare the results relative to neutrally and stably stratified flow. Both Ekman veering and drag coefficient are slightly greater when the flow is stably stratified, but the level of zero turbulence is much lower. Those results confirm a well known statement that stratification affects the depth of the BBL at a rate much greater than that of the level of turbulent activity inside the layer (Weatherly and Martin,1978). Furthermore, since Ekman veering is a measure of the bottom friction forces acting on the flow, an increment of turbulence (u*) must correspond to an analogous increment of Ekman veering.

Our numerical results are consistent with most of the theories and models of turbulence. However, the vertical coarse mesh point sensibly affects the values of Ekman veering and friction velocity. A finer vertical resolution increases those values, but does not particularly change the value of the bottom stress.

In order to verify that those inaccuracies are due to the coarse resolution rather than to a mistake in the scheme (viz, the boundary conditions), we compute the Ekman veering from equation (4.1.2) with the drag coefficient evaluated from u* specified as in equation (3.4.2) or (4.1.4), and we compare those results with the values predicted by Deardoff (1970). As Fig. 4.6 indicates, there are no substantial differences between the values given by the numerical experiments and the Ekman veering as computed from the

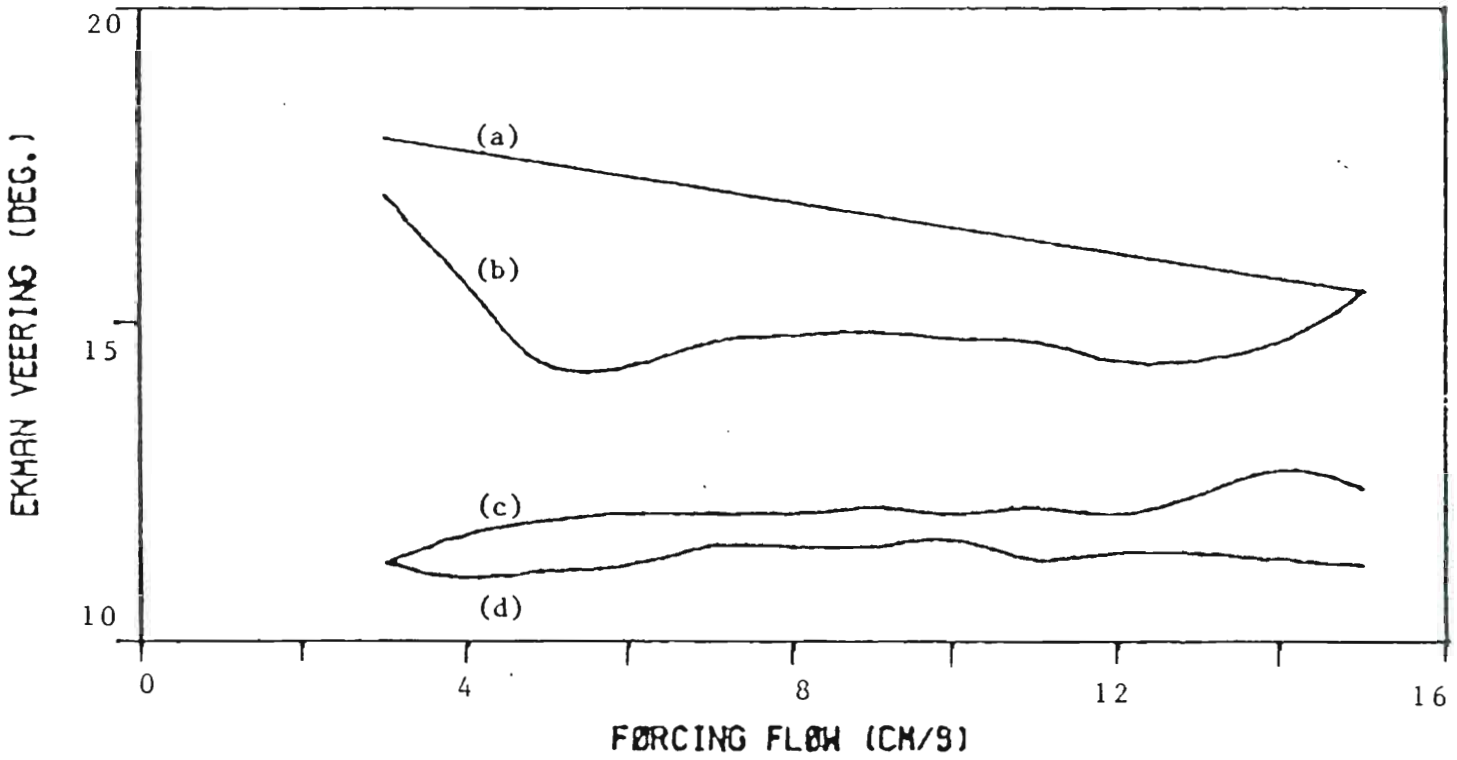

Figure 4.6. The Ekman veering as function of the forcing flow computed from: (a) Deardoff's study; (b) sin α=7.55 $\sqrt{C_D}$ and u_* from bottom stress; (c) numerical experiments; (d) sin α=7.55 $\sqrt{C_D}$ and u_* from the turbulent kinetic energy at the lowest points.

kinetic energy at the lowest level (i.e., a coarse resolution affects turbulent kinetic energy and Ekman veering equally). On the other hand, the best fit between results and Deardoff's predictions is obtained by computing the friction velocity from equation (4.1.4) (i.e., a coarse resolution does not influence the value of the bottom stress).

All things considered, we conclude that the inaccuracies of the scheme do not alter the dynamics of the motion, and the small distortions due to coarse mesh point are compensated for by the computational efficiency of the model.

4.2. The interaction between the Benthic Boundary Layer and mesoscale motions.

In this section we wish to show that the interactions between the Benthic Boundary Layer and a mesoscale eddy-like flow are a consequence of the constraint imposed on the motion by the quasi-geostrophic approximation. Such an assumption requires that the vorticity changes be geostrophic and the temperature changes be hydrostatic (Pedlosky, 1979). The adiabatic temperature variations due to rising (sinking) of water parcels must also keep the vorticity changes geostrophic, and the vertical motion keep the temperature variations hydrostatic (Holton,1979). Since both adiabatic temperature variations and vertical velocity are proportional to the

Rossby number, only the magnitude of those general features of the quasi-geostrophic model are basically affected, if the motion is fully nonlinear.

In view of those observations, we focus our attention to the structure of the Benthic Boundary Layer associated with cyclonic (cold), and anticyclonic (warm) eddies.

There is an old question whether or not the point of maximum velocity of mesoscale flow is close to the edge. The paucity of observations for deep motions makes it impossible to resolve the controversy. Therefore, in order to define the stucture of the motion, we refer to observations made for Gulf Stream rings, which indicate that the point of maximum velocity is more likely to be located at about 2/3 of the radius (Olson, 1980; Joyce, 1984). Therefore, the numerical experiments are performed for deep eddy-like flows of total depth H=4000m, total extension R=150km, and a linear velocity distribution of maximum $U_M = 0.15ms^{-1}$ at 100km from the center. The initial temperature distribution far from the bottom is horizontally homogeneous and stably stratified with a Brunt-Vaiasala frequency $N=7.6x10^{-4}s^{-1}$.

4.2.1. Cyclonic flow.

In order to understand the evolution of the temperature distribution as depicted in Fig. 4.7, we recall that inside a cyclonic

Figure 4.7. The evolution of the temperature distribution relative to the coldest bottom water for a cyclonic (cold) mesoscale eddy-like flow. The ordinate represents the radius of the eddy and is expressed in km; the abscissa represents the height above the bottom and is given in m. Temperature is scaled by 10^4.

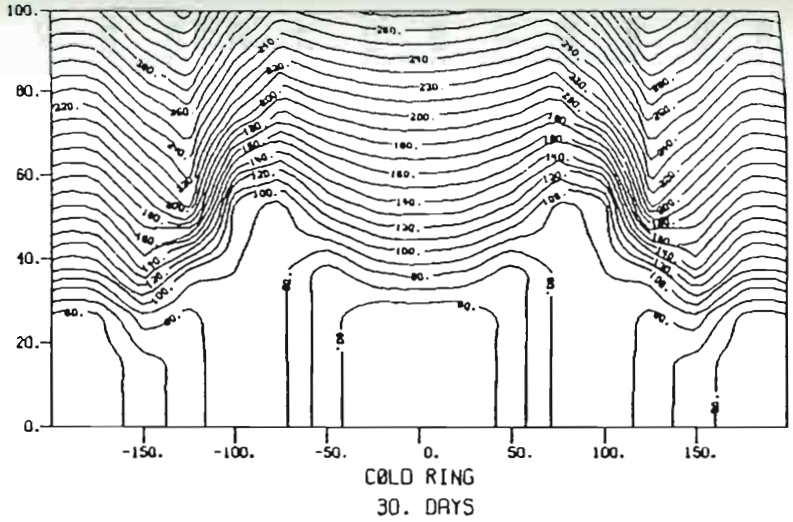

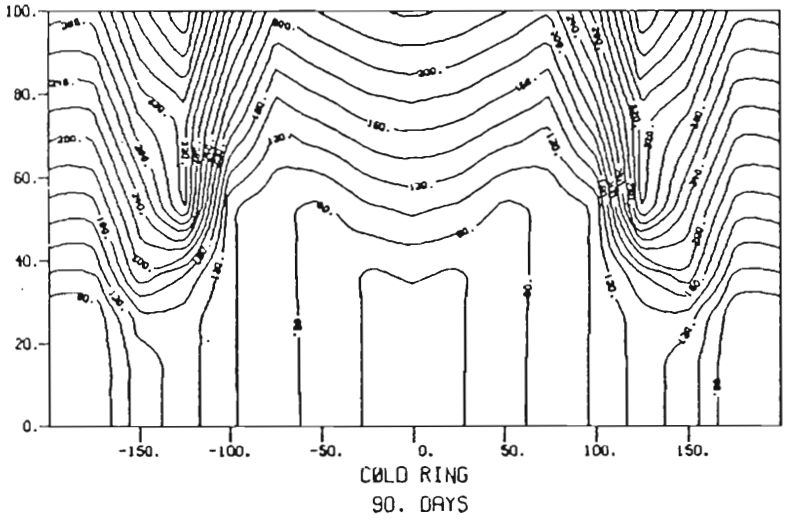

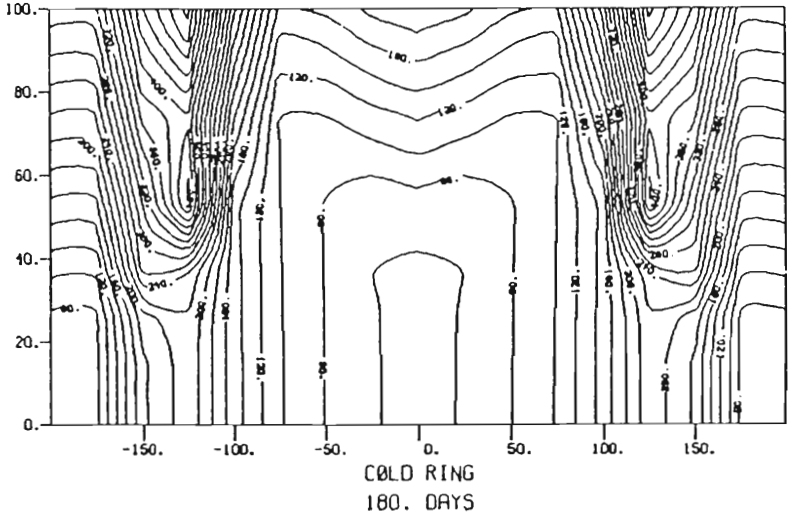

eddy the Ekman velocity associated with the bottom friction forces has the form of an upwelling. Recirculation implies that there must be a downwelling at the edge, which pumps warm water in the lowest levels, removing the original cold bottom water. Conservation of mass requires that the environment supply water to the BBL beneath the eddy. As this water is injected in the BBL, it is advected upwards and mixed by turbulence. Thus the thickness of the mixed layer increases and the isotherms of the interior temperature distribution are lifted upwards. Once the original cold water is removed from the bottom, warm water is supplied to the Benthic Boundary Layer at the edge of the vortex, the temperature of the mixed layer increases, and the sharp interface between the mixed layer and the interior is slowly eroded.

As the thickness of the mixed layer increases, the BBL is imbedded in a neutrally stratified layer, and the level of zero turbulence increases as described in Section 4.1.1. and depicted in Fig.4.8.

4.2.2. Anticyclonic flow.

With respect to cyclonic flows, the distribution of the vertical velocity is reversed. There is a downwelling inside the vortex and an upwelling at the edge. However, the physical mechanisms associated with the vertical velocity are identical to those described in the previous section.

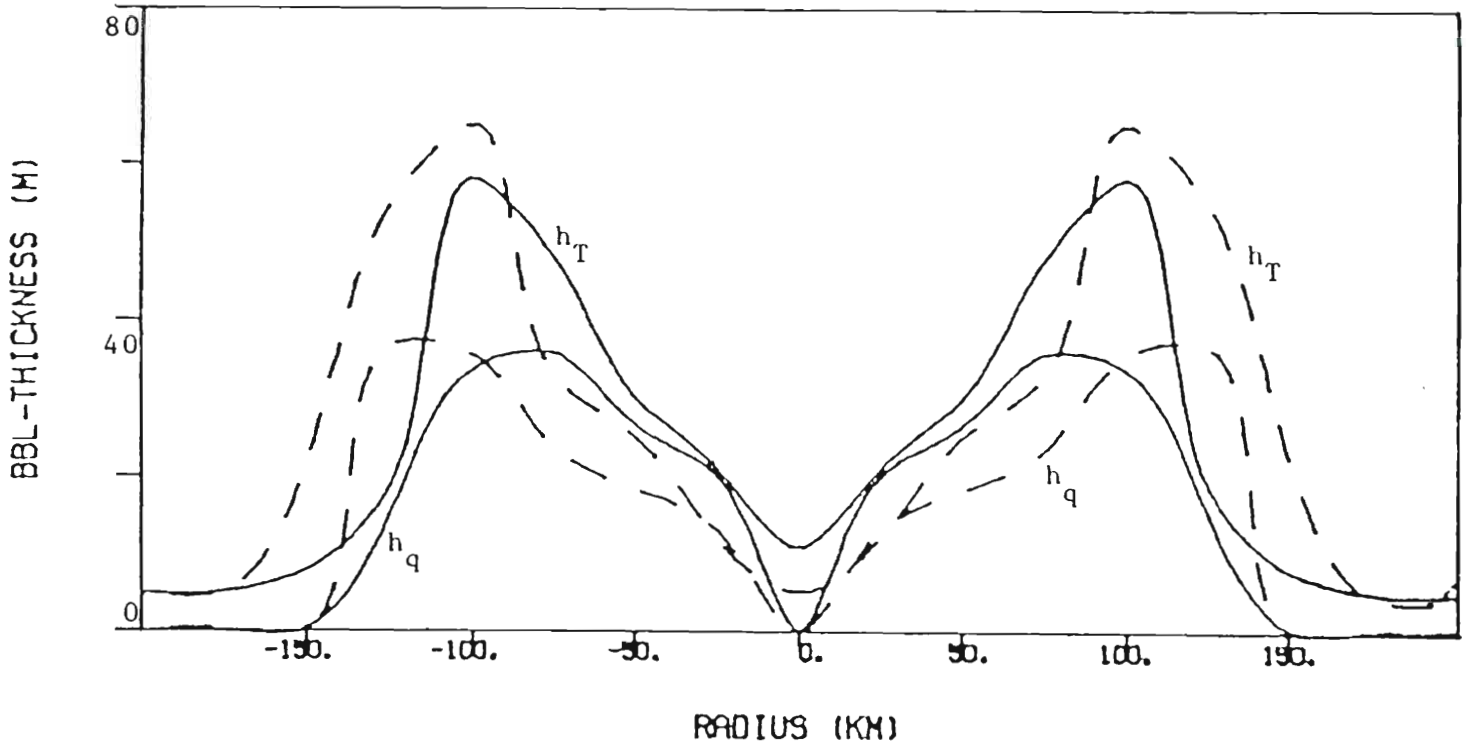

Figure 4.8. The horizontal profile of the mixed layer and BBL thicknesses computed for cyclonic (solid line) and anticyclonic (dashed line) flows at time t=90 days.

Figure 4.9. The evolution of the temperature distribution relative to the coldest bottom water close to the bottom for an anticyclonic (warm) mesoscale eddy-like flow. Same as in Fig. 4.7.

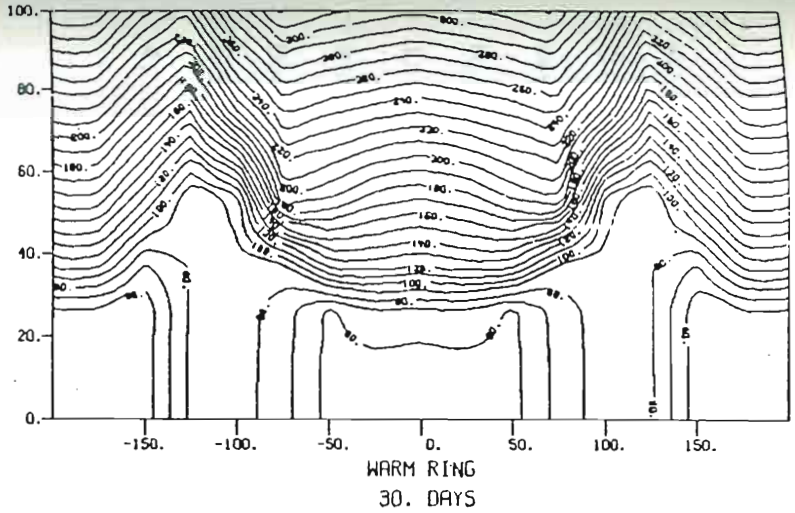

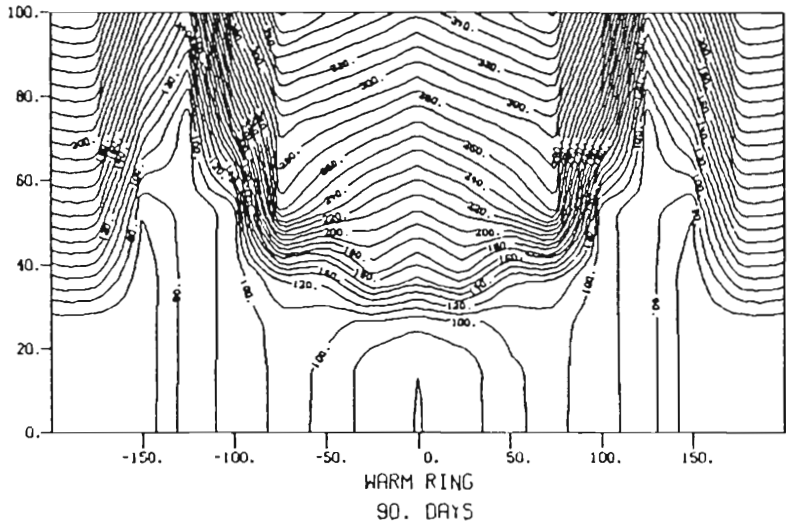

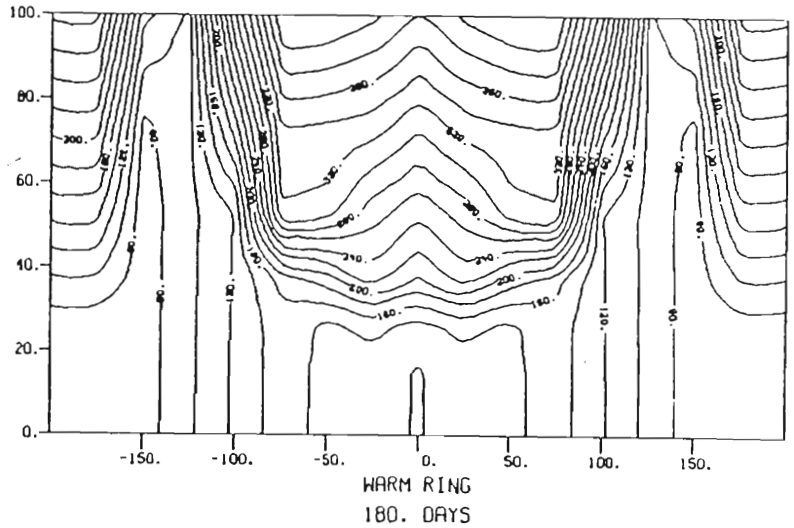

Downwelling inside the eddy has the tendency to remove cold water from the bottom and reduce the thickness of the mixed layer. Turbulence inside the layer, which is primarily determined by the magnitude of the forcing flow, does not allow complete erosion of the mixed layer. Thus as warm water is continuously pumped downwards from the upper levels of the eddy, the interface between mixed layer and interior becomes sharper and sharper, and the bottom layer is heated only by the heat flux across the interface (Fig. 4.9).

4.2.3. Discussion.

The features illustrated in the previous sections indicate that the structure of the Benthic Boundary Layer is quite different for cyclonic and anticyclonic flows.

Under a cyclonic eddy, the structure of the mixed layer is primarly defined by vertical advection. It is warmer and thicker than the mixed layer of a correspondent anticyclonic eddy, and its horizontal extent is equal to the radius of the vortex (Fig. 4.7). The associated BBL is much thinner than the mixed layer and not particularly affected by vertical advection. The dynamics are equivalent to those found for horizontally homogeneous and neutrally stratified flows (Fig. 4.3, 4.8).

On the other hand, the mixed layer of an anticyclonic vortex is the result of both advective and turbulent processes, and the

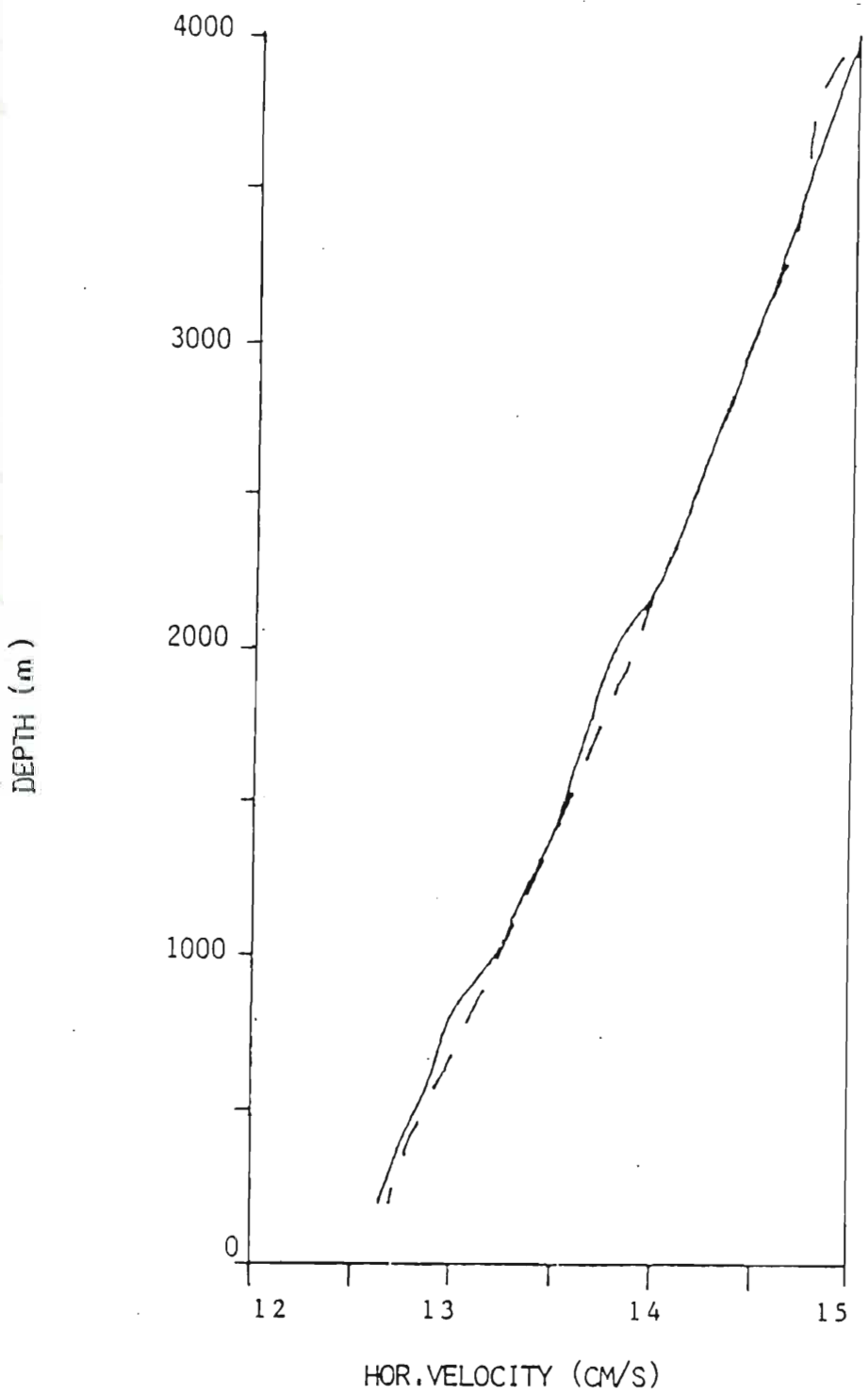

Figure 4.10. The vertical profile of the magnitude of the flow at the location of maximum velocity, and time t=90 days. Cyclonic flow (solid line); anticyclonic flow (dashed line).

ambiguity between the mixed layer and BBL is greatly reduced as for stably stratified flows. Furthermore, since vertical advection tries to remove water from the bottom, the mixed layer spreads outwards and the spatial extent of Benthic Boundary Layer is greater than the radius of the eddy.

Although cyclonic and anticyclonic Benthic Boundary Layers have quite different structures, their influences on the relative forcing flow are comparable. The dynamic of the flow far from the bounadry is primarly affected by the thermal wind effect induced by the vertical advection of temperature, and the motion deviates from its its original barotropic configuration (Fig. 4.10).

5. THE DECAY OF AN HOMOGENEOUS VORTEX UNDER A LINEAR REGIME.

The classical approach in fluid dynamics is to consider the simplest formulation of the problem in order to derive a mathematical framework suitable for analytical diagnostic solutions and to verify whether these simple representations are able to describe gross features of the motion. In general, the mathematical difficulties which arise are nonlinearities due to stratification and the presence of advection in the governing equations. These terms are therefore generally dropped from the model. Thus as a preliminary study of the decay of an isolated vortex, we assume that the flow is linear and homogeneous. A dimensional analysis of the motion equations provides the limits within which the above assumptions might apply.

5.1. The analytical model.

In the following section, we present an analytical model for the decay of a deep eddy-like flow. It is necessary during the formulation of the model to define a correct parameterization of turbulence, suitable for carrying simple analytical solutions. From this point of view, it is appealing to represent turbulence with constant eddy viscosity coefficients, so that the problem becomes equivalent to the usual Ekman Boundary Layer theory. Thus the

starting point of the analysis is to use, as far as possible, of the similarities between Laminar Boundary Layer (LBL; viz, BBL defined by viscosity coefficients that are constant with depth) and Turbulent Boundary Layer (TBL; viz, BBL defined by viscosity coefficients that are function of height) of equal depth and forced by the same flow.

5.1.1. Formulation of the problem.

We consider a deep eddy on a f-plane subjected to bottom friction forces. The eddy is circular and axially symmetric of radius R and total depth H. A cylindrical coordinate system is chosen such that the radial coordinate r^* is zero at the center of the eddy and increases outwards and the vertical coordinate z^* is zero at the bottom and increases upwards. The fluid is assumed to be incompressible and Boussinesq. We neglect horizontal diffusion of momentum and temperature (i.e., there is not substantial exchange between the eddy and the surrounding water). Vertical diffusion is also neglected inside the eddy but not close to the bottom, where it defines a BBL of thickness h^*. Thus the equations for the flow away from the BBL are:

$$u^*_{t^*} + u^* u^*_{r^*} + w^* u^*_{z^*} - \left(f + \frac{v^*}{r^*}\right)v^* = -\frac{1}{\rho_o} p^*_{r^*} \qquad (5.1.1a)$$

$$v^*_{t^*} + u^* v^*_{r^*} + w^* v^*_{z^*} + \left(f + \frac{v^*}{r^*}\right) + u^* = 0 \qquad (5.1.1b)$$

$$0 = -p^*_{z^*} - g\rho^* \tag{5.1.1c}$$

$$\frac{1}{r^*}(r^*u^*)_{r^*} + w^*_{z^*} = 0 \tag{5.1.1d}$$

$$\rho^*_{t^*} + u^*\rho^*_{r^*} + w^*(\rho^*_B + \rho^*)_{z^*} = 0 \tag{5.1.1e}$$

The subscripts (r^*,z^*,t^*) denote partial differentiation, the variables u^*, v^* and w^* are the mean components of the radial, azimuthal, and vertical velocities respectively. The variable ρ^* is the deviation of density from the state of rest, expressed by the linear function $\rho^*_B(z^*)$. The variable p^* is the deviation of the hydrostatic pressure from the hydrostatic pressure associated with the state of rest, g is the gravitational acceleration, f the Coriolis parameter and ρ_o a constant reference value of density.

The variables are nondimensionalized by assuming geostrophic and hydrostatic balances, and scaling the temporal variable with the spin-down time scale for a bottom layer (henceforth LBL) defined by a characteristic thickness D and by an eddy viscosity coefficient constant with depth (Greenspan, 1968). Therefore, the variables are scaled in the following manner:

$$r^* = Rr \qquad z^* = Hz \qquad h^* = Dh$$

$$(u^*, v^*) = U(u,v) \qquad w^* = \frac{UH_w}{R} \qquad p^* = \rho_o fULp \tag{5.1.2}$$

$$\rho^* = \rho_o \frac{fUR}{gH}\rho \qquad t^* = \left(\frac{Df}{H}\right)^{-1} t$$

Introduce the parameters:

(5.1.3a) $\varepsilon = U/fR$ The Rossby number

(5.1.3b) $E = (D/H)^2$ The Ekman number

(5.1.3c) $N^2 = (-g\rho_{Bz}/\rho_o H)$ The square of the Brunt-Vaisala frequency.

(5.1.3d) $s = \frac{N^2H^2}{f^2R^2}$ The stratification parameter

(5.1.3e) $\lambda = \sqrt{E}/\varepsilon$

Therefore, the momentum equations in the nondimensionalized form are:

(5.1.4a) $$\varepsilon \frac{D}{Dt} u - \left(1 + \varepsilon \frac{v}{r}\right) v = - p_r$$

(5.1.4b) $$\varepsilon \frac{D}{Dt} v + \left(1 + \varepsilon \frac{v}{r}\right) u = 0$$

(5.1.4c) $$0 = - p_z - \rho$$

(5.1.4d) $$\frac{1}{r} (ru)_r + w_z = 0$$

(5.1.4e) $$\frac{D}{Dt} \rho - sw = 0$$

where

(5.1.4f) $$\frac{D}{Dt} = \lambda \frac{\partial}{\partial t} + u \frac{\partial}{\partial r} + w \frac{\partial}{\partial z}$$

The boundary and initial conditions of the problem (5.1.4) must be carefully assigned. Since we are concerned with the decay of the eddy, we neglect the early stages of the evolution of the flow.

Thus we assume that dissipation by bottom friction starts being effective after the geostrophic flow of the eddy is fully developed. The equations (5.1.4) are satisfied within the region $0 \leq r \leq 1$, $0 \leq z \leq 1$. The bottom of the eddy is at $z = 0$ and the thermocline displacement at $z = 1$. The azimuthal velocity, v, must vanish at the center of the eddy. We assume that at the edge the pressure is the hydrostatic pressure associated with the state at rest (i.e., the eddy is at rest with respect to the surrounding water). We do not close the problem with lateral boundary layers. This is equivalent to assuming that all the water exchanged between the eddy and the surrounding water is exchanged via the BBL. At the bottom of the eddy the boundary conditions are specified by matching the interior and the boundary layer solutions. In particular, since the BBL is characteristically a well-mixed region, stratification does not affect the order of magnitude of the vertical velocity pumped out of the bottom layer; i.e.,

$$\tilde{w} = \sqrt{E}\ \tilde{w}_o \tag{5.1.5}$$

where the tilde indicates the BBL solution and $w_o = 0(1)$ (Pedlosky, 1979).

Assume:

$$\varepsilon \ll 1 \tag{5.1.6}$$

and expand all the variables in their asymptotic expansion with respect to the parameter ε. Thus the variables are scaled in the following manner:

$$v = v^{o} + \varepsilon v^{1} + \ldots$$

$$u = \varepsilon u^{1} + \ldots$$

$$w = \varepsilon w^{1} + \ldots$$

(5.1.7)

$$\rho = \frac{s\sqrt{E}}{\varepsilon}\,(\bar{\rho}^{o} + \varepsilon\bar{\rho}^{1} + \ldots$$

$$p = \eta^{o} + \varepsilon\eta^{1} + \ldots + \frac{s\sqrt{E}}{\varepsilon}\,(\bar{p}^{o} + \varepsilon\bar{p}^{1} + \ldots .$$

$$\frac{D}{Dt} = \lambda\,\frac{\partial}{\partial t} + 0(\varepsilon)$$

Assume:

(5.1.8) $\quad s\sqrt{E} \ll \varepsilon^{2}$

Thus in first approximation it follows:

(5.1.8a) $\quad v^{o} = -\,\eta^{o}_{r}$

(5.1.8b) $\quad \lambda v^{o}_{t} + u^{1} = 0$

(5.1.8c) $\quad \frac{1}{r}(ru^{1})_{r} + w^{1}_{z} = 0$

(5.1.8d) $\quad 0 = -\,\bar{p}^{o}_{z} - \bar{\rho}^{o}$

(5.1.8e) $\quad \lambda\,\bar{\rho}^{o}_{t} - w^{1} = 0$

Here the variable η represents the displacement of the thermocline.

Thus for the range of the parameters:

(5.1.9) $\quad \frac{s\sqrt{E}}{\varepsilon} \ll \varepsilon \ll 1$

it follows that the effects of bottom friction on stratification are of secondary importance on the spin-down process of the eddy and the eddy decays homogeneously.

In order to verify the applicability of the model to a deep-eddy-like flow, let us consider typical values for such a flow located at middle latitude (Armi and D'Asaro, 1980):

$$\begin{array}{lll} H = 4 \times 10^3 \text{ m} & D = 20 \text{ m} & R = 10^5 \text{ m} \\ U = 15 \text{ cms}^{-1} & f = 10^{-4}\text{s}^{-1} & N^2 = 0.7 \times 10^{-7}\text{s}^{-2} \end{array} \qquad (5.1.10a)$$

These values imply:

$$\begin{aligned} \sqrt{E} &= 0.5 \times 10^{-2} \\ \varepsilon &= 1.5 \times 10^{-2} \\ s &= 1.1 \times 10^{-2} \\ \frac{s\sqrt{E}}{\varepsilon} &= .36 \times 10^{-2} \\ \lambda &= 0.3 \end{aligned} \qquad (5.1.10b)$$

and the relation (5.1.9) is satisfied. Integration over depth of the continuity equation (5.1.8c) and equation (5.1.8b) lead to:

$$\lambda\left(\frac{R}{L_D}\right)^2 \eta_t^o - \lambda^2 h_t - \lambda \tilde{w}_o - \lambda \frac{1}{r}(rv^o)_{rt} = 0 \qquad (5.1.11)$$

where $L_D = \sqrt{gH}/f$ is the barotropic radius of deformation. The term containing η_t represents the contribution of the free surface variations to the potential vorticity by vortex-tube stretching

(Pedlosky, 1979). Since $R << L_D$, this contribution is unimportant and can be neglected (i.e., the free surface appears no different from a rigid lid). Therefore, we simplify equation (5.1.11) by neglecting this term.

5.1.2. The Bottom Boundary Layer solution.

To close the problem, we must now define the functions $\tilde{w}_o$ and h of the equation (5.1.11) from the BBL solutions. The mathematical difficulties of the problem depend on the turbulent nature of the BBL In order to present simple analytical solutions, it is appealing to parameterize turbulence via eddy viscosity coefficients that are constant with depth. Thus we compare the dynamics of a Turbulent Boundary Layer (henceforth TBL) with the dynamics of a LBL of equal depth and forced by the same flow.

Let the superscript L indicate values for the LBL; thus the LBL is defined by the eddy viscosity coefficient ν^L (constant with depth):

$$(5.1.12) \qquad \nu^L(r) = \frac{fD^2}{2\pi 2} h^2(r)$$

In Appendix A we show that the constant eddy viscosity coefficient ν^L is a good estimate of the mean value of the eddy viscosity coefficient $K_M(z)$ which defines the TBL. However, there is a fundamental difference between the assumptions that the eddy

coefficient is constant throughout the boundary layer or that it is a function of height. One of the main disagreements observed between LBLs and TBLs is that close to the rigid wall, the Ekman veering is 45° and 10° respectively, (Weatherly, 1972). Thus phenomenon is a measure of the different friction forces that drive laminar and turbulent motions.

Outside the boundary layer, the Coriolis forces F_c balance the pressure gradient forces F_p exactly (Fig. 5.1a); inside the layer, the forces that act on the layer as a whole are the pressure gradient forces F_p (depending only upon the thickness of the layer and the geostrophic flow of the interior), the friction forces F_f and the Coriolis forces F_c (Fig. 5.1b). If we require that the Ekman veering is at an angle β with respect to the flow above the layer it follows that:

$$\begin{aligned} &- F_p + F_c^\beta \cos\beta + F_f^\beta \sin\beta = 0 \\ &F_c^\beta \sin\beta - F_f^\beta \cos\beta = 0 \end{aligned} \tag{5.1.13}$$

where the superscript β indicates values for the given Ekman veering at the rigid wall. Equations (5.1.13) imply:

$$F_f^\beta / F_p = \sin\beta \tag{5.1.14}$$

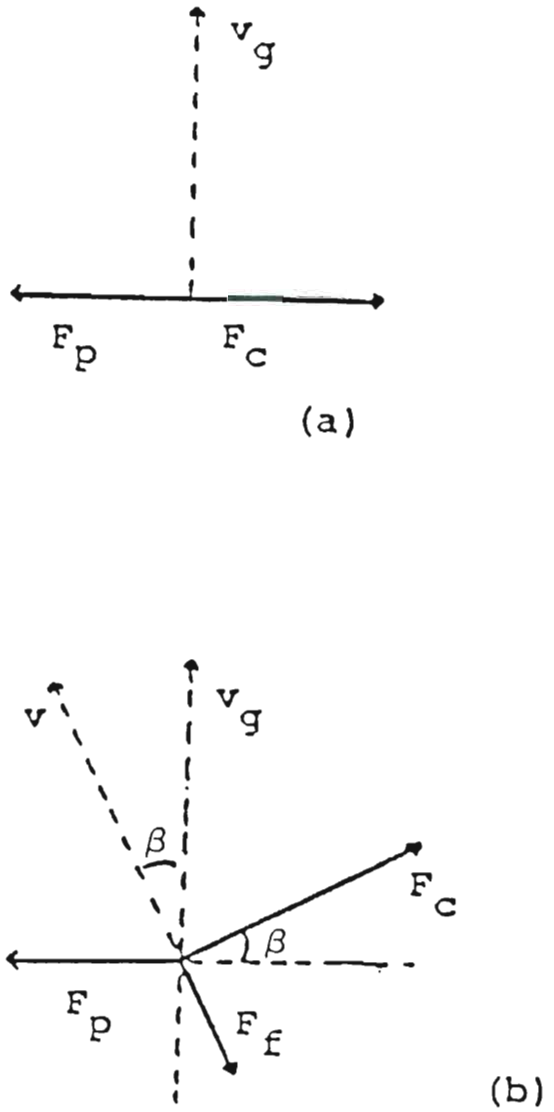

Figure 5.1. The balance of forces acting at the top (a) and at bottom (b) of the boundary layer. F_p=pressure gradient forces; F_c=Coriolis forces; F_f=friction forces; v_g=direction of the forcing flow; v=direction of the flow at the rigid surface.

and therefore,

(5.1.15) $F_f^{10}/F_f^{45} = .25$

Therefore we conclude that LBLs are more dissipative than TBLs for equal boundary layer depth and equal forcing geostrophic flow.

a). The Ekman velocity

As the previous analysis indicates, a LBL cannot satisfactorily parameterize a TBL. Therefore, in order to derive an appropriate expression for the term $\tilde{w}$, we assume that the Ekman Boundary Layer theory is applicable only above the logarithmic layer. Thus the non-slip boundary condition at the rigid surface is transformed into:

(5.1.16) $(u,v) = (u_b\cos\beta, u_b\sin\beta)$

where u_b is the magnitude of the velocity at the top of the logarithmic layer and β the Ekman veering. It can be showed that (Holton, 1979):

$$u_b = (\cos\beta - \sin\beta)(U_g^2 + V_g^2)^{1/2}$$

where (U_g, V_g) are the velocity components of the forcing flow. Thus, neglecting terms $O(\varepsilon)$, the solution above the layer is given by:

(5.1.17a) $u = -v^o e^{-\xi}\sin\xi + v^o(\cos\beta-\sin\beta)e^{-\xi}\sin(\xi-\beta)$

(5.1.17b) $v = v^o(1-e^{-\xi}\cos\xi) + v^o(\cos\beta-\sin\beta)e^{-\xi}\cos(\xi-\beta)$

where

$$\xi = \pi z/(\sqrt{E}\ h(r))$$

Thus the Ekman velocity at the top of a TBL is :

(5.1.18a) $\tilde{w} = \sqrt{E}\ \tilde{w}_o = \sqrt{E}\ k\ddot{w}_o$

(5.1.18b) $k = \frac{\sin 2\beta}{2\pi}$

(5.1.18c) $\ddot{w}_o = \frac{1}{r}(rhv^o)_r$

An Ekman veering $\beta=10°$ leads to the value k=0.08.

b). The thickness of the Bottom Boundary Layer

We first recall that the thickness of a LBL does not vary with time and it is independent of the forcing flow, but the characteristic scale of a TBL thickness must somehow be related to the forcing flow. Usually the thickness of a TBL is taken to be (Wimbush & Munk, 1974; Weatherly, 1972; Weatherly and Martin, 1978):

(5.1.19) $D = 0.4u*/f$

where the friction velocity u* can be related to the flow above the bottom layer:

(5.1.20) $u* = aU$

The constant of proportionality, a, is usually assumed to range from

0.03 to 0.04 (Kundu, 1976). Therefore, with the non-dimensionalized variables we might assume:

$$h = |\underset{\sim}{v}^{o}|_{*} + O(\varepsilon) \qquad (5.1.21)$$

The relation (5.1.21) is particularly appealing because of its simplicity; however, it must be applied under the correct circumstances. As we have pointed out, during the decay of the vortex, the effects of stratification are of secondary importance, but during the phase in which the interior flow builds up the BBL, stratification plays an important dynamic role, mixing the bottom layer and creating the sharp interface that inhibits the upward propagation of turbulence. For steady state flows, the mixed layer is the region in which most of the turbulent activity occurs and the relation (5.1.21) applies. On the other hand, as the forcing flow decays, we might expect a reduction of turbulence and a consequent reduction of the TBL thickness. However, once the initial TBL has been mixed, there are no mechanisms (except molecular diffusion) for reestablishing stratification, and therefore, turbulence can still propagate upward to the upper levels of the mixed layer. Then, the TBL retains some memory of the original forcing flow which highly complicates the relation between the BBL thickness and the interior flow. Thus we can conclude that the relation (5.1.21) might be applied at least in the early stage of the spin-down process, when the mixed layer and the TBL are in balance.

Independent of the validity of equation (5.1.21), substituting (5.1.8), (5.1.9) in (5.1.3e) it follows:

$$(5.1.22) \quad \lambda = \sqrt{E}/\varepsilon = 0.4a\frac{R}{H} = 0\ \frac{R}{H}(\ x\ 10^{-2})$$

Thus the parameter λ is related only to the spatial dimensions of the vortex.

5.1.3. The model equation

Substituting (5.1.16), (5.1.17), and (5.1.21) into (5.1.11) using the rigid lid approximation, the model equation is reduced to:

$$(5.1.23) \quad (rv^o)_{rt} + \lambda r|v^o|_t + k(r|v^o|v^o)_r = 0 \qquad t>0$$

subjected to the boundary and initial conditions:

$$(5.1.24a) \quad v^o(0,t) = 0$$

$$(5.1.24b) \quad v^o(r,0) = V(r) \qquad t<0$$

Furthermore, because of the boundary condition at the center of the eddy, the initial velocity distribution V(r) may be written as follows:

$$(5.1.24c) \quad V(r) = Ar^{\alpha}f(r)$$

where A is constant, $f(0) = 1$, and $\alpha>0$.

Consider equation (5.1.23) and its term $|v^o|_t$. Since the thickness of the BBL is related to the magnitude of the forcing flow,

the term $|v^o|_t$ is always negative and in the decay process of the flow might be considered equivalent to an apparent upwelling. Then, we conclude that the BBL time variations are a dissipative mechanism for cyclonic eddies, but they imply a production of relative vorticity for anticyclonic eddies. Therefore, we expect that cyclonic vortices decay faster than anticyclonic with equivalent features.

Although the nonlinear nature of equation (5.1.23) does not make it possible to present an expression for the general solution of the problem, additional information can be derived. Introduce the new variables :

$$\begin{aligned} \rho &= \lambda r \\ \tau &= kt \end{aligned} \tag{5.1.25}$$

Equations (5.1.23) and (5.1.24c) are transformed into:

$$(\rho v^o)_{\rho\tau} + \rho|v^o|_\tau + (\rho|v^o|v^o)_r = 0 \tag{5.1.26}$$

$$V = A\lambda^{-\alpha}\rho^{\alpha} f(\rho/\lambda) \tag{5.1.27}$$

Equation (5.1.26) implies that the eddy does not respond simultaneously to dissipation by bottom friction, but with a time shift expressed by the factor $\lambda^{-\alpha}$. Then we conclude that the solution is of the form:

$$v^o = v^o(\lambda r, kt + \gamma) \tag{5.1.28}$$

and the associated decay time scale T_d is given by:

$$(5.1.29) \quad T_d = \frac{1}{\sqrt{Efk}} + \gamma$$

where γ represents the shift factor. The essence of the solution (5.1.28) can be summarized as follows:

i) $\lambda >> 1$

During the spin-down process "fat" eddies spread and lose most of their kinetic energy in the early stage of the decay. However, the case is of purely academic interest. "Fat" eddies require a radius so large that the rigid lid approximation is no longer valid and (5.1.26) cannot be applied.

ii) $\lambda << 1$

"Slim" eddies contract and respond with a delay to dissipation by bottom friction. Here, we recognize two different phases of the decay: the early stage during which eddies preserve their initial features almost unchanged, and the final stage during which eddies rapidly lose their kinetic energy.

iii) $\lambda = 1$

We first assume $\lambda = 1$. During the decay the horizontal scale of the eddy does not change, and the eddy responds simultaneously to bottom friction dissipation. On the other hand, if we assume $\lambda \cong 1$, the flow might evolve in accordance with any of the previous cases. We recall that the previous possibilities can never

be found in the decay process of the same eddy; during the spin-down fat eddies become fatter and slim eddies slimmer.

Finally, we recall that according to the values of (5.1.10a) typical deep eddy-like flows evolve as illustrated in case ii), and the associated time scale of the decay is:

(5.1.30) T_d = 1.2 years

On the other hand, if we suppose that the eddy is subjected to a LBL, the associated time scale is :

(5.1.31) $T_d^L = (\sqrt{E}\ f)^{-1}$ = 1 month,

It is unnecessary to emphasize that the T_d value expresses a much more realistic estimate than T_d^L and that the evolution of the flow according to our model is also in good agreement with observations (The Ring Group, 1981).

5.1.4. Discussion.

The model suggests that spin-down occurs on a time scale of about one year. The result is indeed in good agreement with observations and measurments. A dimensional analysis indicates that dissipation affects primarly the barotropic component of the motion, provided that the stratification parameter s and the square root of

the Ekman number E is much smaller than the square of the Rossby number ε. Thus if we assume also that the Rossby number is much less than unity, the eddy might be considered linear and homogeneous.

The results of the model might be summarized as follows:

- LBLs are more dissipative than TBL of equal depth and forced by the same flow. The Ekman velocity at the top of a TBL is proportional to the Ekman velocity of the correspondent LBL through a constant of proportionality which is a function of the Ekman veering at the wall.
- The BBL time variations are a dissipative mechanism of kinetic energy for cyclonic flows, but they imply a production of relative vorticity for anticyclonic flows. Thus cyclonic eddies decay faster than anticyclonic eddies of equal features.
- The evolution of the flow depends upon the range between the radius and the total depth of the vortex. For realistic values of those spatial dimensions, eddies contract and the spin-down occurs in two phases: the early phase, during which eddies preserve their original features, and the final stage, during which eddies rapidly lose their kinetic energy.

5.2. The numerical experiments.

Inspite of the assumptions made throughout the formulation of the problem, the analytical model is able to reproduce most of the features observed during the decay of mesoscale eddies and suggests a simple parameterization for the BBL turbulent activity. Therefore we

apply the numerical model to investigate the decay of a deep eddy-like flow under linear regime. The eddy is assumed to be homogeneous except close to the bottom where density is a linear function of depth. The condition is required for generating a bottom mixed layer and for maintaining a sharp temperature gradient at the top of the layer which inhibits turbulence for propagating upwards.

The eddies considered in the numerical experiments have the typical dimensional values given in (5.1.10), and linear initial velocity distributions.

5.2.1. Cyclonic and anticyclonic flows.

We consider two eddies of equal spatial dimensions, but initial velocity distributions of opposite sign. Numerical simulations indicate that the decay patterns are virtually identical inside the vortices (Fig. 5.2, and 5.3). Both eddies lose more than 80% of their initial energy in the first year of the spin-down. The result is in good agreement with the estimated decay time scale of the analytical model.

On the other hand, cyclonic and anticyclonic eddies induce different circulations in the surrounding waters. As Fig. 5.4 illustrates, the radius of the anticyclonic eddy contracts about 2% of its initial value in the first year of the spin-down, but the

cyclonic eddy preserves its original radius. The features are a consequence of the role played by the BBL time variations during the decay of the flow.

Let us consider a cyclonic eddy. At the edge of the vortex the Ekman velocity has the form of a downwelling, but the BBL time variations are equivalent to an upwelling. Thus each effect opposes the other, tending to preserve the original radius of the eddy. In contrast, at the edge of an anticyclonic eddy both the Ekman upwelling velocity and BBL time variations work to increase the gradient of the forcing flow and an anticyclonic eddy must contract.

5.2.2. The Ekman velocity.

We consider the decay induced by an Ekman velocity computed as:

$$(5.2.1) \qquad w_e = < k(hV_g)_x/(H-h) >$$

where the constant k is defined in (5.1.18b) and < > indicates average value over the period $\Delta\tau$.

As Fig. 5.5 indicates, no substantial differences are found in the evolution of the flow when the Ekman velocity is computed as in (3.1.7b) (the term h_t being neglected) or defined as in (5.2.1). Thus we conclude that the definition (5.1.18) is the correct parameteriziation of the Ekman velocity present at the top of a TBL.

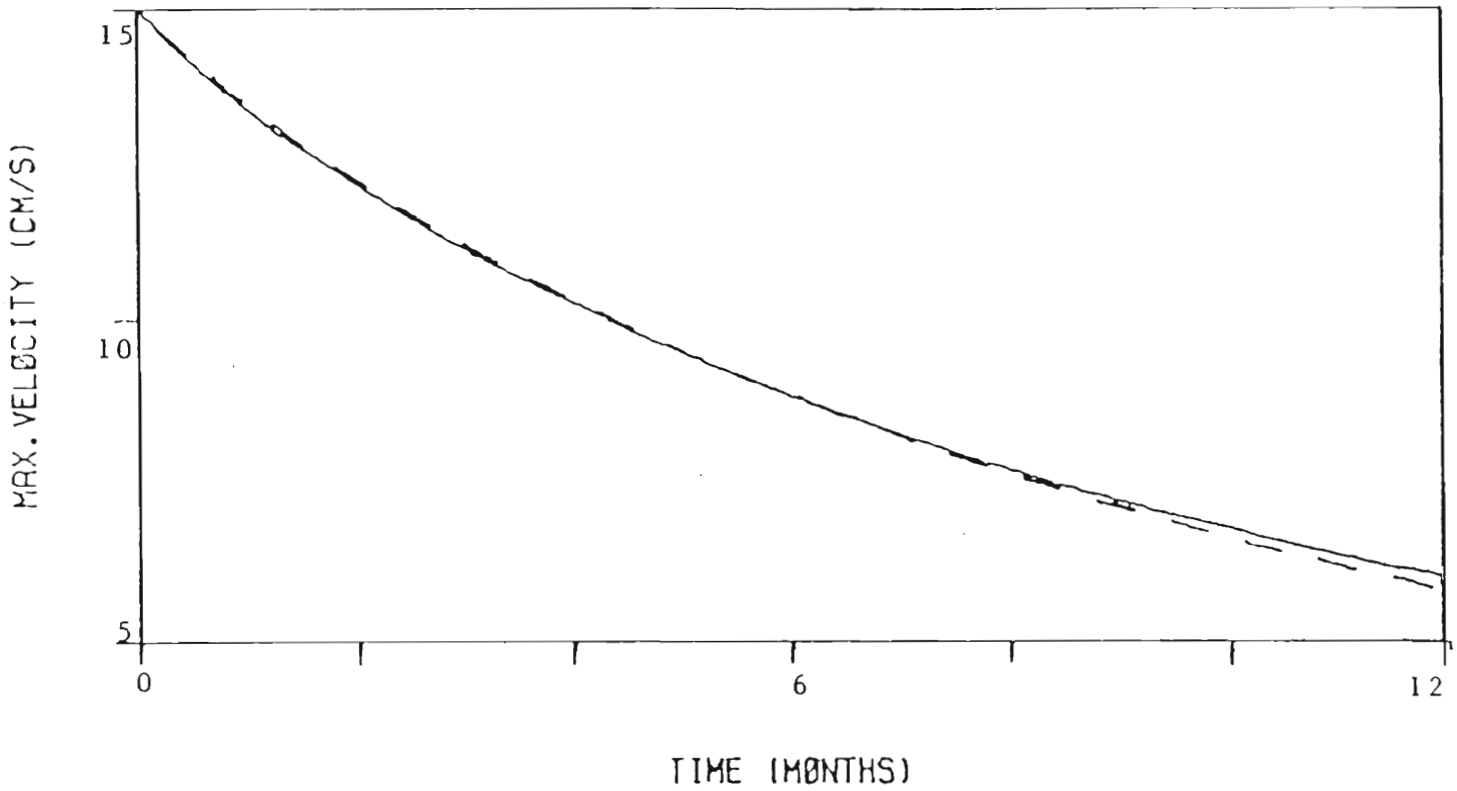

Figure 5.2. The decay of the forcing flow at the location of maximum velocity; cyclonic eddy (solid line), anticyclonic eddy (dashed line).

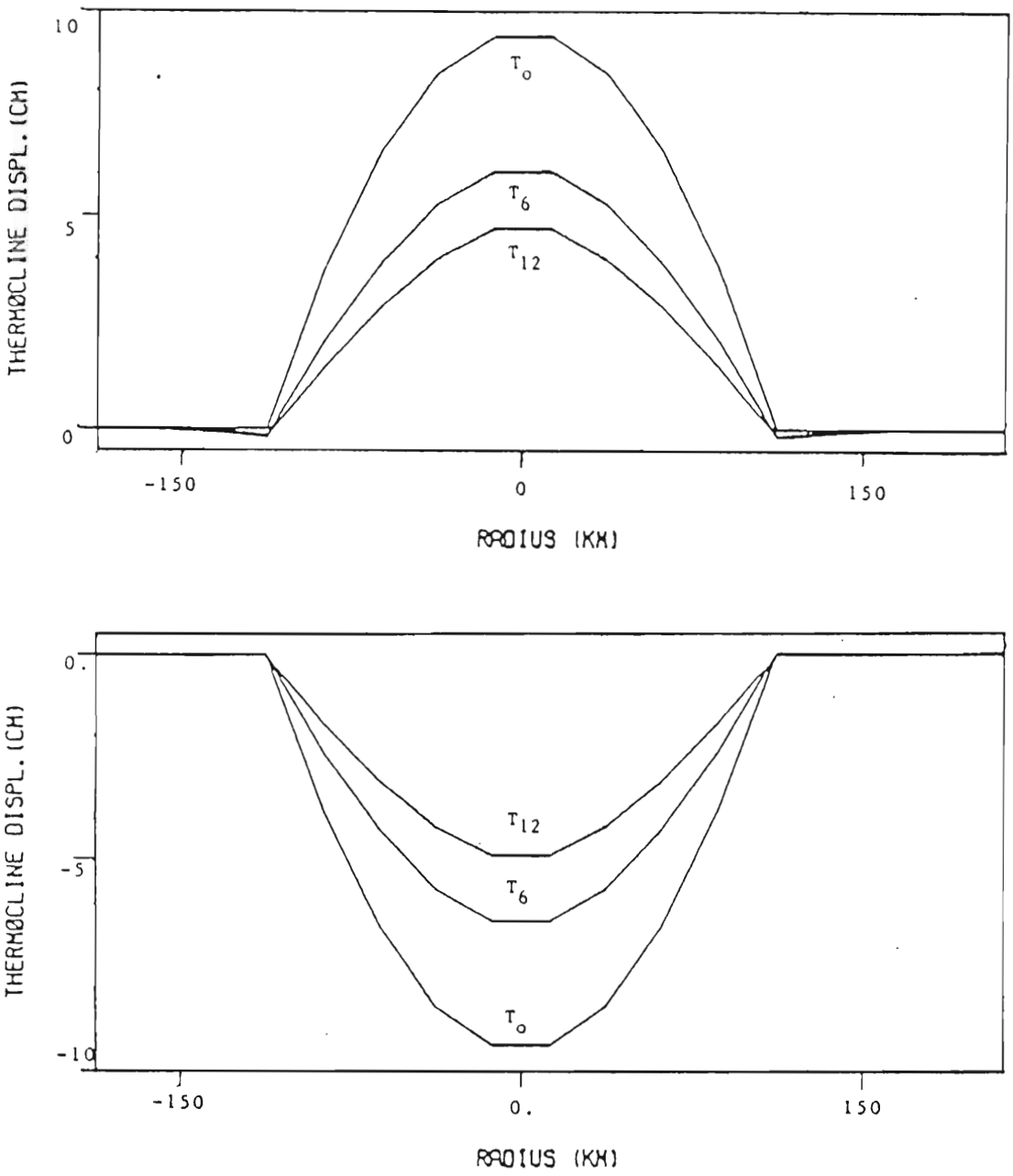

Figure 5.3. The displacement of the thermocline at time t=0, 6,and 12 months from the beginning of the dissipative process; anticyclonic eddy (a), cyclonic eddy (b).

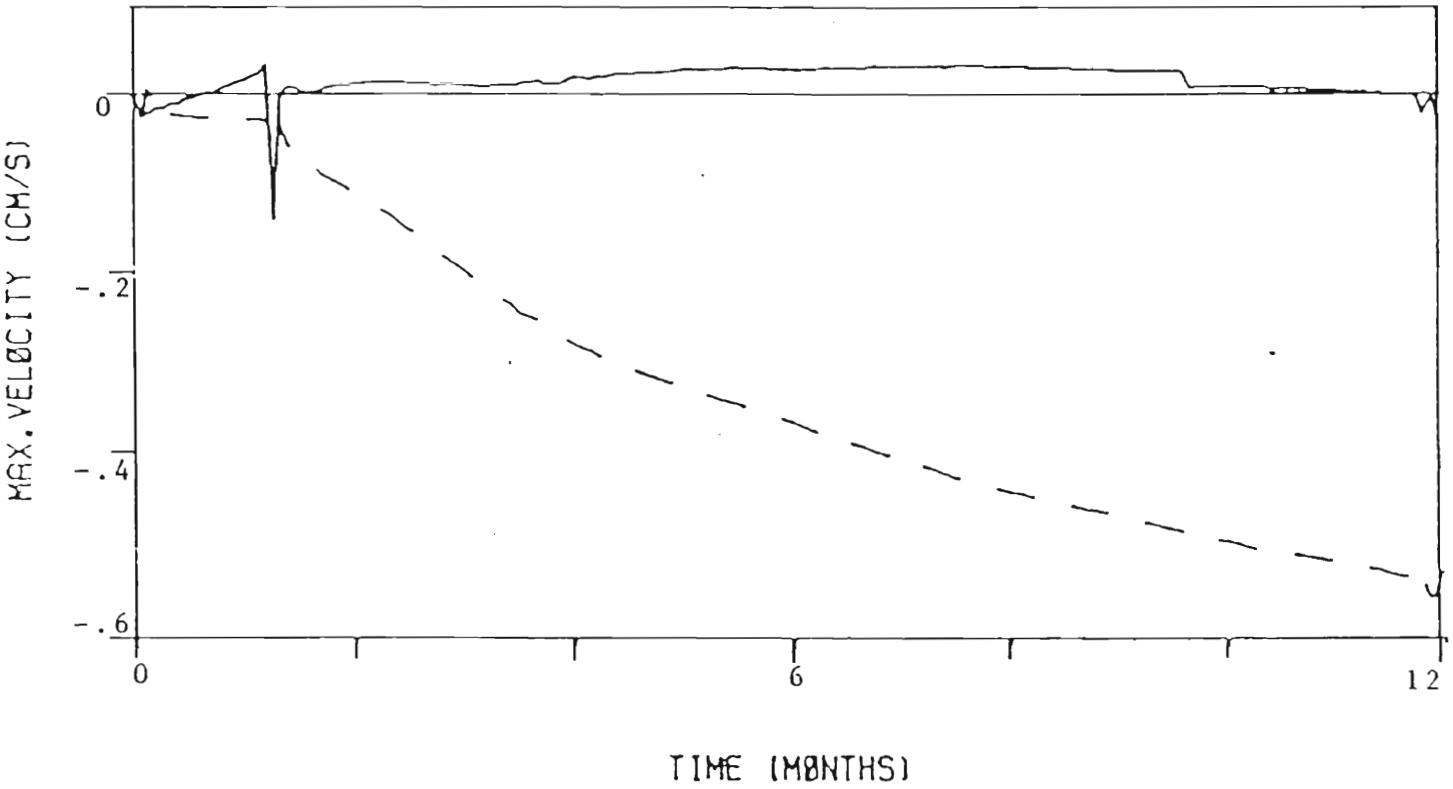

Figure 5.4. The evolution of the poleward velocity at the left edge of mesoscale eddy-like flow computed for cyclonic (solid line) and anticyclonic (dashed line) motion. Positive (negative) velocity for cyclonic flow corresponds to contraction (expansion) of the vortex.

5.2.3. The evolution of the Bottom Boundary Layer

The evolution of the BBL thickness is depicted in Fig. 5.6. Although the rate of the decay for the forcing flow is uniform, the BBL evolves in four distinct phases:

i) The initial stage, during which the BBL decreases (the high frequency noise of Fig. 5.6 is a consequence of the $2\Delta x$-instability and an indication that the inertial oscillations have been excited).

ii) The early stage (about 1.5 months), during which the BBL preserves the new configuration.

iii) The intermediate stage (about 2.5 months), during which the BBL thickness decreases with a well-defined pattern.

iv) The final stage (after 4 months fron the begining of the decay), during which the BBL appears to maintain a steady configuration.

These features might be explained as follows. At time t=0 of the decay, the BBL and mixed layer are in a condition of equilibrium. When dissipation is primed, there is an initial loss of kinetic energy and a reduction of the BBL thickness. Then the BBL is imbedded in a neutrally stratified layer and turbulence, not inhibited by the buoyancy forces, can propagate upwards in the upper levels of the mixed layer. As the forcing flow continues to decay, the supply of kinetic energy from the mean flow cannot support turbulent activity in the upper strata of the mixed layer and the BBL decreases at a rate faster than that of the forcing flow. From Fig. 5.2 and 5.6 we estimated that the BBL thickness is not responsive to

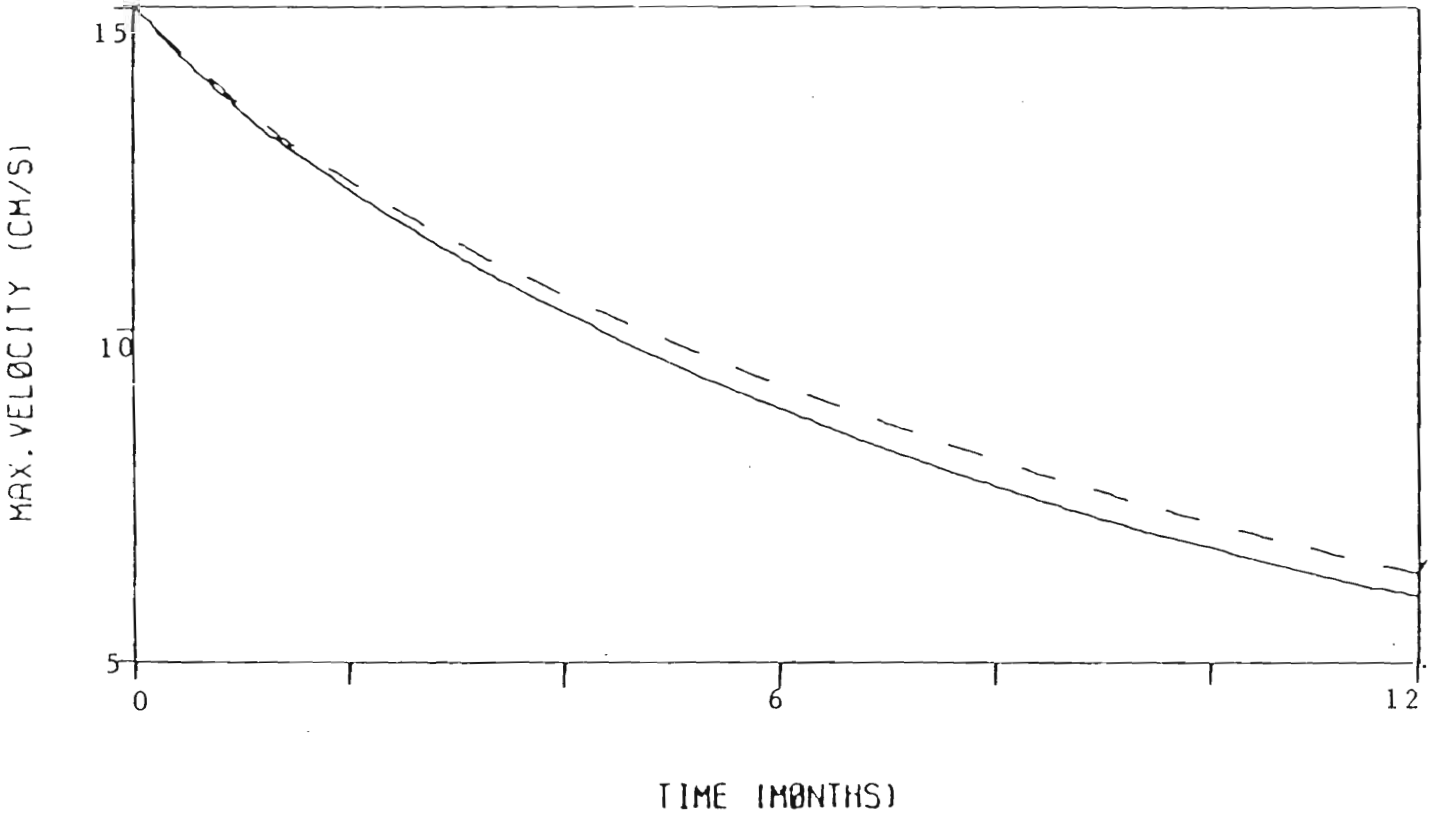

Figure 5.5. The decay at the location of maximum velocity of a cyclonic flow computed with the level 2½ closure scheme (solid line) and relating the Ekman velocity to the Ekman velocity of the correspondent LBL (dashed line).

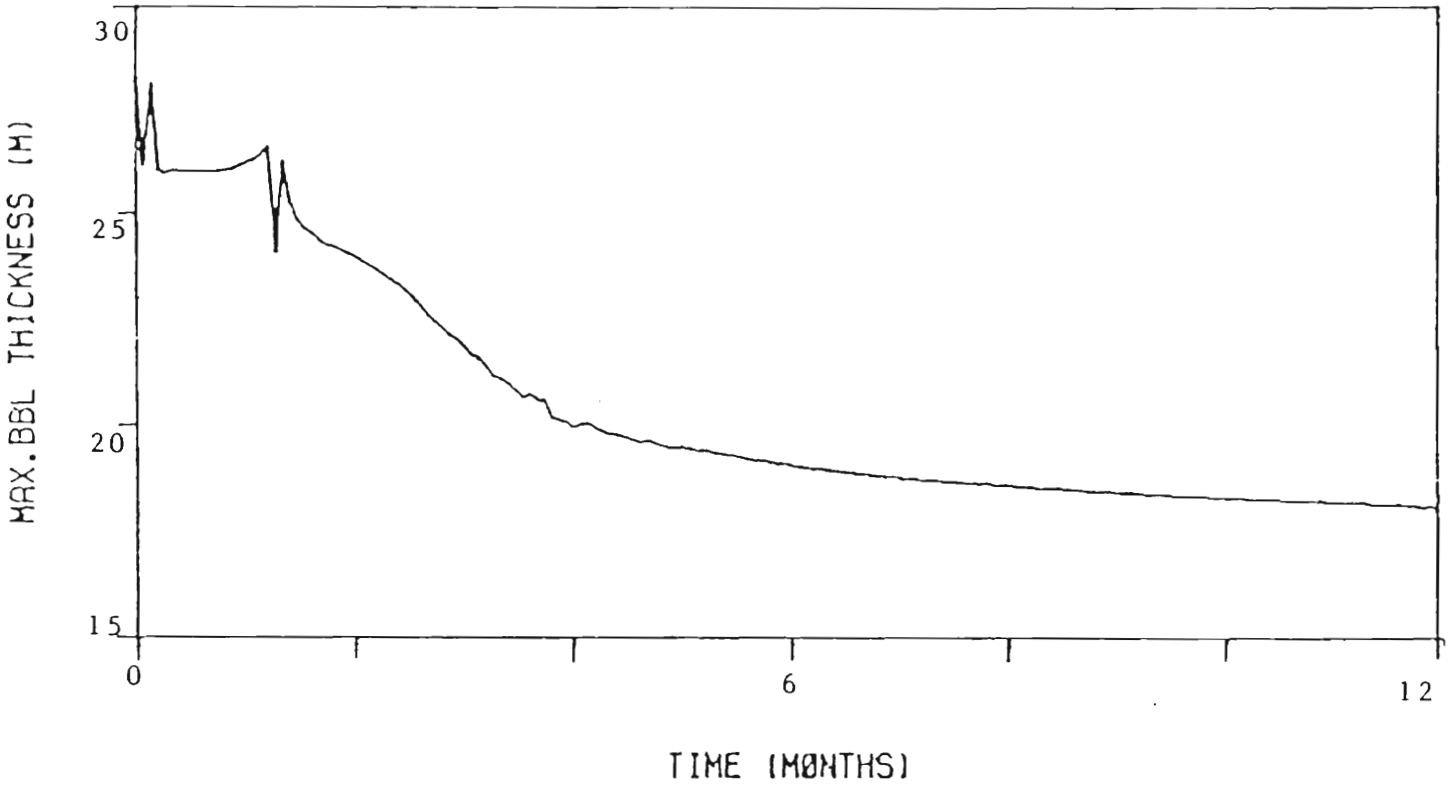

Figure 5.6. The evolution of the BBL thickness at the location of maximum velocity of an anticyclonic eddy-like flow.

a reduction of the kinetic energy of the forcing flow up to 25% of its original value. Four months after the begining of the decay, both BBL and forcing flow are reduced by a factor of 30%, but the mean kinetic energy is now sufficient to mantain turbulence in the upper levels of the new BBL, and the BBL thickness reaches a new constant configuration.

5.3. Comparison between analytical model and numerical experiments.

The numerical experiments confirm most of the results of the analytical model, but some of the features suggested by the model are reproduced only in minimal measure or not at all. The numerical simulations ratify that the Ekman velocity has been correctly parameterized as in (5.1.18), and the decay time scales of both analytical model and numerical tests are in good agreement.

The discrepancies depend upon the dynamic role of the BBL time variations. In the formulation of the analytical model, we have supposed that the BBL thickness is proportional to the magnitude of the forcing flow. This includes the implicit assumption that the BBL time variations are of the same order of magnitude as the time variations of the forcing flow. Under such an hypothesis, the BBL variations become responsible for the different decay pattern for cyclonic and anticyclonic eddies, for the contraction, and for the delay with which the flow responds to dissipation by bottom friction.

Thus the numerical experiments indicate that the weakness of the analytical model is due to the definition of the BBL. The BBL thickness was related to the forcing flow through the friction velocity (equations (5.1.19), (5.1.20)), but the ratio between friction velocity and forcing flow is found to be constant during the spin-down of the motion (Fig. 5.7).

The evolution of the BBL thickness depends upon the dynamic role of the buoyancy forces. Thus a correct parameterization of the BBL thickness presents an intriguing problem which does not have an easy solution. From our analysis, we might propose to modify the relation (5.1.21) as follows:

$$h = \sigma |\underset{\sim}{v}^{o}|_{*} + O(\varepsilon) \qquad (5.3.1)$$

where σ is an empirical (unknown) function dependent upon the magnitude of the initial velocity distribution and stratification. However, the problem requires an analysis which is beyond the bounds of the present research.

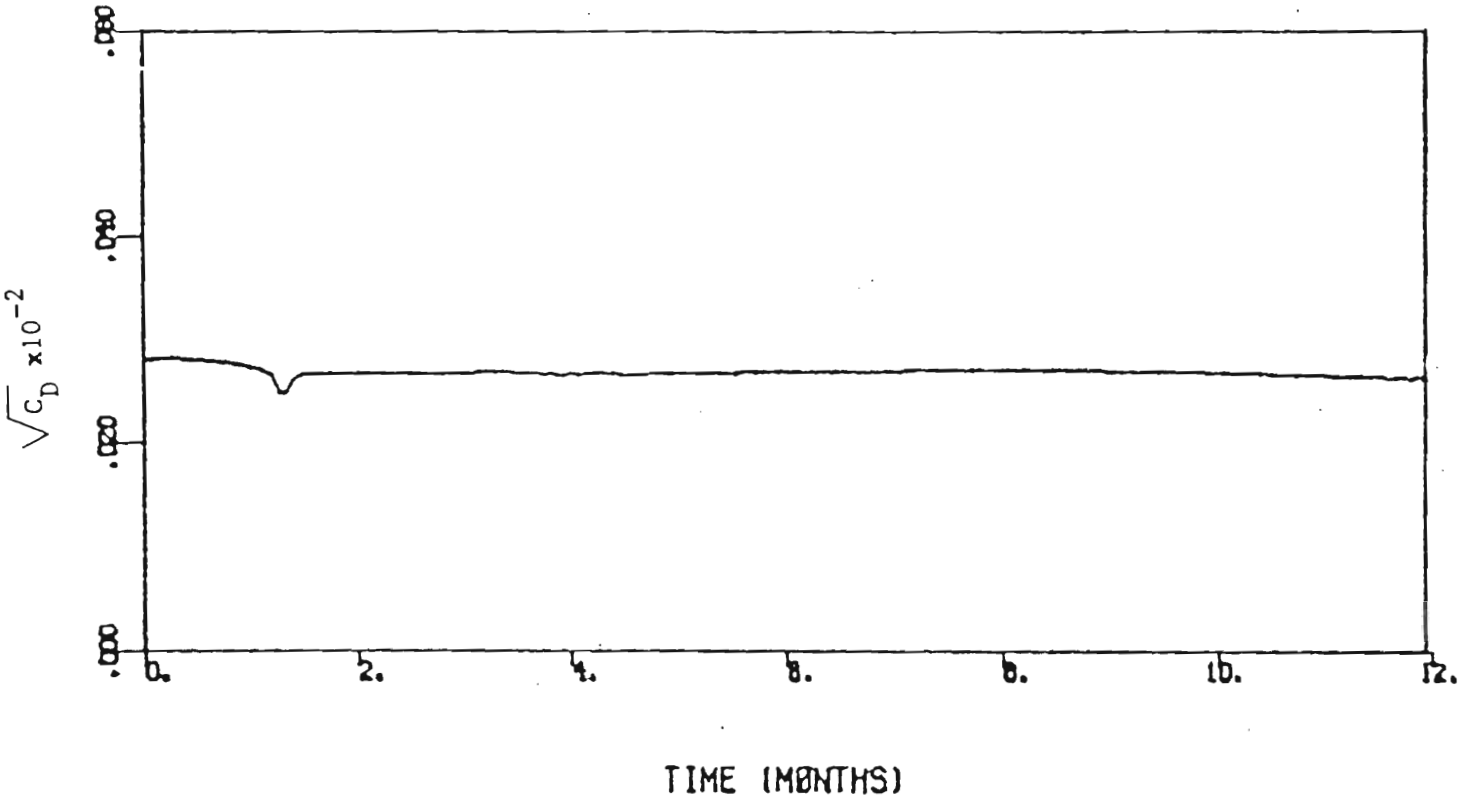

Figure 5.7. The square root of the drag coefficient at the location of maximum velocity as a function of time.

6. THE DECAY OF A DEEP MESOSCALE EDDY-LIKE FLOW.

The analysis presented in the previous section indicates that bottom friction forces are an important mechanism for the decay of isolated vortices. However, the formulation of the model precludes certain types of spin-down mechanisms and observed features. Perhaps the most important omissions are the assumptions that the eddy does not interact with the surrounding water, that the Rossby number, ε, is much less than unity, and that the product of the stratification parameter, s, and the square root of the Ekman number, E, is much less that the square of the Rossby number. Scaling arguments do not completely support the validity of the last conditions. Here we analyze how the physical mechanisms of advection and stratification affect the dynamics of a deep mesoscale flow during the decay induced by bottom friction forces.

Since the simulations are performed for extended periods of time, the numerical scheme is modified to prevent nonlinear instability as has been described in Section 3.3. The correction does not alter the dynamics of the problem (Fig. 4.7a, 6.1a; 4.9a, 6.2a). The new horizontal eddy coefficients affect the structure of the mixed layer, reducing the horizontal gradient of temperature at the edge of the vortex. This also prevents any instability that

might be caused by adiabatically advecting parcels of fluid through a strong thermal front.

6.1. Stationary flow.

Here we analyze the response of stationary flows to dissipation by bottom friction. When it is not indicated otherwise, all the numerical experiments consider the initial values given in Section 4.2. These features imply a Rossby number $\varepsilon=1.5\times10^{-2}$, an Ekman number $E=0.25\times10^{-4}$, and a stratification parameter $s=9.2\times10^{-2}$. In that case the assumptions (5.1.8) of Section 5 are violated. We also assume that spin down starts being effective after one month of numerical simulation, so that the flow may adjust from the initial conditions.

The importance of advection in the dynamics of the motion is represented by the Rossby number, which can be modified by altering either the velocity scale or the spatial scale of the flow. Changes of the velocity field imply changes in the turbulent activity of the BBL and, consequently, changes in the evolution of the decay. On the other hand, changes of the horizontal scale affect both the Rossby number and the stratification parameter without requiring additional alterations of the flow structure. Thus numerical experiments in Section 6.1.2 are performed only for different values of the radius of the vortices.

6.1.1. Cyclonic and anticyclonic flows.

First let us consider the decay pattern of cyclonic and anticyclonic eddies of equal spatial features but with initial velocity distributions of opposite sign.

Fig. 6.1 and 6.2 illustrate the evolution of the mixed layer which might be explained with arguments similar to those used in Section 4.2, and which are therefore not repeated here. The decay of the maximum velocity and the evolution of the thermocline displacement are depicted in Fig. 6.3 and 6.4 respectively. It follows that spin-down occurs mainly in the first six months, after which the flow reaches an almost-steady configuration. Unexpectedly, although both eddies lose approximately 50% of their initial kinetic energy at the location of maximum velocity, in their total extensions the cyclonic eddy decays faster than the anticyclonic. Furthermore, the cyclonic eddy expands and the anticyclonic contracts.

Before explaining these features, let us recall that if the eddy is nonlinear and stratified, the thermal wind effect, caused by vertical advection of temperature, implies a reduction in magnitude of the bottom velocity regardless of its sign at the free surface (Fig. 4.10). Under such a circumstance, turbulent activity inside the BBL is reduced and consequently nonlinear and stratified flows decay on a larger time scale than the time scale of the correspondent linear and homogeneous flows. In addition, most of

Figure 6.1. The evolution of the temperature distribution relative to the coldest bottom water, during the decay of a cyclonic flow. Same as in Fig. 4.7.

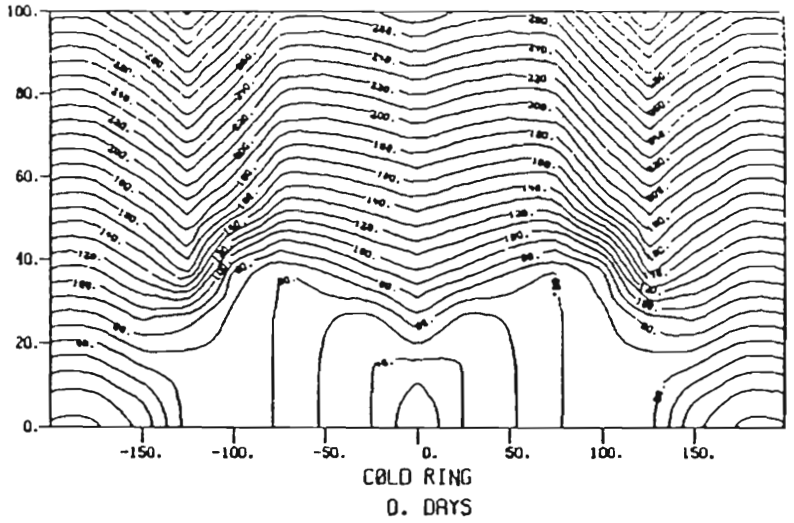

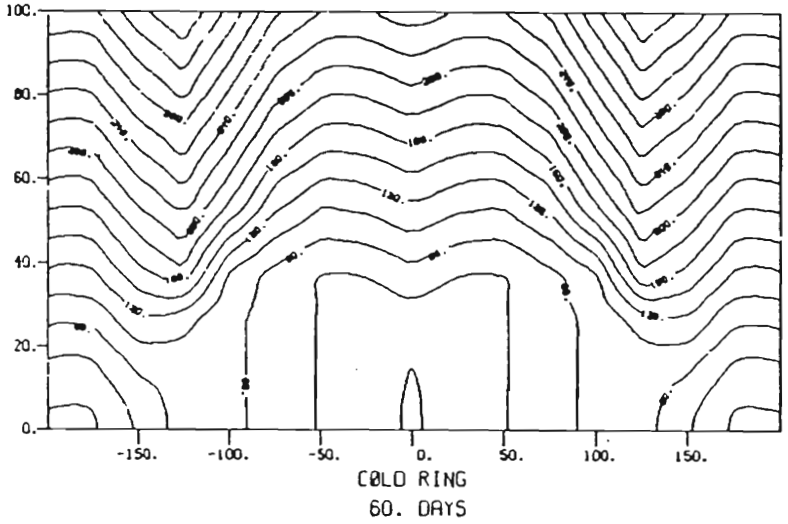

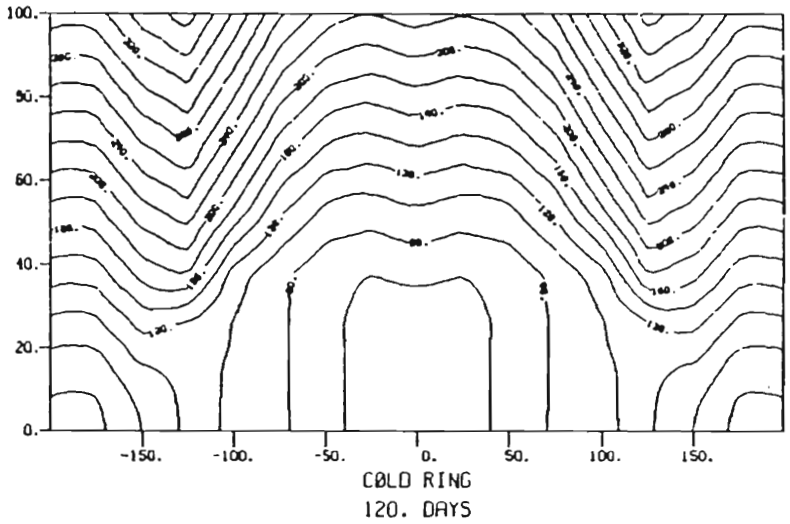

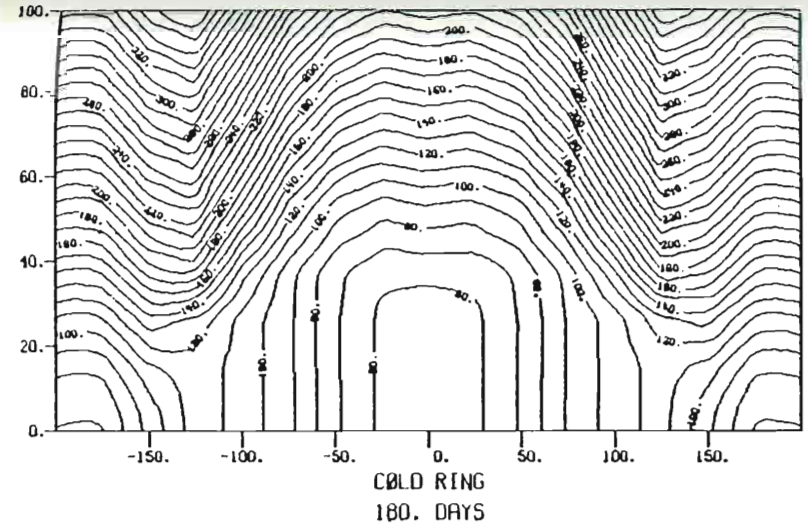

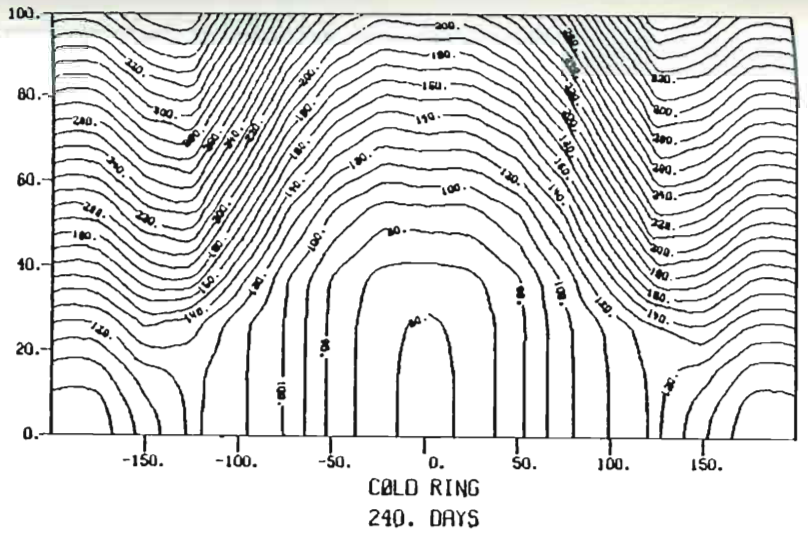

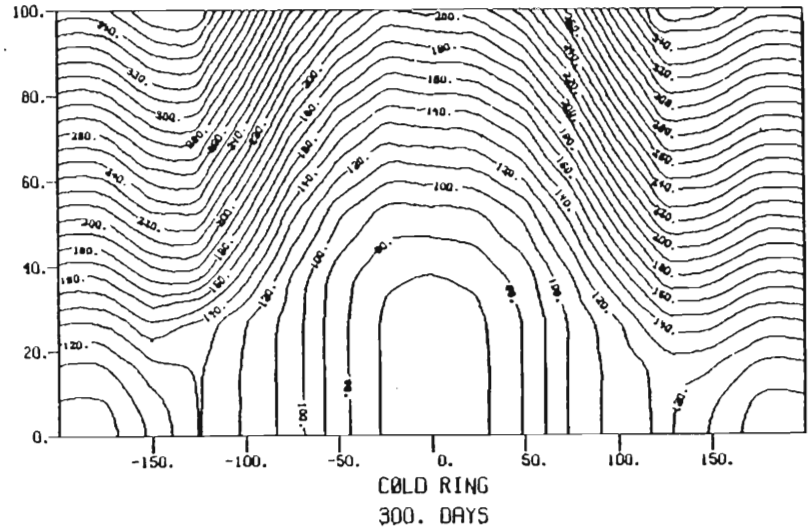

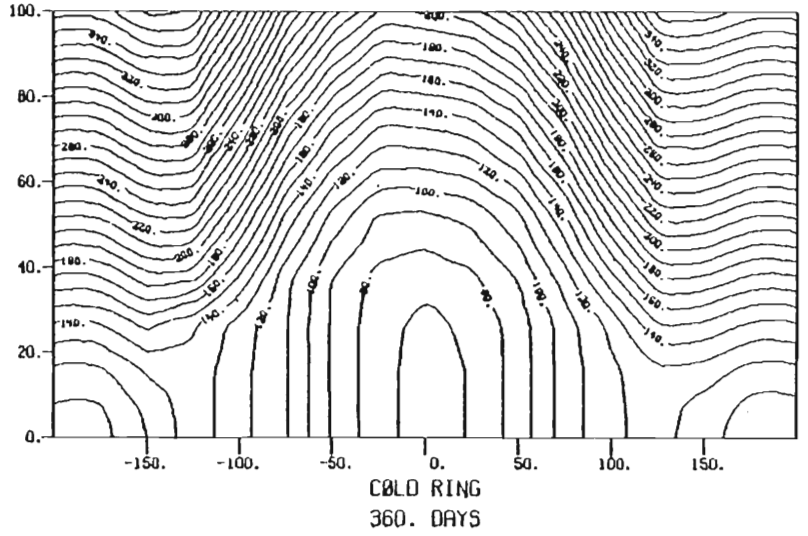

Figure 6.1. Continued.

Figure 6.2. The evolution of the temperature distribution relative to the coldest bottom water, during the decay of an anticyclonic flow. Same as in Fig. 4.7.

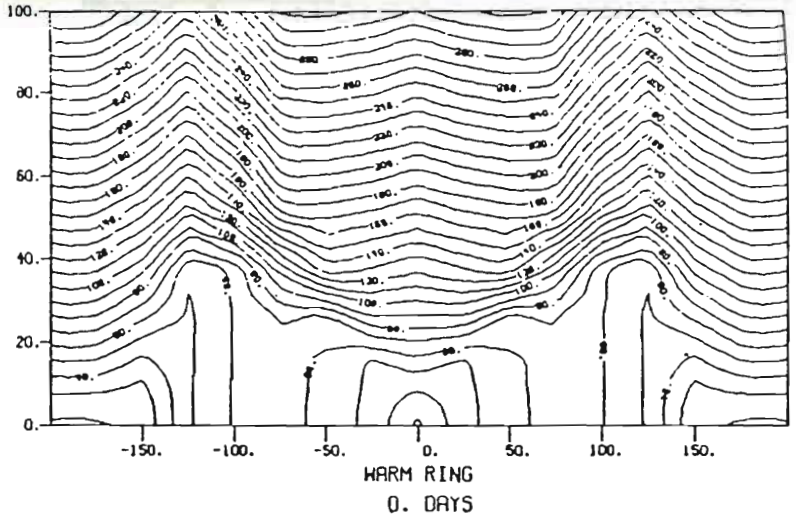

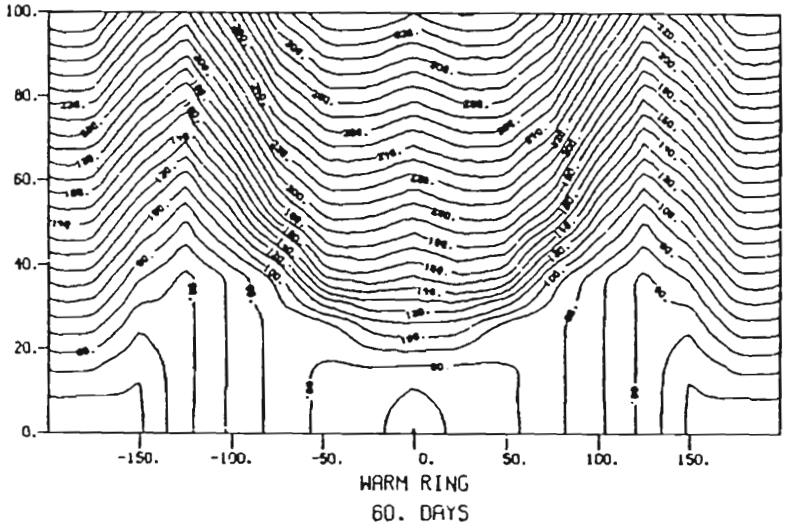

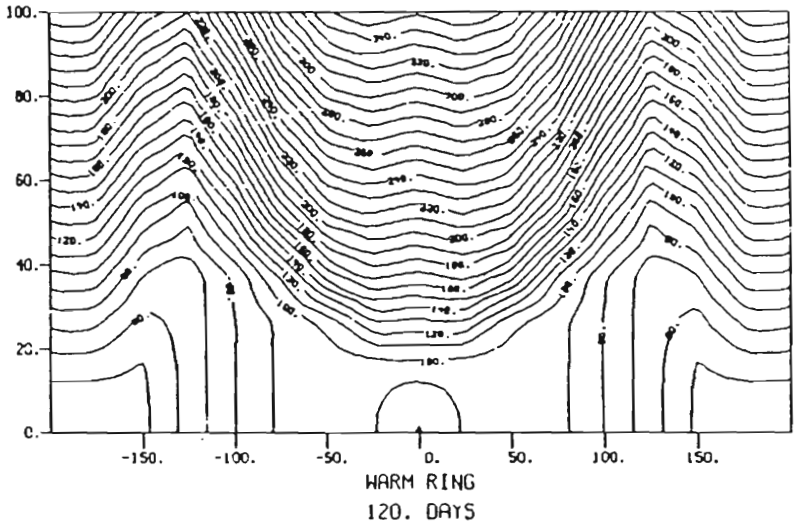

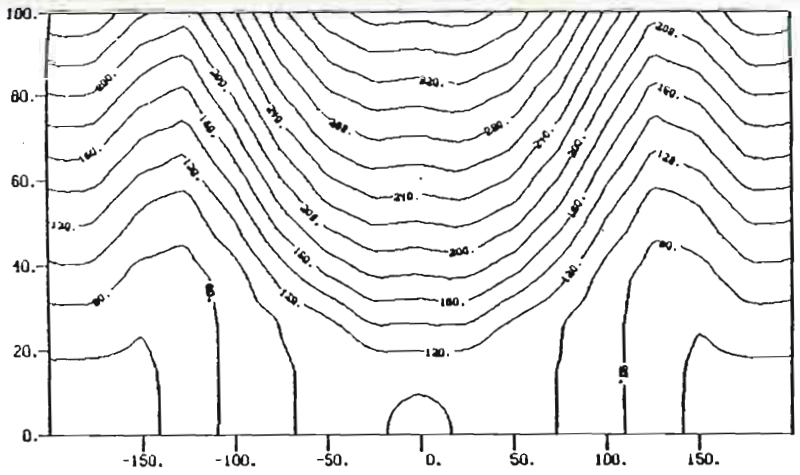

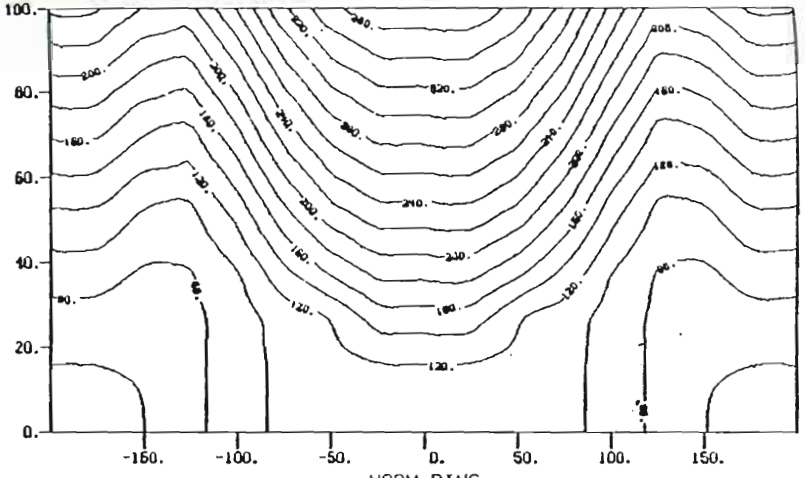

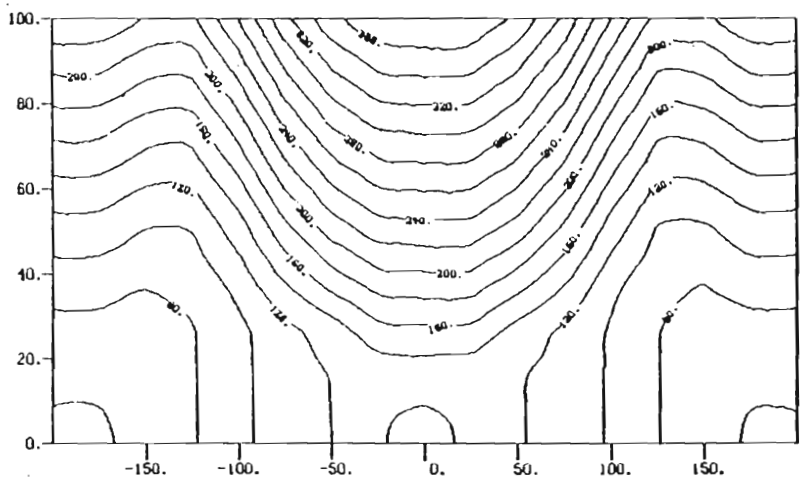

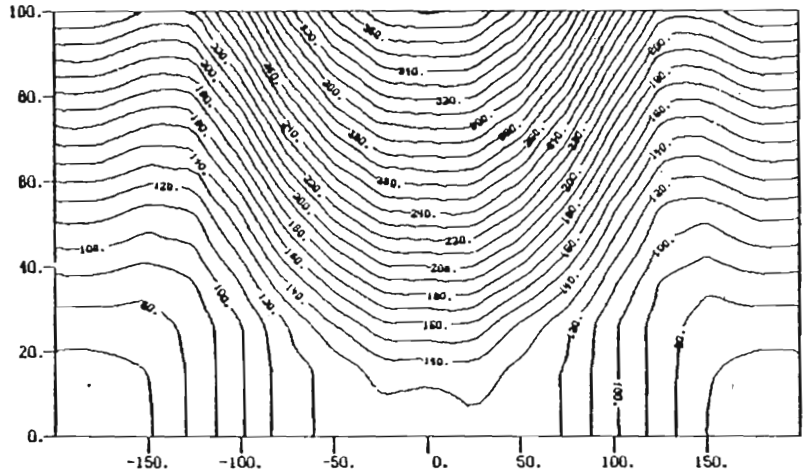

Figure 6.2. Continued.

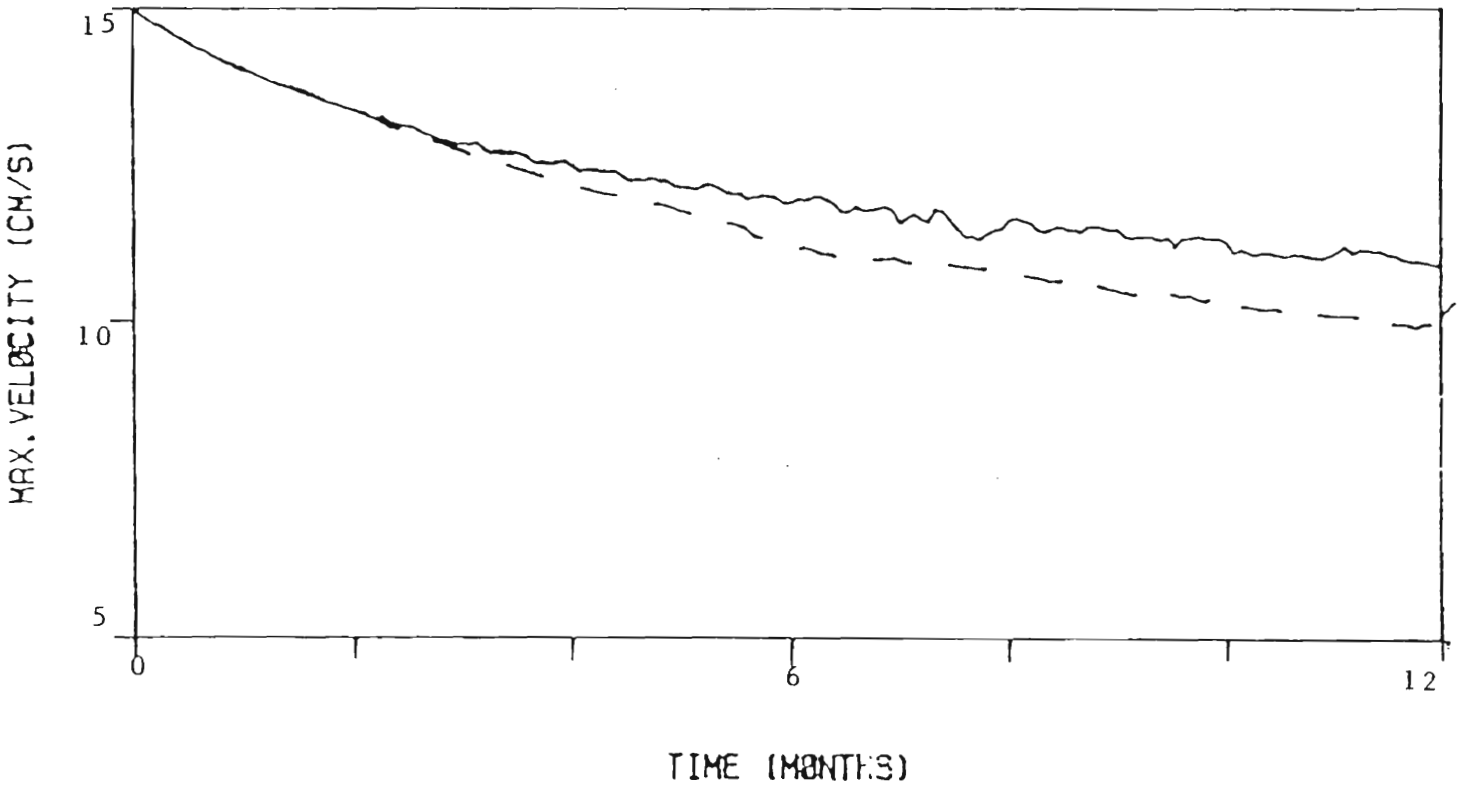

Figure 6.3. The decay of the barotropic component of the flow at the location of maximum velocity; cyclonic flow (solid line), anticyclonic flow (dashed line).

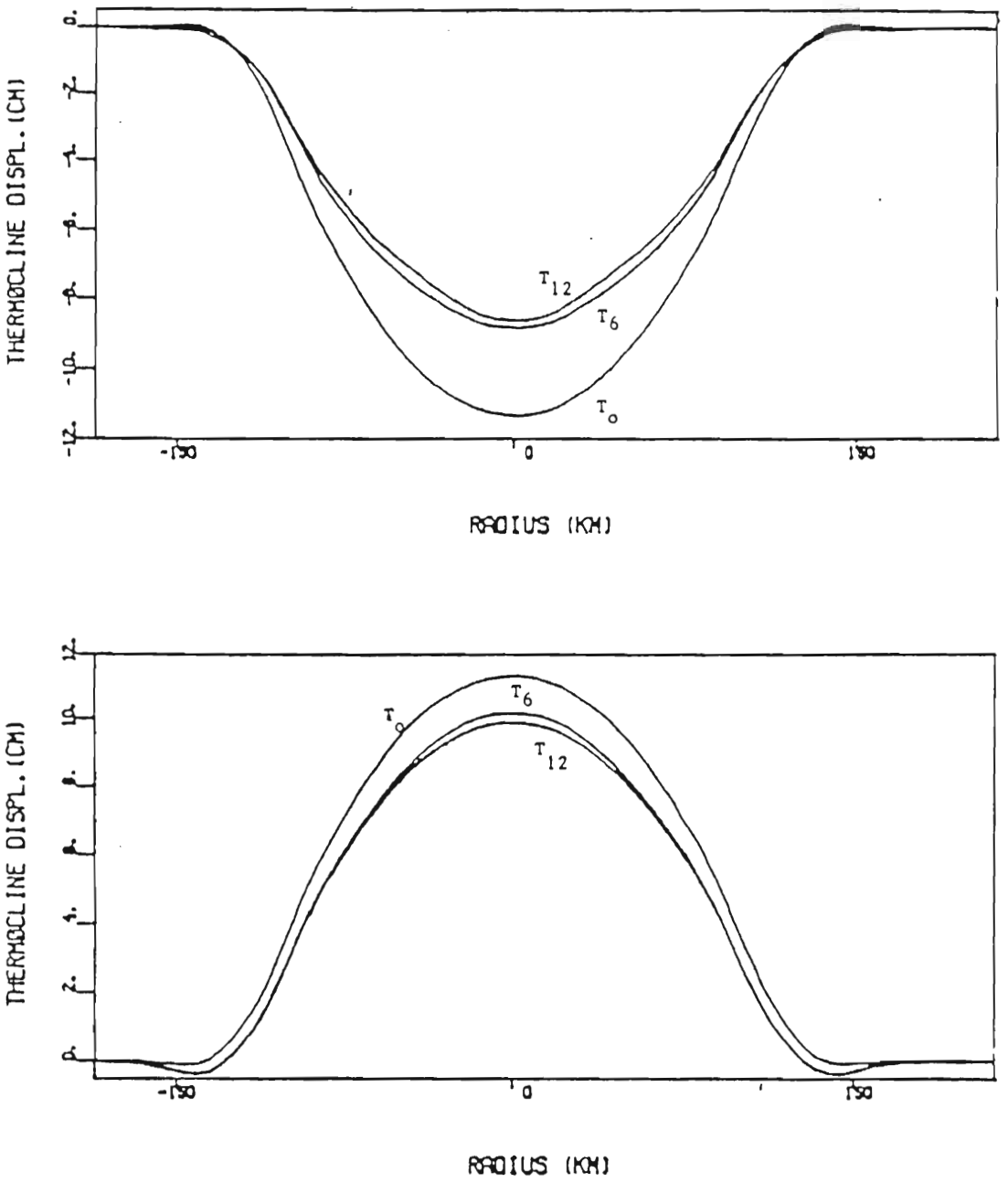

Figure 6.4. The displacement of the thermocline at time t=0, 6, and 12 months; (a) cyclonic flow, (b) anticyclonic flow.

the dissipation must occur in the early stage of the decay, when turbulence inside the BBL is strong enough to control the dynamics of the motion.

From these premises, it follows that both advection and stratification work to amplify the effects of the BBL time variations. Let us consider an anticyclonic eddy. The downwelling inside the vortex has the tendency to reduce the thickness of the mixed layer. If the forcing flow is steady, turbulence inside the BBL does not allow a complete erosion of the mixed layer; but as the forcing flow decays, turbulent activity is reduced and the BBL decreases as a result of both vertical advection and decay. Therefore the BBL time variations are not a dissipative mechanism.

In the case of a cyclonic flow, vertical advection and spin-down play opposite roles in determining the thickness of the BBL. Thus the BBL evolves similarly to the linear case of Section five, and cyclonic eddies decay faster than the correspondent anticyclonic eddies.

Analogous arguments might be applied to the dynamics of the flow at the edge of the vortices to explain the features of Fig. 6.3 and 6.5.

6.1.2. Flows for different spatial extensions.

The numerical simulations described above have indicated that vertical advection of temperature and consequent thermal wind work

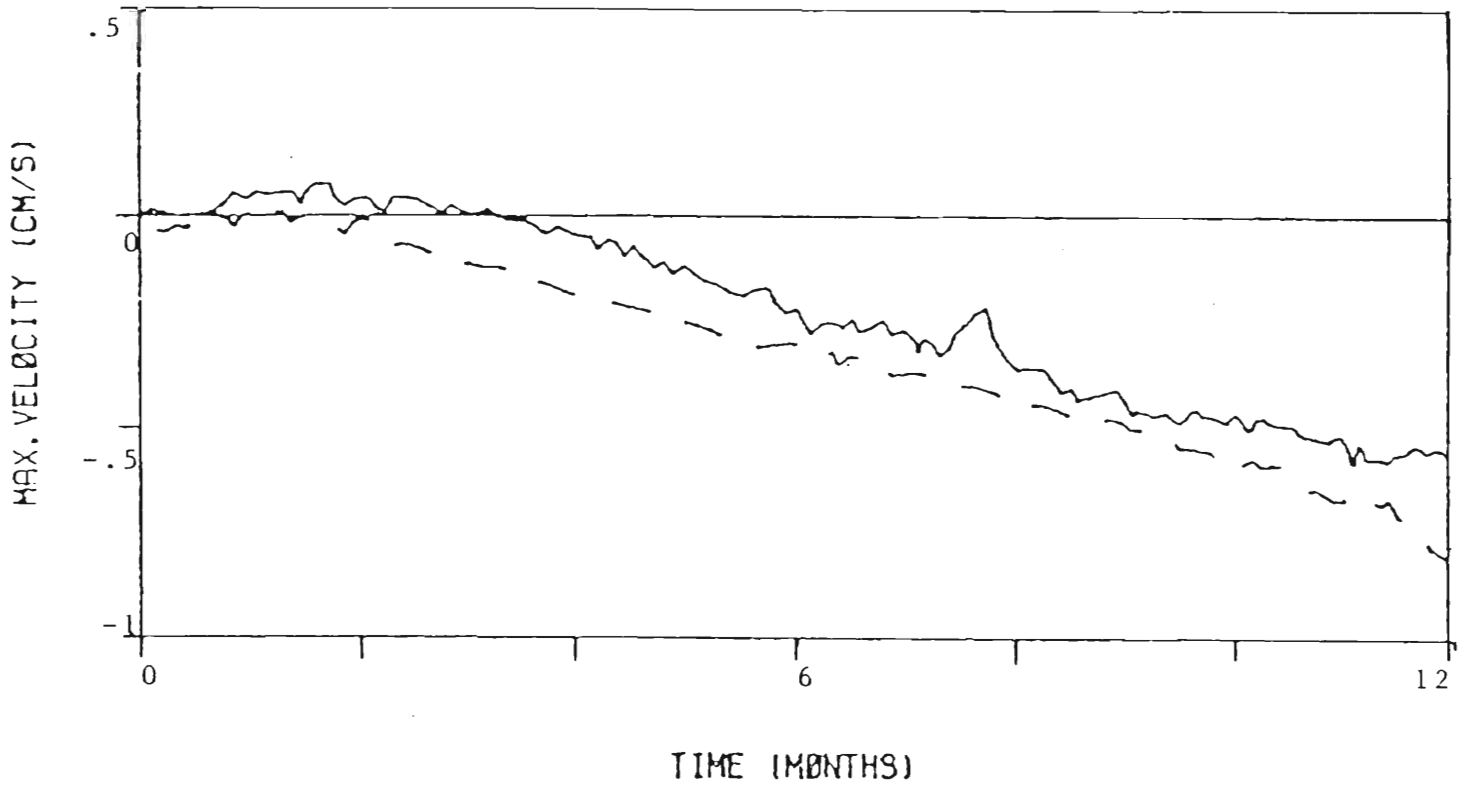

Figure 6.5. The evolution of the poleward velocity at the left edge of mesoscale eddy-like flow computed for cyclonic (solid line) and anticyclonic (dashed line) motion. Positive (negative) velocity for cyclonic flow corresponds to contraction (expansion) of the vortex.

against dissipation by bottom friction, reducing turbulent activity inside the BBL. Furthermore, vertical advection and stratification emphasize the role of the BBL time variations during the decay of the flow.

Although the BBL time variations are an important feature for differentiating the decay of cyclonic and anticyclonic eddies, the thermal wind introduces a much more determinant factor in the dynamics of the motion. Several experiments, whose features and parameters are described in Table 6.1, have been considered. Since the difference between eddies of opposite velocity signs have been discussed in the previous section, we compare results relative to cyclonic and anticyclonic flows separately.

Fig. 6.6 illustrates the evolution of the flows at the location of maximum velocity, whose initial vertical profiles are depicted in Fig. 6.7. We do not present the vertical profiles for cyclonic flows because they are virtually identical to those of the correspondent anticyclonic. Finally, the evolution of the thermocline displacement is depicted in Fig. 6.8.

It is evident that experiments 3 and 7 confirm the validity of the analytical model. If the motion is defined by a small Rossby number and stratification parameter, eddies decay as homogeneous and linear. On the other hand, flows subjected to a stronger thermal wind effect decay on a much larger time scale.

Experim.	R(km)	D(m)	$\varepsilon=\frac{U}{fR}$	$\sqrt{E}=\frac{D}{H}$	$s=\frac{N^2H^2}{f^2R^2}$	$\frac{s\sqrt{E}}{\varepsilon}$
Cyclonic Flow						
1	100	29	1.5×10^{-2}	$.75\times10^{-2}$	0	0
2	100	27	1.5×10^{-2}	$.5\times10^{-2}$	9.2×10^{-2}	$3.\times10^{-2}$
3	200	32	$.75\times10^{-2}$	$.75\times10^{-2}$	2.3×10^{-2}	2.3×10^{-2}
4	50	21	$3.\times10^{-2}$	$.5\times10^{-2}$	3.7×10^{-1}	$6.\times10^{-2}$
Anticyclonic flow						
5	100	28	1.5×10^{-2}	$.75\times10^{-2}$	0	0
6	100	28	1.5×10^{-2}	$.5\times10^{-2}$	9.2×10^{-2}	$3.\times10^{-2}$
7	200	33	$.75\times10^{-2}$	$.75\times10^{-2}$	2.3×10^{-2}	2.3×10^{-2}
8	50	21	$3.\times10^{-2}$	$.5\times10^{-2}$	3.7×10^{-1}	$6.\times10^{-2}$

Table 6.1. The characteristic dimensional scales and parameters relative to the experiments. All the experiments have the following common features: H=4000m, U=0.15ms^{-1}, and N=7.6x10^{-4}s^{-1}. The length scale D is derived from the initial values of the BBL thickness. See section 5.1. for definition of terms.

In order to explain those features, a simple model for the thermal wind is presented in Appendix B. The model furnishes a diagnostic solution to the decay of nonlinear and stratified flows when the velocity at the thermocline and the stratification parameter s are known. As Table 6.2 confirms, the predictions are in good agreement with the numerical simulations. Indeed, the model does not take in account the nonlinear terms of the momentum equation, and in deriving equation (B.4) we referred to predictions relative to linear and homogeneous flows.

We have already discussed how the weakness of the analytical model of Section 5 depends on the definition of the BBL thickness and the consequences of such definition. Nonlinearity and stratification further complicate the evolution of the BBL. Experiment 8 may be considered a good example of the last statement.

The case is defined by a large stratification parameter and Rossby number. The velocity, v_h, at the top of the BBL is very small compared with the velocity, v_H, at the thermocline, and there is a strong downwelling inside the vortex. As the flow decays and turbulent activity is reduced inside the BBL, both mixed layer and BBL decrease. The ultimate configuration is a complete erosion of the Benthic Boundary Layer and, after about three months, the flow decays only from the effects of molecular dissipation. (Fig. 6.9).

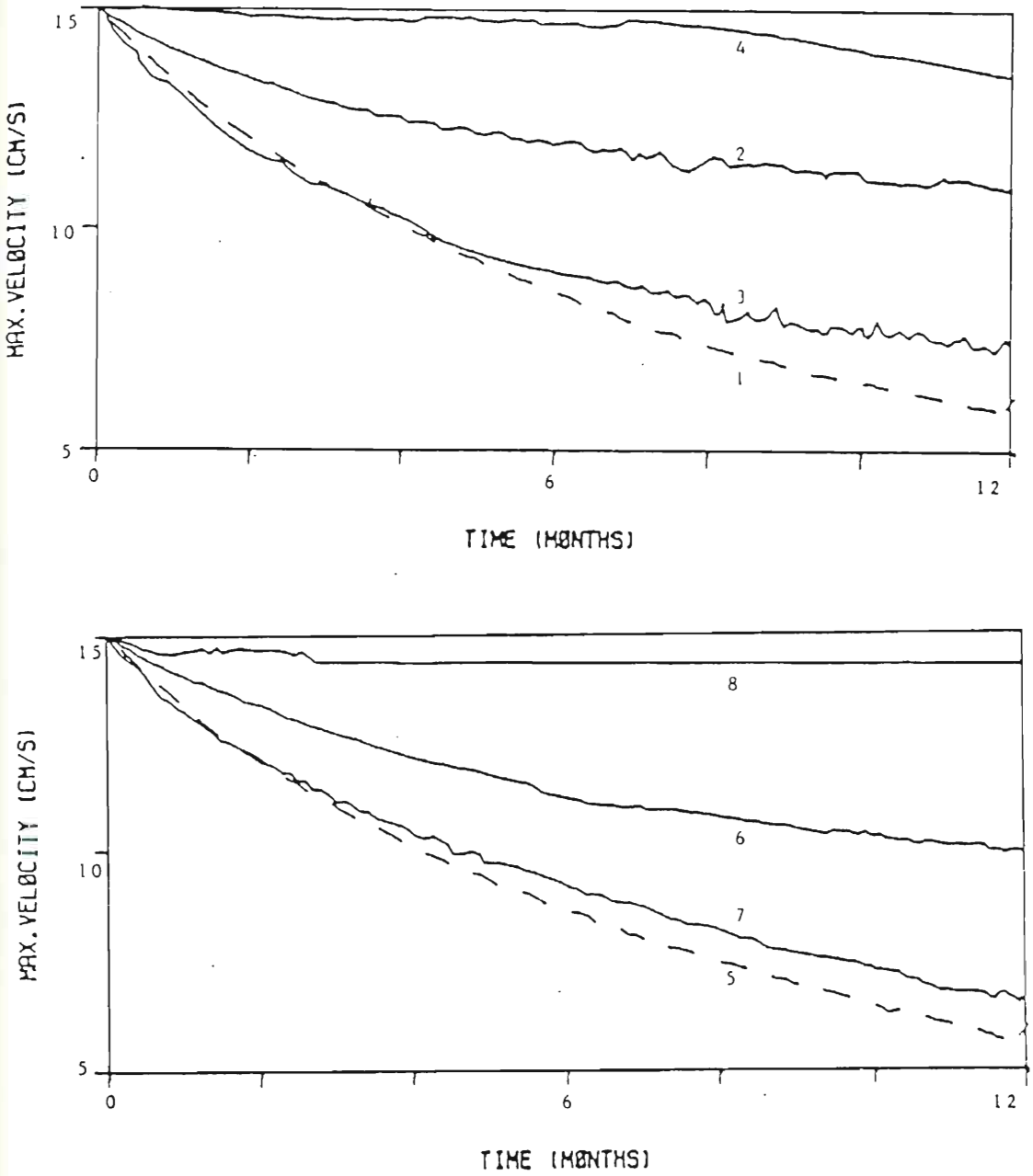

Figure 6.6. The decay of the barotropic component of the flow at the location of maximum velocity; (a) experiments 1-4, (b) experiments 5-8.

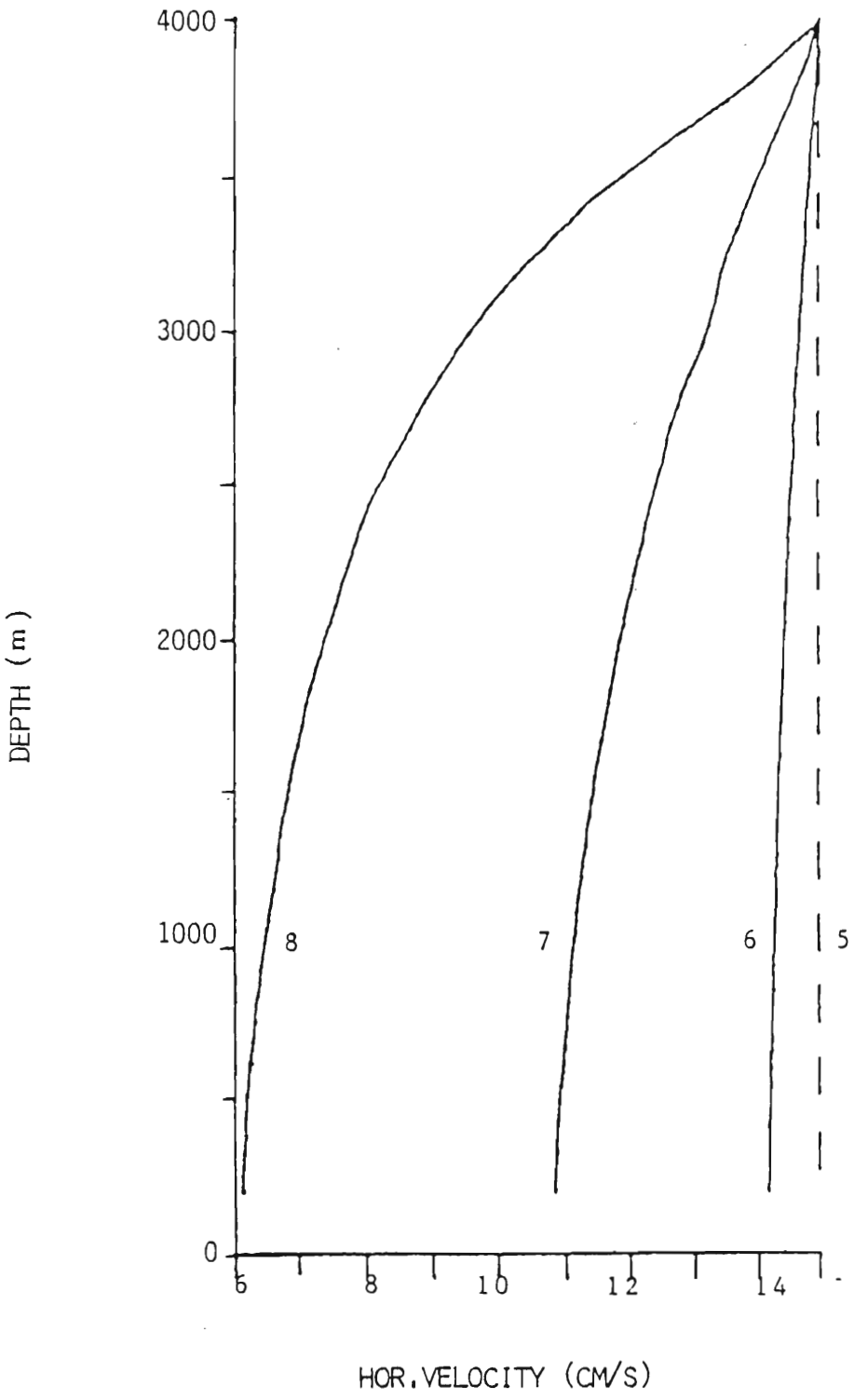

Figure 6.7. The initial vertical velocity profile at the location of maximum velocity relative to experiments 5-8.

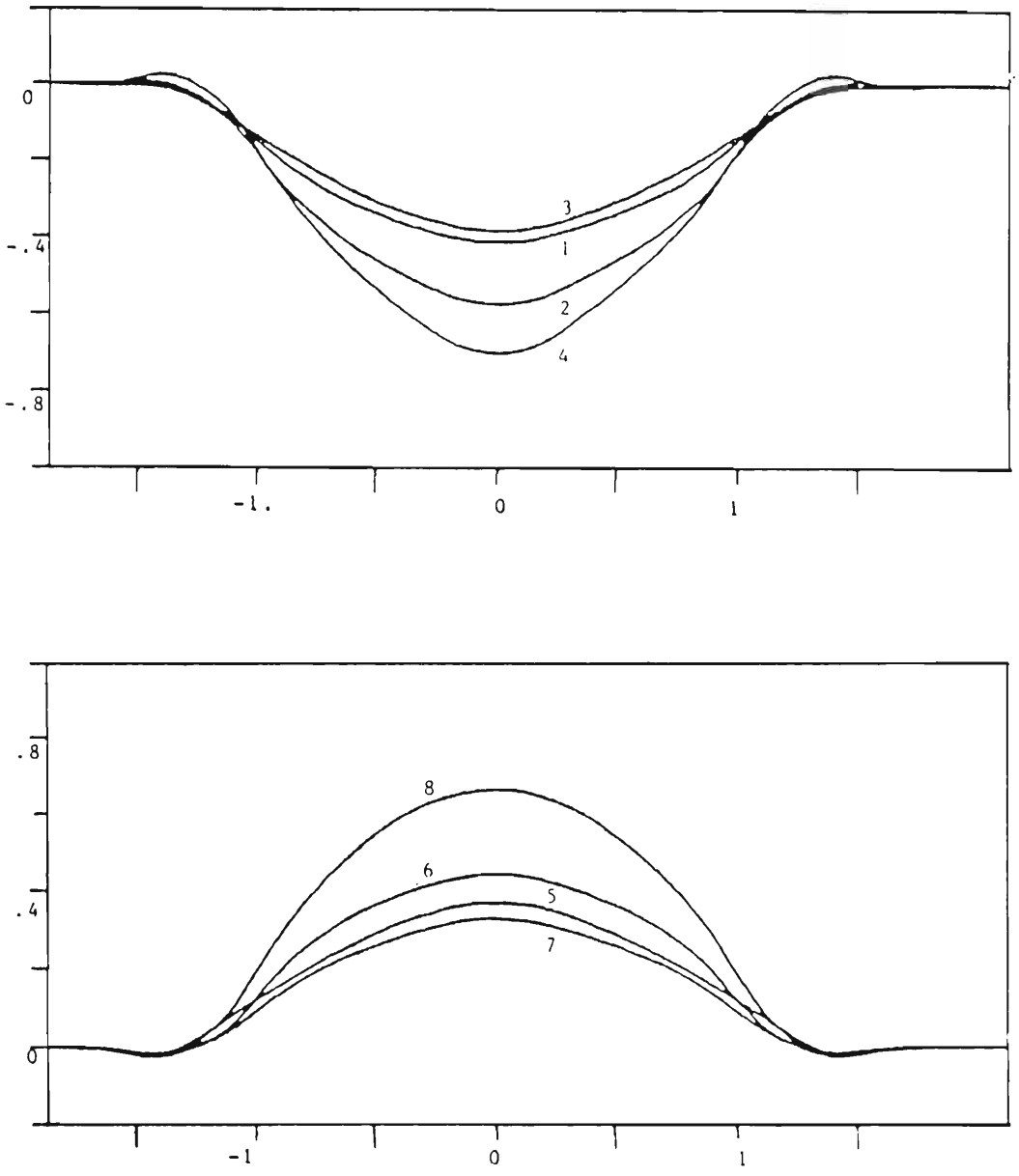

Figure 6.8. The displacement of the thermocline at time t=12months. The ordinate represents the horizontal extent of the eddy nondimensionalized with respect to the original radius of each experiments. The abscissa represents the thermocline displacement nondimensionalized with respect to the initial maximum displacement. (a) experiments 1-4, (b) experiments 5-8.

	Predictions			Values		
Experim.	$v_h^o(ms^{-1})$	T_s(years)	$v_H(ms^{-1})$	$v_h^o(ms^{-1})$	$v_H(ms^{-1})$	K/K^o
Cyclonic flow						
1	.15	1	.055	.15	.06	81%
2	.136	1.1	.11	.109	.109	56%
3	.146	1	.057	.142	.065	86%
4	.094	1.5	.139	.061	.134	23%
Anticyclonic flow						
5	.15	1	.055	.15	.055	81%
6	.136	1.1	.11	.11	.10	40%
7	.146	1	.057	.142	.07	84%
8	.094	1.5	.139	.074	.137	19%

Table 6.2. Comparison between predictions and numerical computations relative to each experiment. The velocity, v_H, is computed after one year of decay. In order to reduce the distorsion due to our paremeterization of the thermal wind, the values in column 3 are computed from the raltive values, v_h^o, of column 4. The last column indicates the fraction of initial kinetic energy which has been dissipated. See Appendix B for definition of terms.

Experiment 8 also highlights the inadequacies of the diagnostic solution that assumes a smooth exponential decay which is not supported by the numerical computations. This may indicate that the agreements between predictions and numerical tests are a result of a mere coincidence rather than of the validity of the model. In defense of the model we present the following arguments.

The model assumes that turbulence is determined by the value of the velocity at the top of the BBL independent of the barotropic component of the motion. It does not seem unreasonable to postulate that although thermal wind does affect bottom friction forces, the barotropic component of the motion also contributes to defining turbulence inside the BBL. This might be confirmed by Tables 6.1 and 6.2: the initial thickness of the BBL is not proportional to the values of the velocity, v_h. In our model we have underestimated the effects of dissipation in the early stage of the decay when dissipation is more efficient, and spread the surplus of friction forces along the time scale of the decay.

6.2. Nonstationary flow.

We have previously considered stationary eddies and a motionless ocean. Both assumptions are unrealistic. It is well known that Gulf Stream rings move westward (The Ring Group, 1981); Nof (1984) indicated that the translation is the result of the balance between pressure, Coriolis and beta-effect forces that act

Figure 6.9. The evolution of the temperature distribution relative to the coldest bottom water of experiment 8. Same as in Fig 4.7.

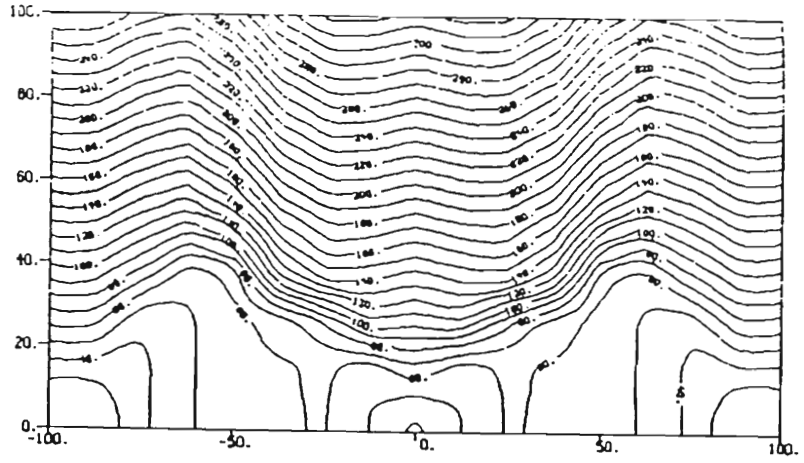

WARM RING.
0. DAYS

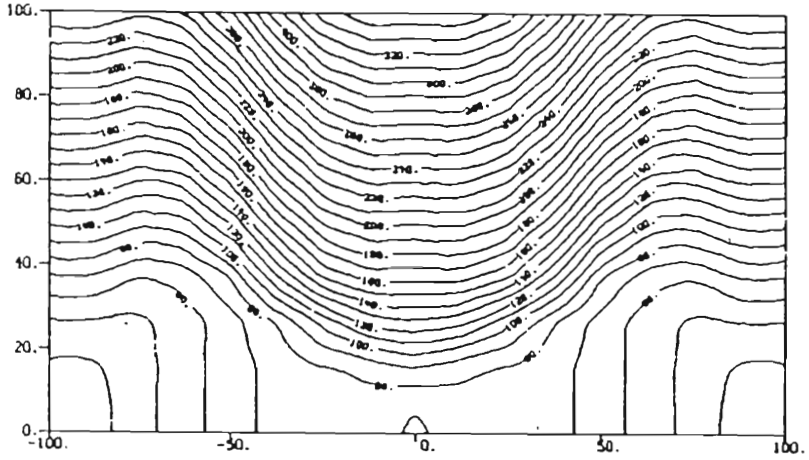

WARM RING
60. DAYS

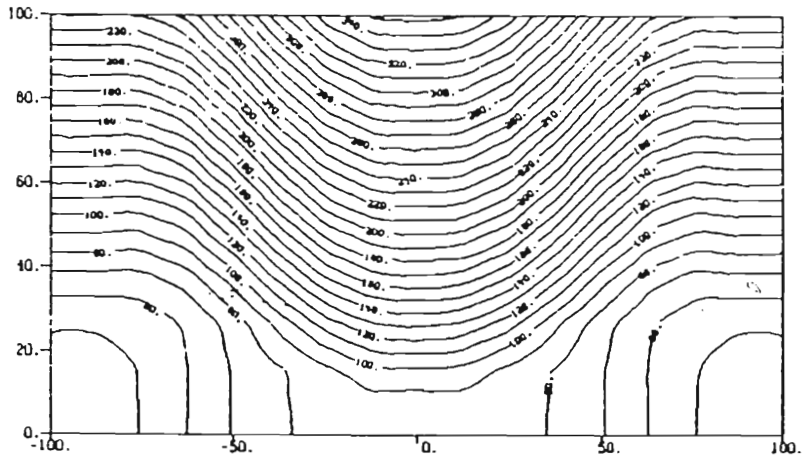

WARM RING
120. DAYS

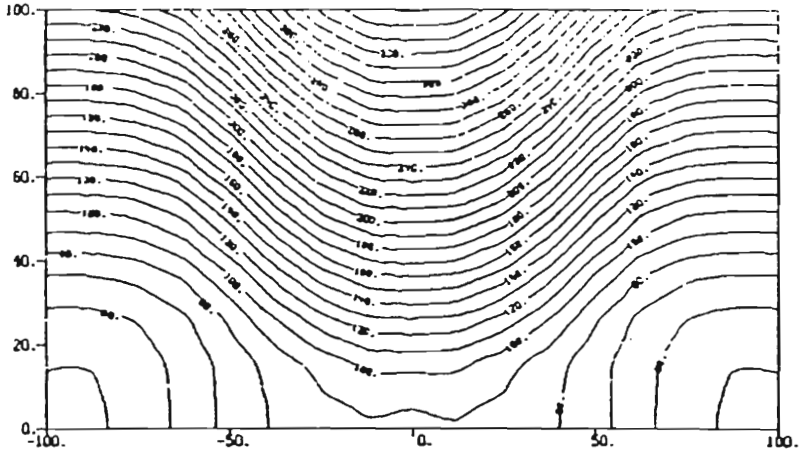

WARM RING
180. DAYS

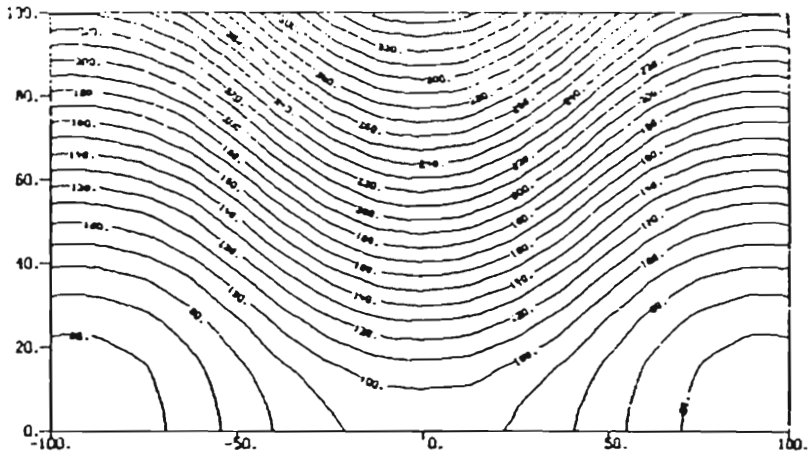

WARM RING
240. DAYS

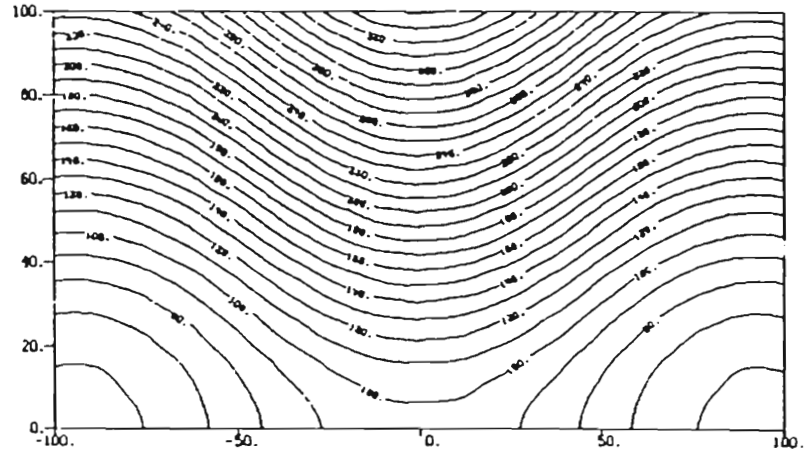

WARM RING
300. DAYS

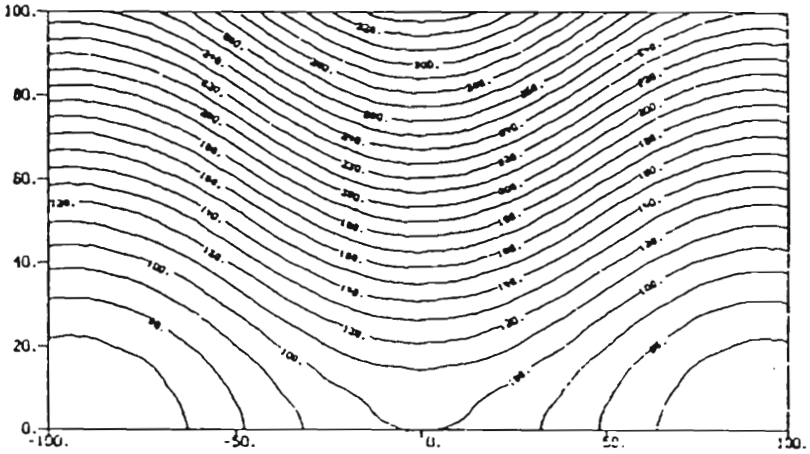

WARM RING
360. DAYS

Figure 6.9. Continued.

over the vortex as a unity. Tides, currents, and large-scale deep ocean circulation models confute the hypothesis of a motionless ocean.

Therefore, we now assume that the vortices move westwards with a uniform and steady velocity. The assumption that the eddy is moving is important in our analysis because the resultant new motion does not preserve symmetric properties, but adds a new source of bottom turbulence, so the migration of the eddy furnishes a background of bottom turbulence available for the spin-down of the mesoscale flow.

Although the direction of the motion has been chosen to be consistent with the features of Gulf Stream rings, the following study cannot be considered an application for investigating the migration of eddies. The correct formulation of the problem is fully three-dimensional and cannot be parameterized by our two-dimensional model. In addition, the original formulation of the problem does not require particular conditions at the center of the vortex. As we have discussed in Section 1, formulating the problem in a more appropriate cylindrical coordinate system does not allow a two-dimensional formulation of the migration of the vortices. Thus the numerical tests described in this section cannot be considered a direct simulation of the decay of nonstationary vortices, but an indication of the tendencies induced by the migration.

6.2.1. Cyclonic and anticyclonic flow.

The numerical tests discussed in this section consider the initial features of experiments 2 and 6 of Section 6.1., with the vortices advected by an uniform oceanic current $u_o = -0.05 ms^{-1}$.

The evolution of temperature distributions near the bottom are depicted in Fig. 6.10, and 6.11. It follows that the mutual interactions between mixed layer and BBL are basically preserved inside the vortices as discussed in the previous sections. However, the background of turbulence due to the translation of the eddies does not allow a complete erosion of the Benthic Boundary Layer when the anticyclonic flow weakens under the effect of the decay. Under such a circumstance, the flow maintains a well defined mixed layer, about 30m thick, separated by a sharp interface from the interior stratified region. Furthermore, the effects of the translation are more determinant in the recirculation of the surrounding water, where a clear downstream wake is generated.

The loss of symmetric properties is even more evident in the evolution of the forcing flow. As Fig. 6.12 indicates, there is a downstream deepening of the thermocline, regardless of the initial velocity distribution, but the location of the maximum thermocline displacement of cyclonic and anticyclonic flows moves downstream and upstream, respectively.

6.2.2. Discussion.

First let us recall that, according to the usual Ekman laminar boundary layer theory, the inclusion of a uniform and steady current modifies the structure of the boundary layer (viz, the vertical profile of the velocity components) without altering the decay of a mesoscale flow (viz, the Ekman velocity at the top of the layer). Under more realistic circumstances, we must always take in account the differences between the structure of the Benthic Boundary Layer and the dissipation induced in the forcing flow. Furthermore, the nonlinear nature of the relationship between turbulent activity and forcing flow does not grant that dissipation is an invariant with respect to stationary and nonstationary flows.

In order to understand how the translation affects the dynamics of the motion, in Appendix C we derive an expression for the Ekman velocity at the top of the BBL. We have assumed constant eddy viscosity coefficients and imposed a given Ekman veering at the top of the logarithmic layer. For the purposes of our study, it is convenient to rewrite the solution (C.3) in nondimensionalized variables as follows:

(6.2.1a) $w_E = w_{ES} + w_{ET}$

where:

(6.2.1b) $w_{ES} = \sqrt{E}\ (\sin 2\beta/2\pi)\ V_{gx}$

Figure 6.10. The evolution of the temperature distribution relative to the coldest bottom water, during the decay of a cyclonic flow under a uniform and steady westward translation. Same as in Fig. 4.7.

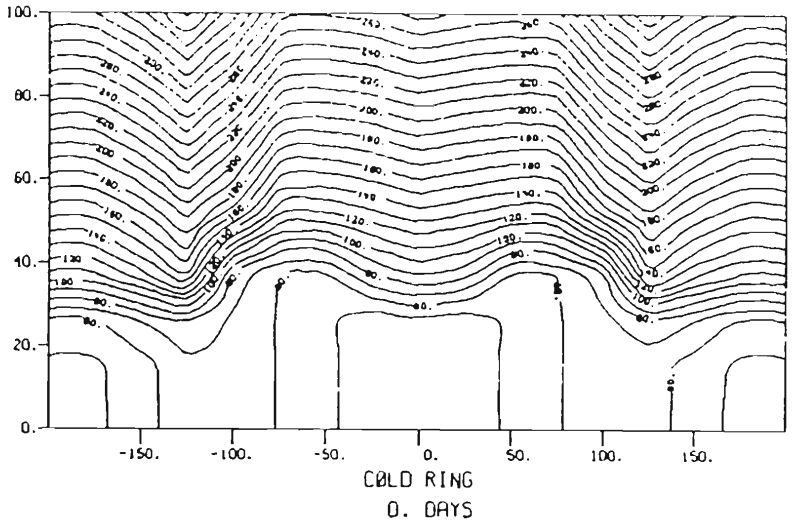

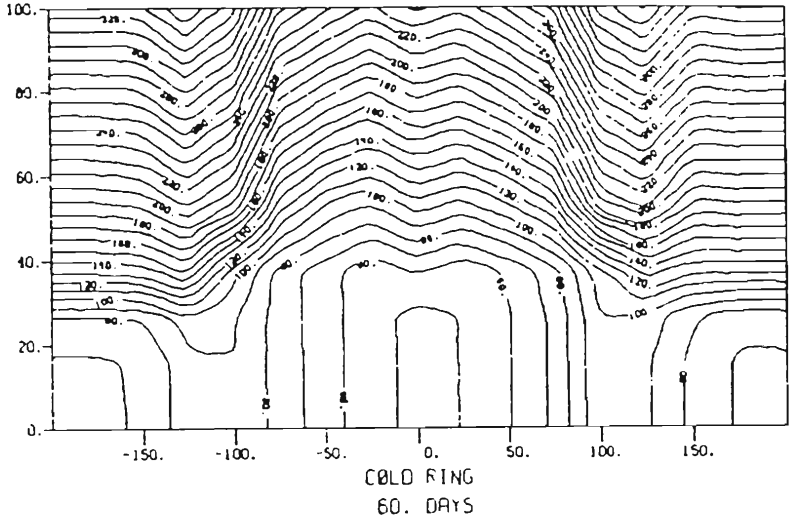

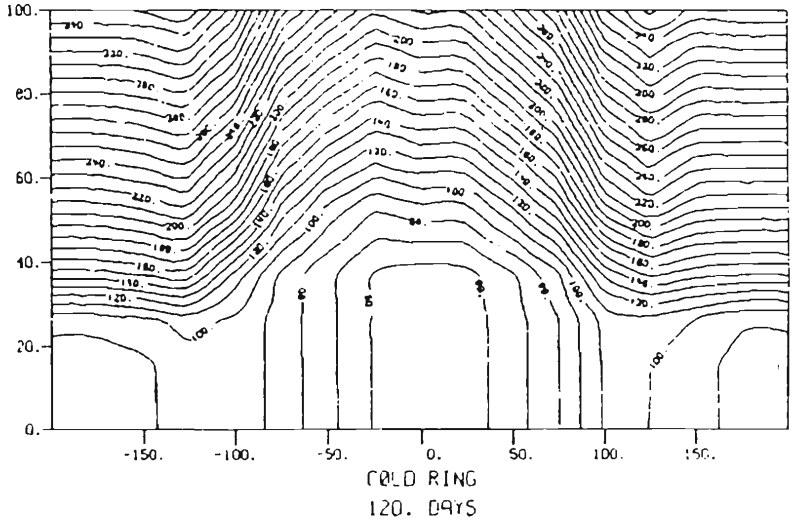

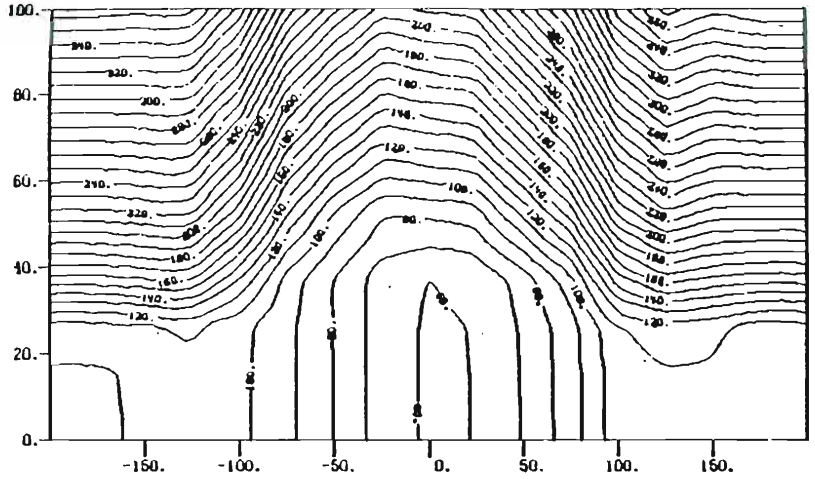

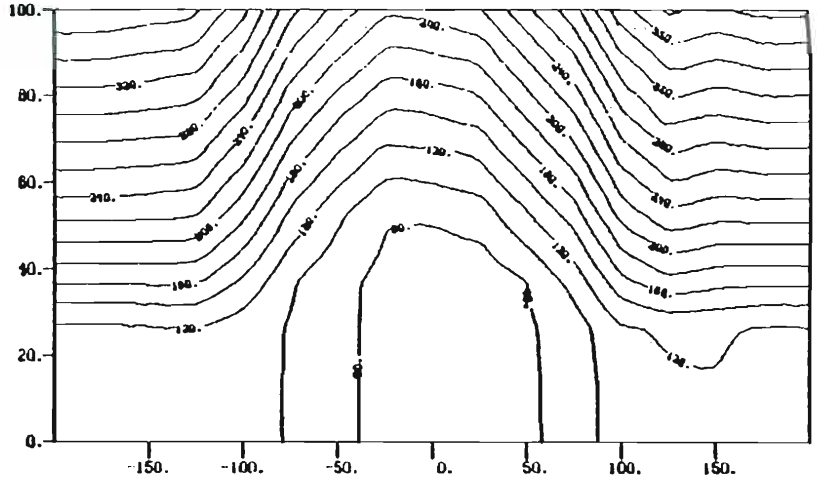

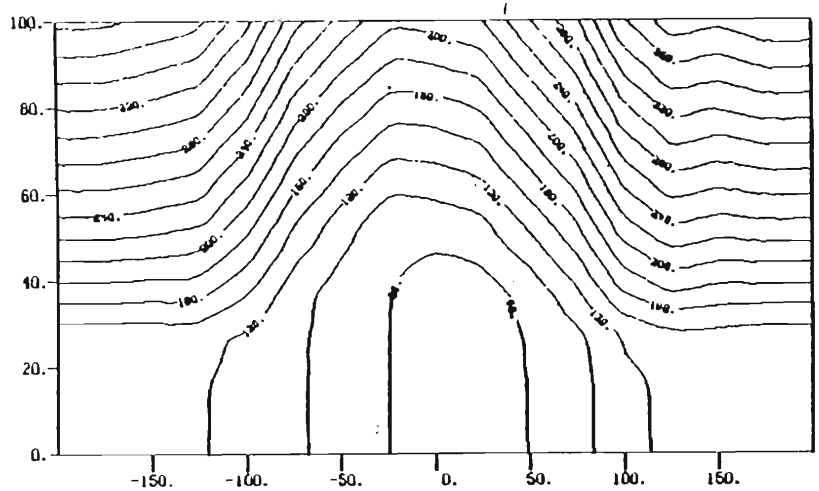

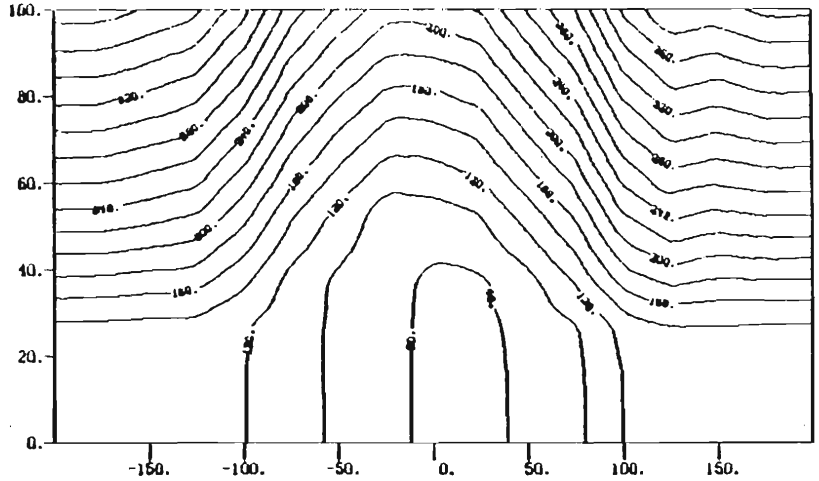

Figure 6.10. Continued.

Figure 6.11. The evolution of the temperature distribution relative to the coldest bottom water, during the decay of an anticyclonic flow under a uniform and steady westward translation. Same as in Fig. 4.7.

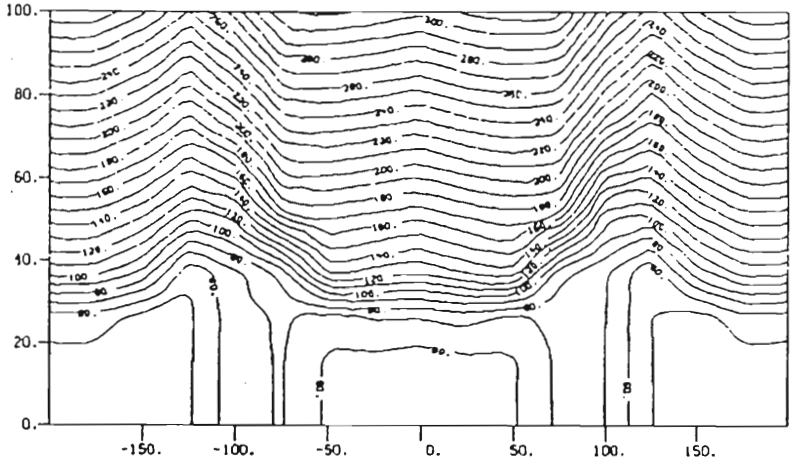

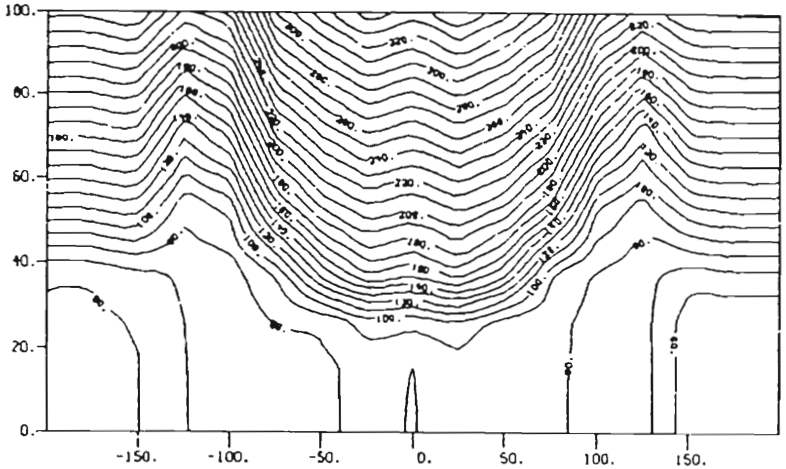

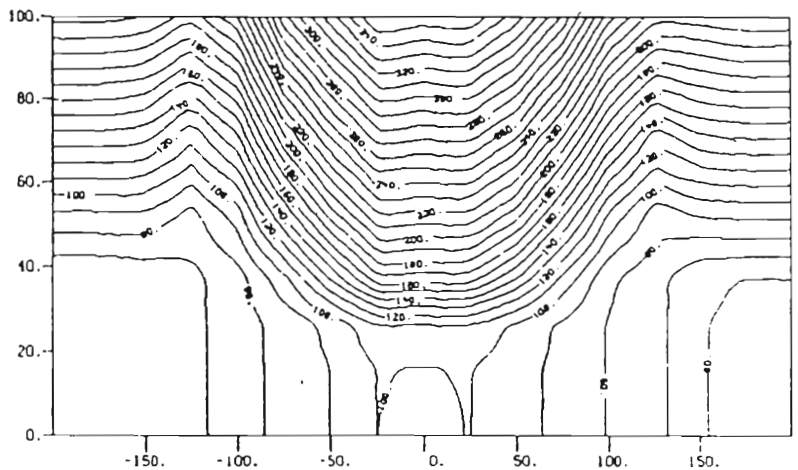

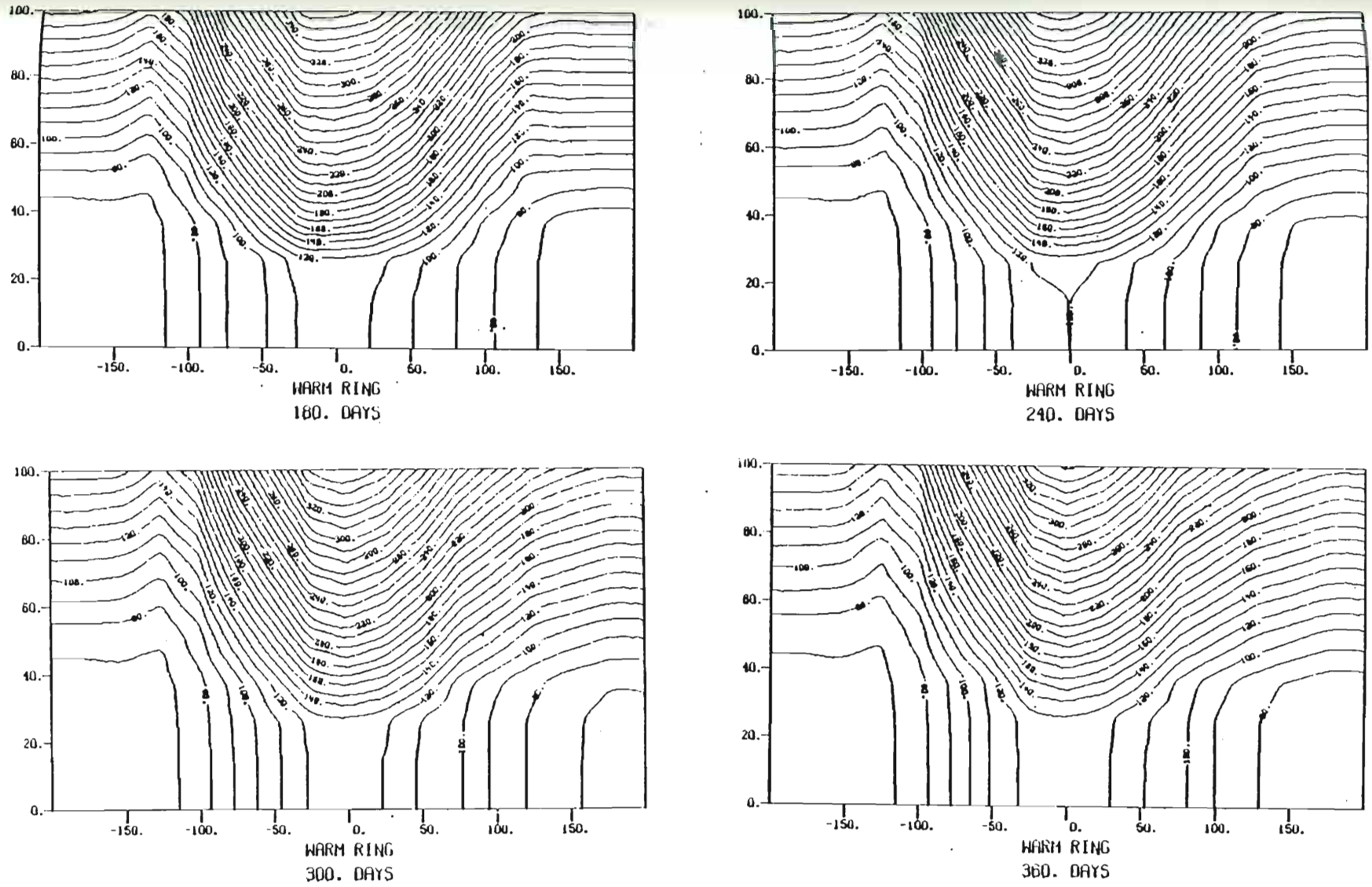

Figure 6.11. Continued.

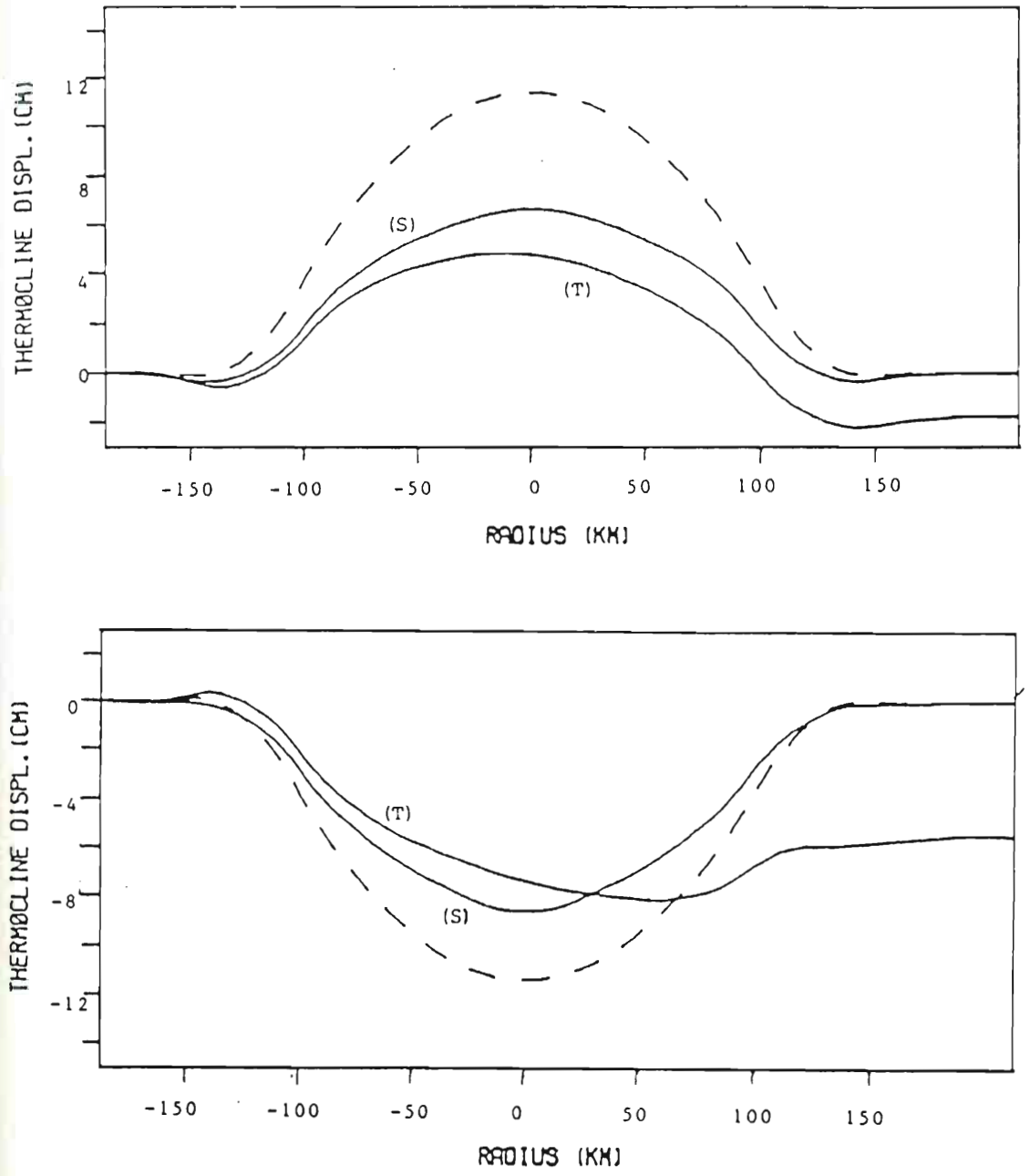

Figure 6.12. The displacement of the thermocline at time t=0 (dashed line) and t=12 months. (S) stationary flow, (T) non-stationary flow. (a) anticyclonic flow, (b) cyclonic flow.

$$(6.2.1c) \qquad w_{ET} = \sqrt{E}\,(U_g^2(1 - \sin 2\beta) - U_g V_g \cos 2\beta)V_{gx}/(2\pi(U_g^2 + V_g^2))$$

where w_{ES} is the Ekman velocity relative to stationary flow, and w_{ET} the perturbation due to the uniform translation.

With the aid of equations (6.2.1) we are able to attempt an explanation for the features described in Section 6.2.1. However, before proceeding in our analysis it is necessary to remember that the ultimate aim of spin-down is not a zero forcing flow or a zero thermocline displacement, but is rather constant values of these variables.

Let us consider an anticyclonic flow. In Fig. 6.13 we briefly sketch how translation affects the decay of the flow with respect to its correspondent stationary eddy. The assumption that the flow is unperturbed upstream, and the fact that dissipation is more efficient at the left edge assure a greater smoothing of the thermocline than that of the correspondent stationary flow. In region B, where friction forces are less dissipative, the thermocline preserves most of its original gradient. The matching condition between regions A and B leads to the downstream deepening of the thermocline. Since Ekman pumping is more efficient at the left side of the center of the vortex than at the right side, it follows that the location of maximum thermocline displacement (viz, the location of zero forcing flow) moves upstream, implying a contraction of the region of positive forcing flow (Fig. 6.12a).

The differences between regions A and B are also responsible for the temperature distribution near the bottom. At the left edge of the eddy, the upwelling is stronger than at the right, leading to the features as depicted in Fig. 6.11.

Reverse arguments must be applied when the flow is cyclonic. The eddy contracts at the left edge under the influence of translation, and the gradient of the thermocline is not sufficiently smoothed inside region B. Since the friction forces are more dissipative in region A, the thermocline deepeens slightly in the first portion of this region (viz, the forcing flow preserves negative values). Thus there is a contraction of the region of positive forcing flow and a downstream deepening of the thermocline (Fig. 6.12b). Once more, the differences between regions A and B lead to the temperature distribution depicted in Fig. 6.10.

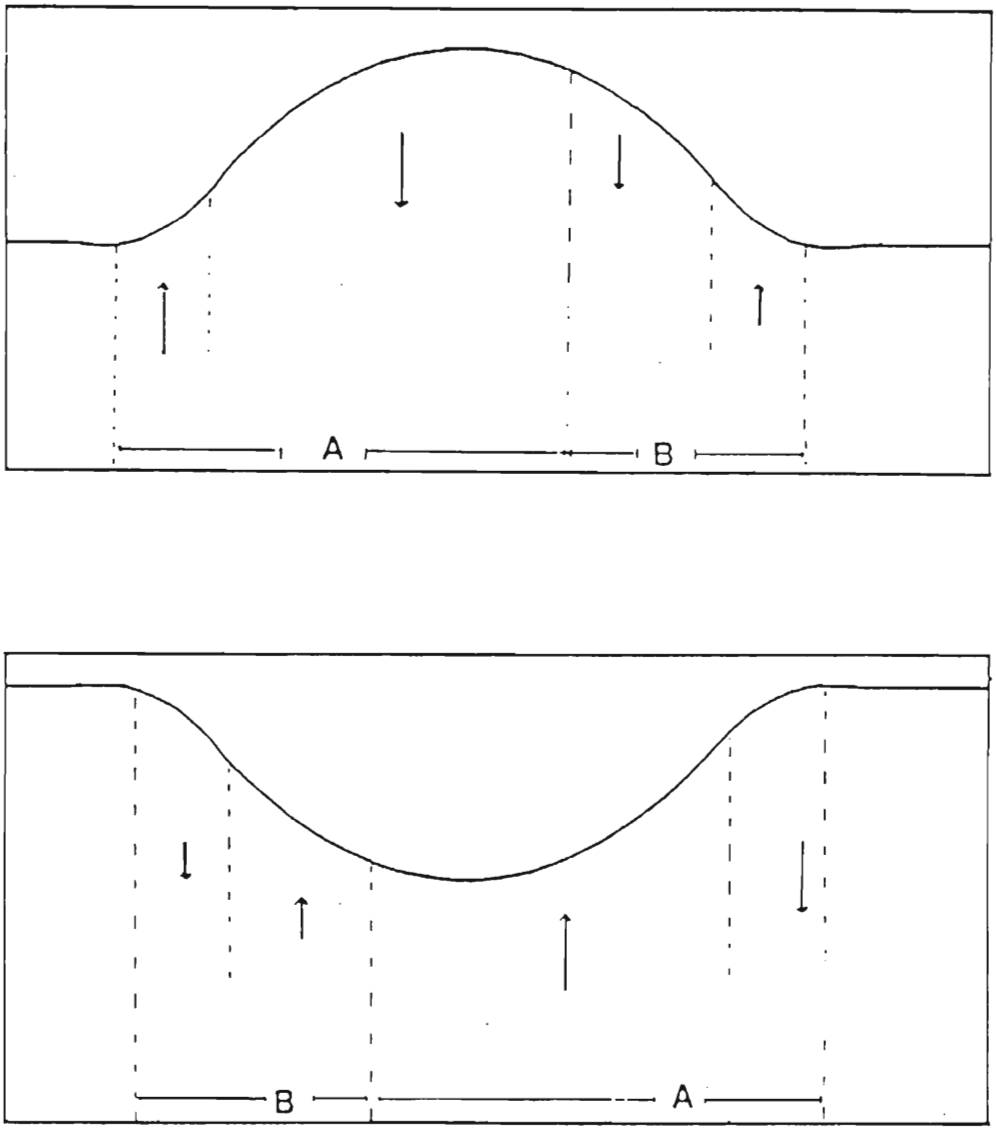

Figure 6.13. The effects of a uniform westward translation on the decay of anticyclonic (a), and cyclonic flow (b). Regions A and B indicate regions where dissipation is more and less effective with respect to the correspondent stationary flow, respectively. Arrows represent the direction of the Ekman velocity at the top of the BBL.

7. SUMMARY AND CONCLUSIONS.

Although the primary goal of the present research has been to analyze the effects of the Benthic Boundary Layer on the decay of an isolated vortex, the study also provides additional contributions to the understanding of the nature of turbulent motions and of the structure of the Benthic Boundary Layer. For this reason, we prefer to describe the findings of the investigation in three different statements.

i) Methods of analysis of turbulent flow.

In this research we are using the principle that: "In the absence of a general and rigorous approach to the solution of problems in turbulence, it is impossible to make accurate quantitative predictions without relying heavily on empirical data" (Tennekes and Lumley, 1972). Therefore our analysis develops from the classical Ekman Boundary Layer theory, corrected with the introduction of new elements derived from observations and measurements. Basically we have depended strongly upon the existence of a near bottom logarithmic layer and upon a priori knowledge of the thickness of the bottom layer and of the Ekman veering close to the wall.

It is found that the depth of the BBL furnishes an appropriate reference for defining a laminar-constant eddy viscosity

coefficient, which is a good estimate of the mean value of the turbulent momentum eddy coefficient, and that the Ekman veering is a suitable measure of the friction forces that drive the motion.

Therefore we have concluded that laminar boundary layers are more dissipative than turbulent boundary layers of equal depth and forced by the same flow. The Ekman velocity at the top of a TBL is proportional to the Ekman velocity of the correspondent LBL through a constant of proportionality which is a function of the Ekman veering at the rigid surface. Furthermore, the assumption that at the rigid wall the flow is not at an angle $\beta = \pi/4$ (counterclockwise looking down) with the forcing flow implies that dissipation is not an invariant with respect to an uniform and steady translation of the mesoscale flow.

Comparisons between the model and numerical simulations confirm that this modified Ekman Boundary Layer solution is suitable for deriving satisfactory diagnostic estimates of the frictional forces associated with the Benthic Boundary Layer.

ii) The structure of the Benthic Boundary Layer

A numerical model based on the level 2 1/2 closure scheme of Mellor and Yamada (1982) has been applied to investigate the structure of the Benthic Boundary Layer. The study ratifies that "a clear distinction should be made between the height of the mixed layer and the height at which the flow is affected by the presence of the boundary" (Richards, 1984). More precisely, a preliminary

analysis on horizontally homogeneous flows confirms that the most appropriate definition of the BBL thickness is the height at which the BBL-generated turbulent kinetic energy goes to zero, that the stratification reduces the depth of the BBL, and that the mixed layer is thicker than BBL.

On the other hand, if the Benthic Boundary Layer is forced by a mesoscale activity, the dynamics are strongly affected by vertical advection. A near-bottom downwelling has the tendency of removing the mixed layer, but turbulence inside the layer does not allow a complete erosion of the layer. The resultant balance leads to a Benthic Boundary Layer structure equivalent to that associated with horizontally homogeneous and stably stratified flows. On the contrary, a near-bottom upwelling implies the growth of the mixed layer. The BBL is then imbedded in an homogeneous region and the Benthic Boundary Layer evolves as expected for horizontally homogeneous and neutrally stratified flows.

Furthermore, recirculation outside the mesoscale activity implies different temperature distributions for cyclonic and anticyclonic motions. If the motion is cyclonic, the mixed layer receives the warm water which is adiabatically advected downwards at the edge of the flow. Cyclonic flows usually develop a mixed layer warmer than the mixed layer associated with equivalent anticyclonic activities.

These findings are in good agreement with the observations on the Madeira Abyssal Plain reported by Saunders (1983) and Thorpe

(1983). In our study, two major events occurred at the mooring sites: the passages of an anticyclonic and a cyclonic flow at days 70 and 130 respectively, as indicated by Saunder's figure 9. In the first case, before the transit of the flow (viz, during an upwelling activity), stratification is weak in the whole sample column (about 80 m), but the depth of the mixed layer is clearly reduced when the high pressure is over the site (viz, during a downwelling activity). On the other hand, the passage of the cyclonic flow is related to marked evidences of a near bottom warm front.

Another interesting place for our study is the station DEEP (39° 53'N, 62° 82'W) in the HEBBLE Area. This mooring site is particularly important because Koenig, Harkema, and Weatherly (1983) made a complete compilation of the data from Oct. 1980 to Oct. 1981, and Kelley (1984) represented the frontal position of the Gulf Stream and rings relative to the station for the same period of time. Although the records present several events that might reinforce the validity of our results, we focus our attention to the period Dec. 28, 1980 - Jan. 9, 1981.

For almost the entire length of that period, the mooring site is clearly under the influence of the recirculation associated with a Gulf Stream meander (viz, an upwelling region), and the Benthic Boundary Layer presents a warm mixed layer about 50 m thick. The region above the mixed layer is weakly stratified. On January 4,

1981 the station appears to be under the direct influences of the Gulf Stream meander (viz, a downwelling region), and the mixed layer becomes colder. Its thickness decreases and the region above is more stratified. Furthermore, the records confirm that the thickness of the mixed layer is not proportional to the magnitude of the forcing flow: the maximum bottom velocity occurred during January 1-3, when the depth of the mixed layer started to decrease.

iii) The effects of the Benthic Boundary Layer on the decay of isolated vortices.

The approach to the problem is to develop an analytical model for investigating the decay of linear and homogeneous flows. The study indicates that the spin-down occurs on a time scale proportional to the order of magnitude of the vertical velocity pumped in (out) the bottom layer. During the decay, reductions of the BBL thickness are dynamically equivalent to an apparent upwelling. Furthermore, under the assumption that the BBL time variations are of the same order of magnitude as the forcing flow variations, and for realistic values of the spatial dimensions of the vortices, eddies contract.

Comparisons between the model and numerical simulations confirm the dynamic role of the BBL time variations. However, the numerical experiments emphasize that during the decay of the flow, the evolution of the BBL depends strongly on the dynamic role of the

buoyancy forces, so that the relation between BBL thickness and forcing flow is complex and not easily understood.

With the assumption that the flow is stably stratified and nonlinear, the study suggests that vertical advection of temperature and consequent thermal wind effect work against dissipation by bottom friction and reduce turbulent activity inside the BBL. Furthermore, both vertical advection and stratification amplify the role of the BBL time variations during the spin-down of the eddies.

Finally, this work investigates the decay of a mesoscale flow advected by an uniform and steady oceanic current. The analysis indicates that a translation of the mesoscale flow implies a loss of symmetry of the motion features and a downstream deepening of the thermocline regardless of the initial velocity distribution.

Two fundamental questions remain unanswered. Are the bottom friction forces a capable dissipative mechanism? If so, in which regions of the ocean are they dominant? A satisfactory answer to these questions can be given only by applying the results of this work to the general ocean circulation. As representative samples we choose three regions: the Florida Current, the Gulf Stream warm core rings 81D, and the Subtropical Gyre.

- The Florida Current

This region has been selected as representative of flow characterized by a marked vertical shear for which the effects of bottom frictions are rather small (Weatherly, 1972).

Typical values of the Florida Currents are total depth H = 700 m, width L = 50 km, near surface velocities ranging from 1-2ms^{-1}, bottom currents of about 0.3 ms^{-1}, and a Brunt-Vaiasala frequency N = 7.2x10^{-3}s^{-1} (Brooks and Niiler, 1977; Weatherly, 1972). Those features imply a Rossby number ε=0.5, and a stratification parameter s = 0.94. From these parameters, we estimate that the thermal wind implies a reduction of the bottom velocity of about 94% with respect to the near-surface current and that therefore bottom friction cannot be dynamically efficient.

- The Gulf Stream warm-core ring 81D.

Following Joyce (1984), the features of the ring can be parameterized by a two layer system of radius R = 100 km, with the upper layer of depth H_u = 1000 m, and maximum near surface velocity v_u = 1 ms^{-1}; and the lower layer of depth H_ℓ = 4000 m, and maximum velocity v_ℓ = 0.15 ms^{-1}. In the lower layer, the flow appears to be cyclonic and essentially barotropic.

Our study predicts that the BBL dissipates about 84% of the kinetic energy contained in the lower layer during the first year of life of the ring. If we assume that velocity distribution of the upper layer is linear with depth, we estimate that the kinetic energy of the lower layer is about 54% of the kinetic energy of the upper strata. Consequently, the BBL dissipates about 25% of the kinetic energy contained in the whole water column.

Dissipation by bottom friction could have been an important mechanism in the spin-down process of ring 81D.

- The Subtropical Gyre.

Weatherly (1984) indicated that the interactions of the Gulf Stream and rings with the bottom dissipate something between 50-100% of the energy input by the wind in the subtropical gyre and that this dissipation occurs in only about 20% of the total extent of the gyre. Fofonoff (1980) estimated the rate of energy input by the wind for unit area to be about 2 ergs s^{-1}.

From the point of view of our analysis, the subtropical gyre can be considered a large-scale eddy-like flow. The system is therefore represented by very small Rossby number and stratification parameter. We might expect that bottom friction is dynamically important. Using the values of the area between estimated contours of the deep kinetic energy reported in Weatherly's Table 3 and from the modified Ekman Boundary Layer solutions, we compute the dissipation rate, P, of the system, assuming that the thickness of the BBL is $D = 0.04\ v_g/f$ and the Ekman veering is $\beta = 10°$. It follows that the dissipation rate per unit area in the region of the Gulf Stream is $P = 8.82$ ergs s^{-1}. Since the Gulf Stream System covers only 20% of the total area of the gyre, the rate of dissipation for unit area in the whole subtropical gyre is about 1.7 ergs s^{-1} or about 86% of the energy input by the wind in the same region. Therefore, our estimates are in very good agreement with Weatherly's study.

In conclusion, our answer to the questions at the opening of this discussion is: Yes, bottom friction forces are a capable dissipative mechanism, provided that the flow is represented by a small stratification parameter and a small Rossby number. Bottom friction is dynamically important for large scale motions, such as the subtropical gyre, or for weakly stratified mesoscale flows, such as deep eddies.

References

Armi, L. and D'Asaro, E., 1980: Flow structure of the benthic ocean. J. Phys. Oceanogr., 3, 245-57.

Armi, L. and Millard, R. C., 1976: The Bottom Boundary Layer of the deep ocean. J. Geophys. Res., 81, 4983-4990.

Blackdar, A. K. and Tennekes, H., 1968: Asymptotic similarity in neutral barotropic planetary boundary layer. J. Atmos. Sci., 25, 1015-20.

Bowden, K. F., 1978: Physical problems of the Benthic Boundary Layer. Geophys. Surv., 3, 225-96.

Brown, R. A., 1970: A secondary flow model for the planetary boundary layer. J. Atmos. Sci., 27, 742-57.

Caldwell, D. R., 1976: Fine-scale temperature structure in the bottom mixed layer on the Oregon shelf. Deep-Sea Res., 23, 1025-36.

Carnahan, B., and Luther, H. A. and Wilkes, J. O., 1969: Applied numerical methods. Wiley, New York, 604 pp.

Clarke, R. A., 1976: Measurements of small near-bottom cyclonic circulation near the Gulf Stream axis. J. Fish. Res. Board Can., 8, 47-62.

Csanady, G. T., 1967: On the "resistance law" of a turbulent Ekman layer. J. Atmos. Sci., 24, 467-71.

_____, 1978: The arrested topographic wave. J. Phys. Oceanogr., 8, 47-62.

D'Asaro, E., 1982: Velocity structure of the benthic ocean. J. Phys. Oceanogr., 12, 313-22.

_____, 1982: Absorption of internal waves by the Benthic Boundary Layer. J. Phys. Oceanogr., 12, 323-36.

Deardoff, J. W., 1970: A three-dimensional numerical investigation of the idealized planetary boundary layer. J. Geophys. Fluid Mech., 1, 377-410.

_____, 1973: Three-dimensional numerical modelling of the planetary boundary layer. J. Atmos. Sci., 29, 91-115.

Flierl, G. R., 1977: The application of linear quasigeostrophic dynamics to Gulf Stream rings. J. Phys. Oceanogr., 7, 365-79.

Fofonoff, N. P., 1962: Dynamics of ocean currenys. In The Sea, vol.1, Wiley,New York,498pp.

_____, 1981: The Gulf Stream System. In Evolution of Physical Oceanography, B. Warren and C. Wunsch eds., The MIT Press, Cambridge, 623 pp.

Greenspan, H. P., 1968: The theory of rotating fluids. Cambridge University Press, 327 pp.

Grotjahn, R., and O'Brien, J. J., 1976: Some inaccuracies in finite differencing hyperbolic equations. Mon. Wea. Rev., 104, 180-94.

Holland, W., 1978: The role of mesoscale eddies in the general circulation of the ocean. Numerical experiments using a wind-driven quasigeostrophic model. J. Phys. Oceanogr., 8, 363-92.

Holton, J. R., 1979: An introduction to dynamic Meteorology. Academic Press, New York, 391 pp.

Joyce, T. M., 1984: Velocity and hydrographic structure of a Gulf Stream warm-core ring. J. Phys. Oceanogr., 14, 936-47.

Kelley, E. A., 1984: A study of highly energetic near-bottom ocean flow at the base of the Scotian Rise. Ph.D. dissertation, Florida State University, Tallahassee, Florida.

Kelley, E. A., and Weatherly, G. and Evans, J. C., 1982: Correlation between surface Gulf Stream and bottom flow near 5000 m depth. J. Phys. Oceanogr., 12, 1150-53.

Koenig, P., and Harkema, R. and Weatherly, G., 1983: A compilation of moored current meter data in HEBBLE area, Oct. 1980- Oct. 1981. Dept. of Oceanography, Florida State University. Technical Report 83-01.

Krauss, E. B., 1972: Atmosphere-Ocean interaction. Claredon Press, Oxford, 275 pp.

Kundu, P. K., 1976: Ekman veering observed near the ocean bottom. J. Phys. Oceanogr., 12, 1150-53.

_____, 1984: Numerical calculations of coastal flow with turbulent dynamics. Deep-Sea Res., 31, 39-60.

Lilly, D. K., 1965: On the computational stability of numerical solutions of time-dependent non-linear geophysical fluid dynamics problems. Mon. Wea. Rev., 93, 11-25.

McCartney, M. S., and Worthington, I. V. and Schmitz, W. J., 1978: Large cyclonic rings from the northeast Saragasso Sea. J. Geophys. Res., 83, 901-14.

McWilliams, J. C., and Flierl, G. R., 1979: On the evolution of isolated nonlinear vortices. J. Phys. Oceanogr., 7, 1155-82.

Mason, P. J., and Sykes, R. I., 1980: A two-dimensional numerical study of horizontal roll vortices in the neutral atmospheric boundary layer. Quart. J. R. Met. Soc., 106, 351-66.

Mellor, G. L., and Yamada, T., 1974: A hierarchy of turbulence closure models for planetary boundary layers. J. Atmos. Sci., 31, 1791-1806.

_____, 1982: Development of a turbulence closure model for geostrophic fluid problems. Rev. Geophys. Space Phys., 20, 851-75.

Mied, R. P., and Lindemann, G. J., 1979: The propagation and evolution of cyclonic gulf stream rings. J. Phys. Oceanogr., 9, 1183-1206.

Molinari, R. L., 1970: Cyclonic ring spin-down in the North Atlantic. Ph.D. dissertation, Texas A & M University, College Station, Texas.

Monin, A. S., and Yaglom, A. M., 1971: Statistical Fluid Mechanics. Vol. 1, The MIT Press, Cambridge, 769 pp.

Nihoul, J. J. C., 1977: Bottom Turbulence. Elsevier Scientific Publ. Comp., Amsterdam, 306 pp.

Nof, D., 1983: On the migration of isolated eddies with application to Gulf Stream rings. J. Mar. Res., 41, 399-425.

Nowell, A. R., 1983: The Benthic Boundary Layer sediment transport in U. S. National Report to International Union of Geodesy and Geophysics, 1979-82. A.G.U., Washington, D. C.

Olson, D. B., 1980: The physical oceanography of two rings observed by the cyclonic ring experiment. Part II: Dynamics. J. Phys. Oceanogr., 10, 514-28.

Phillips, N. A., 1959: An example of non-linear computational instability. In The Atmosphere and the Sea in Motion. Rossby Memorial Volume, Rockefeller Institute Press, New York.

Pedlosky, J., 1979: Geophysical Fluid Dynamics, Spring Verlag, New York, 624 pp.

Ragallo, R. S., and Moin, P., 1984: Numerical Simulation of turbulent flows. Ann. Rev. Fluid Mech., 16, 99-137.

Richards, K. J., 1982a: Modelling the Benthic Boundary Layer. J. Phys. Oceanogr., 12, 428-39.

_____, 1982b: The effect of a Bottom Boundary Layer on the stability of a baroclinic zonal current. J. Phys. Oceanogr., 12, 1493-1505.

_____, 1984: The interaction between the bottom mixed layer and mesoscale motions of the ocean. A numerical study. J. Phys. Oceanogr., 14, 754-68.

Richardson, P. L., 1983: Eddy kinetic energy in the North Atlantic from surface drifters. J. Geophys. Res., 88, 4355-67.

Richardson, M. J., and Wimbush, M. and Mayer, L., 1981: Exceptionally strong near-bottom flows on the continental rise of Nova Scotia. Science, 231, 887-88.

Ring Group, the, 1981: Gulf Stream cold-core rings: their Physics, Chemistry, and Biology. Science, 212,1091-1100.

Rotta, J. C., 1951: Statistische theorie nichthomogener turbulenz. Z. Phys., 129, 547-572.

Saunders, P. M., 1983: Benthic observations on the Madeira Abyssal Plain: Currents and dispersions. J. Phys. Oceanogr., 13, 1416-29.

Schmitz, W. J., 1977: On the deep general circulation in the western North Atlantic. J. Mar. Res., 35, 21-28.

Schmitz, W. J., and Holland, W., 1982: Numerical eddy-resolving general circulation experiments: preliminary comparison with observations. J. Mar. Res., 40, 75-117.

Sommeria, G., 1976: Three-dimensional simulation of turbulent process in an undisturbed trade wind boundary layer. J. Atmos. Sci., 33, 216-41.

Tennekes, H., and Lumley, J. L., 1972: A first course in turbulence. The MIT Press, Cambridge, 300 pp.

Thorpe, S. A., 1983: Benthic observations on the Madeira Abyssal Plain: Fronts. J. Phys. Oceanogr., 13, 1430-40.

Vager, B. G., and Nadezhina, Ye. D., 1975: The structure of the atmospheric boundary layer under horizontal homogeneous conditions. Izv. Atmos. and Oceanic Physic., 11, 565-73.

Weatherly, G., 1972: A study of the Bottom Boundary Layer of the Florida Current. J. Phys. Oceanogr., 2, 54-72.

_____, 1977: Bottom Boundary Layer observations in the Florida Current, In Bottom Turbulence. Nihoul ed., Elseviar Sci. Publ. Comp., Amsterdam, 306 pp.

_____, 1984: An estimate of bottom frictional dissipation of Gulf Stream fluctuations. J. Mar. Res., 42, 289-301.

Weatherly, G., and Kelley, E. A., 1984: Abyssal currents: Storms and flow reversals. Submitted to ?

Weatherly, G., and Martin, P. J., 1978: On the structure and dynamics of the ocean Bottom Boundary Layer. J. Phys. Oceanogr., 8, 557-70.

Wimbush, M., and Munk, W., 1970: The Benthic Boundary Layer. In The Sea, Vol 4, Part 1. Wiley, New York.

Worthington, L., 1976: On the North Atlantic Circulation, The Johns Hopkins University Press, Baltimore, 110 pp.

Wyngaard, J. C., and Cote', O. R. and Rao, K. S., 1974: Modelling the atmospheric boundary layer. In Turbulent diffusion in environmental pollution, Advances in Geophysic series, Vol. 18a, Academic Press, New York, 426 pp.

Yamada, T., 1975: The critical Richardson number and the ratio of the eddy transport coefficients obtained from a turbulence closure model. J. Atmos. Sci., 32, 926-33.

_____, 1978: A three-dimensional second-order closure numerical model of mesoscale circulations in the lower atmosphere: Description of the basic model and application to the simulation of the environmental effects of a large cooling pond. Radiological and Environmental Res. Div., Argonne Nat., Lab., Top. Rep. ANL RER-78-1, 67 pp.

_____, 1979: An application of a three-dimensional simplified second-order closure numerical model to study atmospheric effects of a large cooling pond. J. Atmos. Environ., 13, 693-704.

_____, 1982: A numerical model study of turbulent airflow in and above a forest canopy. J. Meteor. Soc. Japan, 439-54.

_____, 1983: Simulations of nocturnal drainage flows by a q^2-ℓ turbulence closure model. J. Atmos. Sci., 40, 91-106.

Appendix A. An approximated vertical profile of the turbulent eddy viscosity coeffiecient.

It is well known that close to the rigid surface, in the log-layer, eddy viscosity coefficients are linear functions of height (Krauss, 1972) and it is usually observed that they are monotonic decreasing functions from the top of log-layer to the top of the total boundary layer (Wyngaard et al., 1974). Therefore, with the boundary condition that the eddy viscosity coefficient K_M goes to zero at the rigid wall and at the top of the TBL, it is possible to approximate $K_M(z)$ by linear interpolation once the thickness D_{log} of the log-layer and the value $K_{max} = K_M(D_{log})$ are known.

From this vertical profile we deduce that:

$$(A.1) \qquad \langle K_M \rangle = \frac{1}{D} \int_0^D K_M(z)dz = 0.5\ K_{max}$$

In order to estimate the variable D_{log} and K_{max}, we refer to the studies of Weatherly (1972) and Wyngaard et al. (1974), respectively:

$$(A.2) \qquad D_{log} = 0.1\ D$$

$$(A.3) \qquad K_{max} = 0.02\ u_*^2/f$$

Therefore,

(A.4) $\langle K_M \rangle = 1.x10^{-2}\ u_*^2/f$

Equations (5.1.12) and (5.1.19) imply:

(A.5) $\langle K_M \rangle = 0.04\ D^2 f = 0.82\ \nu^L$

Appendix B. The effect of stratification on the decay of a deep mesoscale flow: a diagnostic solution.

Assume that the flow is uniform in the poleward direction, geostrophic and Boussinesq. Assume that density distribution is under a purely advective balance. Thus the motion equations might be written as follows:

$$fv_z = - g \frac{1}{\rho_o} \rho x \qquad \text{(B.1a)}$$

$$u\rho_x + w\rho_z = 0 \qquad \text{(B.1b)}$$

Scaling the equations as in (5.1.2) leads to:

$$\tilde{v}_{\tilde{z}} = - \tilde{\rho}_{\tilde{x}} \qquad \text{(B.2a)}$$

$$\tilde{u}\tilde{\rho}_{\tilde{x}} - s\tilde{w} = 0 \qquad \text{(B.2b)}$$

where tilde indicates nondimensionalized variables. Equation (B.2b) implies $\tilde{\rho}_{\tilde{x}} = 0(s)$, and therefore:

$$v_h = v_H(1-s) \qquad \text{(B.3)}$$

where the subscripts h and H represent values at the top of the BBL and at the thermocline, respectively.

As preliminary results we conclude that the thermal wind reduces the velocity at the top of the BBL by a factor (1-s) with respect to the value at the free surface. If we assume that the initial thickness of the BBL is proportional to the magnitude of the velocity v_h, it follows that the time scale of the decay T_s is given by:

$$T_s = 1/(\sqrt{E}\, fk|1-s|) \tag{B.4}$$

Thus we estimate that the decay of the velocity v_h is expressed as:

$$v_h = v_h^o \exp(-t/T_s) \tag{B.5}$$

where the superscript o refers to initial values. From equation (B.5) we are finally able to derive an expression for the evolution of the flow at the thermocline. Since we have assumed that spin-down acts only on the barotropic component of the motion, V_g; the velocities v_h and v_H can be written as follows:

$$v_H = V_g + v_H^o - V_g^o$$

$$v_h = Vg + v_h^o - V_g^o$$

or,

$$v_H = v_h + v_H^o - v_h^o \tag{B.6}$$

Substitution of (B.3), (B.5) into (B.6) leads to:

$$v_H = v_H^o((1-s)\exp(-t/T_s) + s) \tag{B.7}$$

Appendix C. An analytical expression for the Ekman velocity at the top of the Bottom Boundary Layer.

Following the analysis and the symbolisms of Section 5, we consider a laminar boundary layer of constant height D, forced by a geostrophic flow of components (U_g, V_g). Generalizing the study presented in Section 5, the velocity components at the top of the logarithmic layer are:

$$(C.1a) \qquad (u,v) = (u_b\cos(\gamma + \beta),\ u_b\sin(\gamma + \beta))$$

where β is the Ekman veering and

$$(C.1b) \qquad u_b = (\cos\beta - \sin\beta)(U_g^2 + V_g^2)^{1/2}$$

$$(C.1c) \qquad \gamma = \mathrm{atan}(U_g/V_g)$$

The solution above the logarithmic layer is:

$$(C.2a) \qquad u = U_g(1-e^{-\xi}\cos\xi) - V_g e^{-\xi}\sin\xi + (\cos\beta - \sin\beta)(U_g^2 + V_g^2)^{1/2} e^{-\xi}\cos(\xi - \gamma - \beta)$$

$$(C.2b) \qquad v = U_g e^{-\xi}\sin\xi + V_g(1-e^{-\xi}\cos\xi) + -(\cos\beta - \sin\beta)(U_g^2 + V_g^2)^{1/2} e^{-\xi}\sin(\xi - \gamma - \beta)$$

where

(C.2c) $$\xi = \pi z/D$$

In deriving (C.2), we have repeatedly used the relationships:

$$\cos\gamma = U_g/(U_g^2 + V_g^2)^{1/2};\ \sin\gamma = V_g/(U_g^2 + V_g^2)^{1/2}$$

Assume that U_g is constant; then the Ekman velocity at the top of the layer is given by:

(C.3) $$W_E = -\int_o^D u_x dz = -\frac{D}{\pi}\int_o^\infty u_x d\xi =$$

$$\frac{D}{2\pi}\left(\sin 2\beta + \frac{U_g^2(1-\sin 2\beta) - 2U_gV_g\cos 2\beta}{U_g^2 + V_g^2}\right)V_{gx}$$

For $\beta = \pi/4$, the modified spiral (C.2) and the Ekman velocity (C.3) reduce to the solution of the classical Ekman Boundary Layer theory.